SAND REPORT

SAND 2001-3397
Unlimited Release
Printed November 2001

Functional Materials for Microsystems: Smart Self-Assembled Photochromic Films: Final Report

A. R. Burns, D. Y. Sasaki, R. W. Carpick, J. A. Shelnutt, and C. J. Brinker

Prepared by
Sandia National Laboratories
Albuquerque, New Mexico 87185 and Livermore, California 94550

Sandia is a multiprogram laboratory operated by Sandia Corporation, a Lockheed Martin Company, for the United States Department of Energy under Contract DE-AC04-94AL85000.

Issued by Sandia National Laboratories, operated for the United States Department of Energy by Sandia Corporation.

Available to DOE and DOE contractors from
U.S. Department of Energy
Office of Scientific and Technical Information
P.O. Box 62
Oak Ridge, TN 37831

Telephone: (865)576-8401
Facsimile: (865)576-5728
E-Mail: reports@adonis.osti.gov
Online ordering: http://www.doe.gov/bridge

Available to the public from
U.S. Department of Commerce
National Technical Information Service
5285 Port Royal Rd
Springfield, VA 22161

Telephone: (800)553-6847
Facsimile: (703)605-6900
E-Mail: orders@ntis.fedworld.gov
Online order: http://www.ntis.gov/ordering.htm

SAND 2001-3397
Unlimited Release
Printed November 2001

Functional Materials for Microsystems: Smart Self-Assembled Photochromic Films: Final Report

A. R. Burns, D. Y. Sasaki, R. W. Carpick*, J. A. Shelnutt
Biomolecular Materials and Interfaces Dept.

C. J. Brinker
Materials Chemistry Dept.

Sandia National Laboratories
P. O. Box 5800
Albuquerque, NM 87185-1413

*Present address: Dept. of Engineering Physics
University of Wisconsin
Madison, WI 53706

ABSTRACT

This project set out to scientifically-tailor "smart" interfacial films and 3-D composite nanostructures to exhibit photochromic responses to specific, highly-localized chemical and/or mechanical stimuli, and to integrate them into optical microsystems. The project involved the design of functionalized chromophoric self-assembled materials that possessed intense and environmentally-sensitive optical properties (absorbance, fluorescence) enabling their use as detectors of specific stimuli and transducers when interfaced with optical probes. The conjugated polymer polydiacetylene (PDA) proved to be the most promising material in many respects, although it had some drawbacks concerning reversibility. Throughout his work we used multi-task scanning probes (AFM, NSOM), offering simultaneous optical and interfacial force capabilities, to actuate and characterize the PDA with localized and specific interactions for detailed characterization of physical mechanisms and parameters. In addition to forming high quality mono-, bi-, and tri-layers of PDA *via* Langmuir-Blodgett deposition, we were

successful in using the diacetylene monomer precursor as a surfactant that directed the self-assembly of an ordered, mesostructured inorganic host matrix. Remarkably, the diacetylene was polymerized in the matrix, thus providing a PDA-silica composite. The inorganic matrix serves as a perm-selective barrier to chemical and biological agents and provides structural support for improved material durability in microsystems. Our original goal was to use the composite films as a direct interface with microscale devices as optical elements (e.g., intracavity mirrors, diffraction gratings), taking advantage of the very high sensitivity of device performance to real-time dielectric changes in the films. However, our optical physics colleagues (M. Crawford and S. Kemme) were unsuccessful in these efforts, mainly due to the poor optical quality of the composite films.

Table of Contents

1. Summary of accomplishments

The ability of certain organic molecules to form densely-packed and even self-organized films at surfaces and interfaces provides systems whose chemical, structural, and mechanical properties can be controlled for specific applications. For example, functionalized organic thin films can produce optical responses to specific molecular recognition events, thus providing molecular sensing capabilities. The optical response of these films is often due to molecular rearrangements or stresses on the chromophoric element. A detailed understanding of the response of such molecules to applied stresses is necessary for further development of these unique sensing materials. The family of polydiacetylenes (PDAs) is of particular interest as these molecules exhibit strong optical absorption and fluorescence properties that can dramatically change with applied stress (*mechanochromism*). PDAs exhibit chromatic transitions in response to other stimuli, including heat (*thermochromism*), changes in chemical environment such as pH, and binding of specific biological targets (*affinochromism/biochromism*). In general, the observed transition involves a significant shift in absorption from low to high energy bands of the visible spectrum, thus the PDA appears to transform from a blue to a red color. In addition, the red form is highly fluorescent, while the blue form is not. As will be shown here, fluorescence intensity is a sensitive gauge of the color transition.

Preparation of PDA films

We use Langmuir-Blodgett techniques for the formation of mono- and trilayer films of polydiacetylenes. The amphiphile monomers are polymerized at the air-water interface on a pure water subphase. The blue or red films are subsequently transferred onto mica, silicon, or glass substrates using a horizontal deposition technique to capture innate features in the polymerized films. A carboxylic acid functionalized amphiphile, 10,12-pentacosadiynoic acid (PCA), unstable on a pure water subphase as a monolayer, forms a stable trilayer that is readily polymerized and deposited onto substrates. Stable polydiacetylene monolayer structures could

be prepared in the absence of salts using an ethanolamido functionalized analog of PCA, N-(2-ethanol)-10,12-pentacosadiynamide (PCEA). The amide functionality provided some stabilization of the monolayer through lateral intermolecular hydrogen bonded networks at the headgroup position. Highly oriented, crystalline-like polydiacetylene mono- and tri-layer films of PCA and PCEA respectively, were been prepared in both blue and red forms. Due to the stiffness of the polymerized films, orientation of the substrate, and mild conditions of the deposition we believe the features in the film to be identical to those formed on the air-water interface. AFM images of the deposited films reveal highly oriented nano-scale features that extend for tens to hundreds of micrometers within a discrete domain for both monolayer and trilayer structures. A complete report on LB film preparation is found under the section "High molecular orientation in mono- and tri-layer polydiacetylene films imaged by atomic force microscopy."

Scanning probe induced mechanochromism

The exact mechanism(s) driving the various chromatic transitions are not fully understood. In general, it is believed that molecular conformational changes, such as side chain ordering and orientation, impart stresses that lead to different backbone conformation, thus changing the electronic states and the corresponding optical absorption. It is also not established whether the blue-to-red transition is a continuous transition, or a discrete transition between two states separated by an energy barrier. The factors governing the degree of reversibility of the transition are also not understood. To better understand these chromatic transitions in general, and mechanochromism in particular, we embarked on scanning probe microscopy (SPM) studies of PDA thin films. A SPM tip can be thought of as both an imaging probe and a localized stress actuator. With the appropriate tip structure and using low applied loads, the SPM tip forms a nanometer-scale single asperity contact point with a flat sample. Depending on the specific SPM instrument (as described below), the tip can be used to measure the sample's topographic, frictional, and/or optical responses. Using these tools with PDA samples, we have obtained the first observation of mechanochromism at the nanometer scale.

In our paper "First observation of mechanochromism at the nanometer scale," we discuss the blue-to-red chromatic transition of a trilayer polydiacetylene thin film that is induced by a nanometer-scale probe tip. Shear forces between the tip and PDA molecules in the blue phase create nanometer-scale red domains that preferentially nucleate at film defects and propagate along the polymer backbone. The transition is irreversible and appears to be discrete. Significant displacement of the PDA molecules is observed within the red domains. Removal of the uppermost bilayer appears to be correlated with the transition, where the remaining monolayer exists in the red phase. The transition is reproducibly observed with both AFM and NSOM probe tips. The rate of domain formation increases with applied load and hence with higher shear forces and is favored when shear forces are applied perpendicular to the backbones. The shear force-induced transition is consistent with models that invoke side-chain rotation about the conjugated backbone.

The first study of mechanochromism was restricted to trilayers, since LB monolayers of the 10,12-pentacosadiynoic acid monomer precursor are not stable on a pure water subphase. We found that the shear-induced blue-to-red transformations were complicated by the removal of the top bilayer, revealing an seemingly "flattened" monolayer underneath. Thus molecular-scale aspects of conformation changes in the transformation were obscured by the trilayer geometry. It became clear that stable monolayer films were required to simplify characterization of the transformation. Since then, we have been able to produce stable monolayers by synthesizing the monomer N-(2-ethanol)-10,12-pentacosadinamide. Thus in a subsequent paper, "Shear-induced mechanochromism in polydiacetylene monolayers," we find explicit evidence that the irreversible blue-to-red transformation is caused by shear forces exerted normal to the polydiacetylene polymer backbone. The anisotropic probe-induced transformation is characterized by a significant change in the tilt orientation of the side chains with respect to the surface normal. We also perform preliminary molecular dynamics simulations and electronic structure calculations on 12-unit polydiacetylene oligomers that allow us to correlate the transformation with bond-angle changes in the conjugated polymer backbone. So far, we find that dihedral angle deviations from the blue planar form must be in the range of 40°-60°, every

six units, in order to see shifts in the absorption spectra that compare with those observed experimentally.

Friction anisotropy of PDA monolayers

Fundamental studies of friction at the atomic or molecular level have revealed dependence upon sliding velocity and direction. The dependence of friction upon sliding direction arises from structural properties of the materials in contact. As such, friction measurements can reveal specific structural properties, such as molecular or crystallographic orientation, which may not be seen in topographic images. Such experiments can then elucidate how friction is fundamentally related to these structural properties. In our paper "Large friction anisotropy of a polydiacetylene monolayer, " friction force microscopy measurements of a PDA monolayer film reveal a 300% friction anisotropy that is correlated with the film structure. The film consists of a monolayer of the red form of N-(2-ethanol)-10,12 pentacosadiynamide, prepared on a Langmuir trough and deposited on a mica substrate. As confirmed by atomic force microscopy and fluorescence microscopy, the monolayer consists of domains of linearly oriented conjugated backbones with pendant hydrocarbon side chains above and below the backbones. Maximum friction occurs when the sliding direction is perpendicular to the backbones. We propose that this effect is due to anisotropic film stiffness, which is a result of anisotropic side chain packing and/or anisotropic stiffness of the backbone itself. Friction anisotropy is therefore a sensitive, optically-independent indicator of polymer backbone direction and monolayer structural properties

Thermochromism of PDA films

In the paper "Spectroscopic ellipsometry and fluorescence study of thermochromism in an ultrathin polydiacetylene film…," we investigated the thermochromic transition of a trilayer PDA film organized into crystalline domains on a silicon substrate. Spectroscopic ellipsometry and fluorescence intensity measurements are obtained with *in-situ* temperature control. PDA films exhibit a reversible thermal transition between the initial blue form and an intermediate

"purple" form that exists only at elevated temperature (between 303 – 333 K), followed by an irreversible transition to the red form after annealing above 320 K. We propose that the purple form is thermally distorted blue poly-PCDA, and may represent a transitional configuration in the irreversible conversion to red. This hypothesis is supported by the appearance of unique features in the absorption spectra for each form as derived from the ellipsometry measurements. Significant fluorescence emission occurs only with the red form, and is reduced at elevated temperatures while the absorption remains unchanged. Reduced emission is likely related to thermal fluctuations of the hydrocarbon side chains. Time-resolved fluorescence measurements of the irreversible transition have been performed. Using a first-order kinetic analysis of these measurements we deduce an energy barrier of 17.6±1.1 kcal mol^{-1} between the blue and red forms.

PDA/silica nanocomposites

Composite architectures composed of hard and soft materials can provide both useful functionality and mechanical integrity. In our paper "Self-assembly of mesoscopically ordered chromatic polydiacetylene/silica nanocomposites," we report the self-assembly of conjugated polymer/silica nanocomposite films with hexagonal, cubic, or lamellar mesoscopic order using polymerizable amphiphilic diacetylene molecules as both structure-directing agents and monomers. The self-assembly procedure is rapid and incorporates the organic monomers uniformly within a highly ordered, inorganic environment. Polymerization results in polydiacetylene (PDA)/silica nanocomposites that are optically transparent and mechanically robust. Compared to the corresponding ordered, diacetylene-containing films prepared as Langmuir monolayers or by Langmuir-Blodgett deposition the nanostructured inorganic host alters the diacetylene polymerization behavior, and the resulting nanocomposite exhibits unique thermo-, mechano-, and solvato-chromic properties. We believe self-assembly to be an efficient, general approach to the formation of conjugated polymer/inorganic nanocomposites, wherein the inorganic framework serves to protect, stabilize, and orient the polymer, mediate its

performance, and provide sufficient mechanical integrity to enable integration into devices and microsystems.

Microsystem Optical Platforms

Due to poor film quality of the PDA/silica nanocomposites and background fluorescence in LB films, progress was limited in implementing PDA films as sensors in micro-optical systems. Optical sensitivity of the films as they undergo the blue-red phase transformation in response to external perturbations is enhanced by the observation that the blue form does not fluoresce, whereas the red form does. Thus our goal was to quantitatively determine the dynamic range of fluorescence as the films underwent the transformation. Starting with blue phase films, red phase regions were patterned with a 10 minute deep UV exposure through a photomask. With 1 mW 488 nm excitation, we were surprised to discover that the excitation itself had a strong effect on the blue regions: a 5 minute exposure increased the fluorescence intensity by a factor of approximately 8. Red phase regions were unaffected by laser exposure. Since the blue-red conversion occurs thermally at >60° C, we do not think this effect is due to laser heating. However, our results suggest that care must be taken to use very low powers or short exposure times in any fluorescence-based sensor using these films. When we excited the films for short exposure times (10 seconds), there was no detectable change in the blue phase film's fluorescence with multiple exposures. Under these conditions, the red phase regions had only a 28X increase in fluorescence intensity over the blue phase. This is a poor dynamic range, and suggests that during initial polymerization some red phase regions were created, thereby giving the "blue" film a significant amount of fluorescence.

Journal of Colloid and Interface Science 229, 490–496 (2000)
doi:10.1006/jcis.2000.7043, available online at http://www.idealibrary.com on IDEAL®

High Molecular Orientation in Mono- and Trilayer Polydiacetylene Films Imaged by Atomic Force Microscopy

Darryl Y. Sasaki,[1] Robert W. Carpick,[2] and Alan R. Burns

Biomolecular Materials and Interface Science Department, Sandia National Laboratories, Albuquerque, New Mexico 87185–1413

Received December 22, 1999; accepted June 12, 2000

Atomically flat monolayer and trilayer films of polydiacetylenes have been prepared on mica and silicon using a horizontal deposition technique from a pure water subphase. Langmuir films of 10,12-pentacosadiynoic acid (I) and *N*-(2-ethanol)-10,12-pentacosadiynamide (II) were compressed to 20 mN/m and subsequently polymerized by UV irradiation at the air–water interface. Blue and red forms of the films were prepared by varying exposure times and incident power. Polymerization to the blue-phase films produced slight contractions of 2 and 5% for the films of II and I, respectively. Longer UV exposures yielded red-phase films with dramatic film contraction of 15 and 32% for II and I, respectively. The horizontal deposition technique provided transfer ratios of unity with minimal film stress or structure modification. Atomic force microscopy images revealed nearly complete coverage of the substrate with atomically flat films. Crystalline domains of up to 100 micrometers of highly oriented polydiacetylene molecules were observed. The results reported herein provide insight into the roles of molecular packing and chain orientations in converting the monomeric film to the polymerized blue and red phases.

Key Words: polydiacetylene; Langmuir films; AFM; horizontal deposition; molecular orientation.

INTRODUCTION

Polymerization of oriented mono- and multilayer structures containing diacetylene functionality has produced an assortment of colored, robust, highly oriented, and environmentally responsive films (1). These two-dimensional polydiacetylene films, where the conjugation runs parallel to the film surface, have been prepared as Langmuir monolayers (2), Langmuir–Blodgett (LB) multilayer films (3), bilayer systems (4), and self-assembled monolayers (SAM) (5). Numerous applications for these films have been explored, including biomimetic surfaces for protein studies (6), biosensors (7), NLO materials (8), and biomineralization templates (9).

These materials exhibit high structural order in the many different forms yielding colored films that range from blue to red. The color of each material results from the conformation of the conjugated backbone. The conformation is in turn affected by the orientation and packing of the hydrocarbon side chains pendant to the backbone that can either alter the length or change the mode of π conjugation (10). A variety of analytical techniques, such as electron diffraction (11), Fourier transform infrared spectroscopy (12), resonance Raman (13), and fluorescence polarization (14), have been employed to identify the molecular orientation of the side chains and backbones.

Recently, atomic force microscopy (AFM) has been used to image polydiacetylene films at the nanometer scale to evaluate film structure based on topography (15), friction anisotropy (16), and surface features (12, 17, 18). Although the technique is quite powerful, the images reveal a wide range in film quality. Previous work involving LB films of polydiacetylenes required the use of metal ion salts (e.g., $CdCl_2$, $CaCl_2$) to stabilize the carboxylic acid headgroups for deposition of the monolayer (3, 18, 19). The use of metal ion salts, however, can complicate the structures by either altering molecular orientation through metal ion chelation (14, 20) or by depositing salt crystals in or on the LB film.

In this paper, we will describe the formation of mono- and trilayer films of polydiacetylenes polymerized at the air–water interface on a pure water subphase. The colored films were subsequently transferred onto mica, silicon, or glass substrates using a horizontal deposition technique to capture innate features in the polymerized films. For the carboxylic acid functionalized amphiphile, 10,12-pentacosadiynoic acid (**I**), a stable trilayer structure was prepared on the pure water subphase through overcompression of the monolayer. Stable monolayers of **I** could not be obtained in the absence of metal ion salts. Stable polydiacetylene monolayers could, however, be prepared in the absence of salts using an ethanolamido functionalized analog of **I**, *N*-(2-ethanol)-10,12-pentacosadiynamide (**II**) (Scheme 1). The amide functionality adds stability to the monolayer through lateral intermolecular hydrogen-bonded networks at the headgroup position. The deposited films were subsequently characterized with AFM and fluorescence microscopy to reveal highly oriented crystalline-like domains that extend for tens to hundreds of micrometers for both monolayer and trilayer films. Film shrinkage and changes in film height upon UV-induced polymerization indicated a reorganization of the alkyl side chains as the film transitions from the blue to red phase.

[1] To whom correspondence should be addressed. Fax: (505) 844–5470. E-mail: dysasak@sandia.gov.

[2] Present address: Department of Engineering Physics, University of Wisconsin–Madison, 1500 Engineering Drive, Madison, WI 53706.

0021-9797/00 $35.00

for the blue films of both **I** and **II**, only a few small ($<1\ cm^2$) film fragments would break off and transfer onto the substrate (4×2.5 cm). Because of the crystalline-like structure of the blue films, the total area would remain constant at a pressure of 20 mN/m, but a visible hole in the film would persist where the transfer took place. Unlike the homogeneously continuous and stiff blue-phase films, the red-phase films had visible cracks throughout. This allowed the film to compress with vertical deposition so that film transfer was significantly improved. However, even in this case the transfer was less than 70% and the film exhibited oriented features induced from the transfer process.

To capture the innate features of the polymerized films on the pure water subphase, as well as achieving high transfer ratios, a horizontal deposition method was employed. Substrates were situated on a support at a depth of 1–2 mm below the air–water interface and oriented plane-parallel to the surface. Following UV exposure, the film was transferred onto the solid substrate by lowering the water level by aspiration. Once the film draped over the substrate, excess film was removed from the outside edges of the substrate using the aspirator. The substrate was removed and the trapped water between the film and substrate was allowed to evaporate in clean-room air. Visual inspection indicated no macroscopic changes in the transferred blue- and red-phase films relative to their appearance on the air–water interface.

UV–vis spectra of the polydiacetylene films were typical of blue- and red-phase forms. Figure 3 displays the absorption spectra of poly(**I**) trilayer films after 30 s at 40 $\mu W/cm^2$ (blue-phase) and one after a 5-min exposure at 500 $\mu W/cm^2$ (red-phase). Poly(**II**) monolayer films gave nearly identical spectra although with about 70% less intensity, as would be expected for a sample one-third the thickness of the poly(**I**) trilayer.

AFM images of the blue- and red-phase forms of poly(**I**) and poly(**II**) on mica are shown in Fig. 4. The coverage for all films was nearly uniform for the entire mica substrate. The topographic images in Fig. 4 are of areas with cracks or defects in the film to allow for some contrast. Over 95% of the transferred film was flat to within 2–3 Å with up to 100-μm crystalline-like domains observed. Films produced on silicon substrates with both native and thermally grown oxide possessed the same quality.

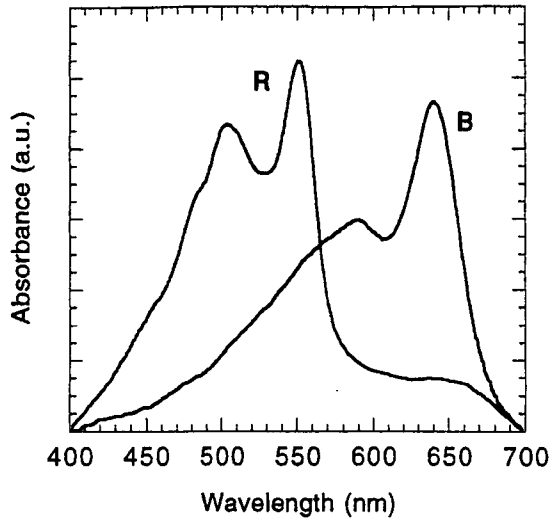

FIG. 3. UV–vis absorption spectra of blue-phase (B) and red-phase (R) poly(**I**) trilayer films deposited on glass substrates.

The choice of a pure water subphase was a result of our initial attempts to prepare mono- and multilayer films using metal ion salts of **I**. $CdCl_2$ and $CaCl_2$ salts, at concentrations from 1 μM to 3 mM, were used in the subphase to prepare stable monolayers of **I**. Following both vertical and horizontal deposition, AFM images revealed micrometer-scale salt crystals dispersed throughout the samples. An example of such an image is shown in Fig. 5. It was clear that such contaminated films would not be amenable to any molecular level studies, not only because of the surface roughness produced by the crystallites, but also from their effects on the chromatic molecular actuation of the film (15).

The 50-μm images of the films formed on pure water subphase show overall polydiacetylene morphology and film structure (Fig. 4). For the blue-phase film of **I**, square edges and straight-line cracks were observed giving the film a crystalline-like morphology (Fig. 4A). In the red-phase films of **I** (Fig. 4B), straight-line cracks were also observed, but not always with square edges. Some curved cracks were also present. The increased number of cracks compared with the blue-phase films was coincident with the film contraction that was observed on the trough.

Polarized fluorescence microscopy of the red films has shown that the polydiacetylene backbones in a single domain are highly oriented (15). By setting the analyzing polarizers at 90° to the backbone direction the emission of a given trilayer domain could be extinguished by a factor of at least 100. This confirms that the conjugated backbones within each domain are highly ordered and that there is structural registry between the three layers of the red phase of **I**. Thus, the crystallinity of the domains exists not only parallel to the substrate, but normal to it as well. Similarly, high polarization contrast was also observed for fluorescence from the red-phase film of **II**, indicating that the backbones are also highly oriented in the monolayer. AFM imaging also confirms the presence of straight-line cracks in films of **II** (Figs. 4C and 4D), although far fewer cracks are observed than with films of **I**. These results indicate a high degree of crystalline ordering in all films.

AFM imaging could also resolve structural differences between the blue- and red-phase films of both **I** and **II**. Distinct height differences (relative to bare substrate) between the blue- and red-phase trilayer stacks of poly(**I**) were measured at 7.4 ± 0.8 and 9.0 ± 0.9 nm, respectively. Similarly, the blue- and red-phase poly(**II**) monolayer films exhibited proportional height differences of 2.7 ± 0.3 and 3.1 ± 0.3 nm, respectively.

Figure 6 shows higher resolution views of the blue-phase films for **I** and **II** revealing the molecular orientation and highly regular structures within the materials. We have previously determined that the striated patterns observed in Fig. 6 run

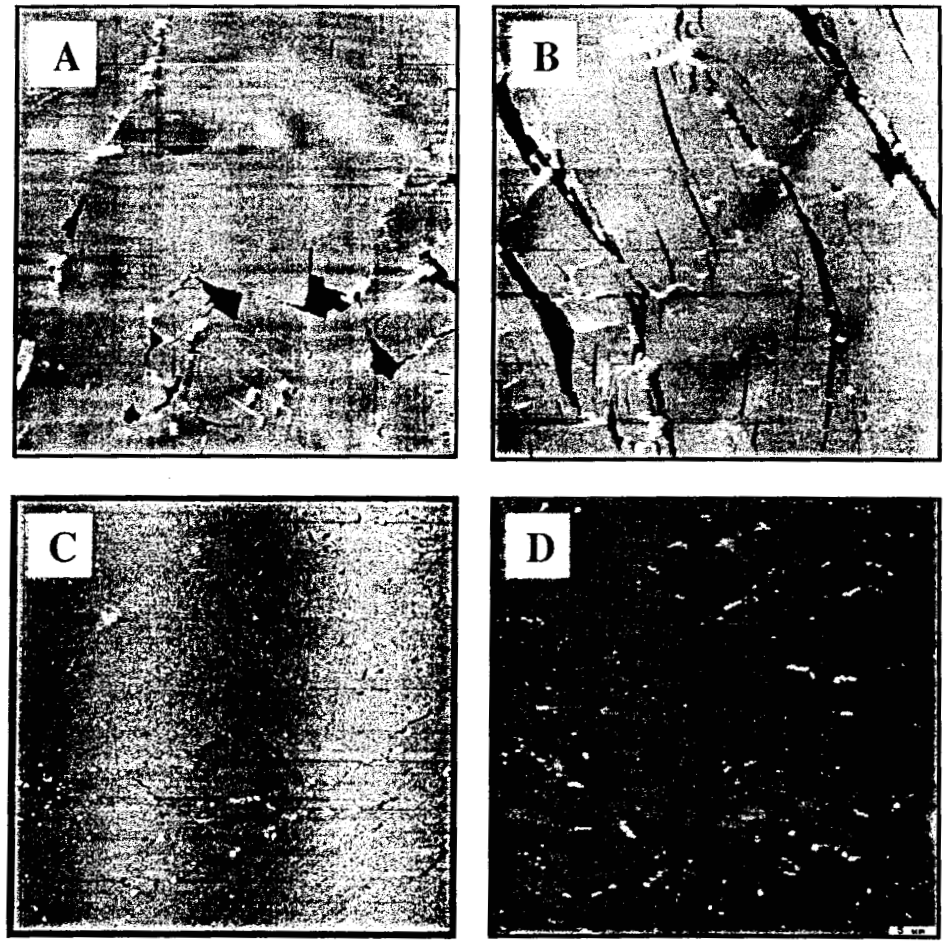

FIG. 4. 50-μm topographic AFM images of poly(**I**) in the blue phase (A) and red phase (B) and poly(**II**) in the blue phase (C) and red phase (D) on mica.

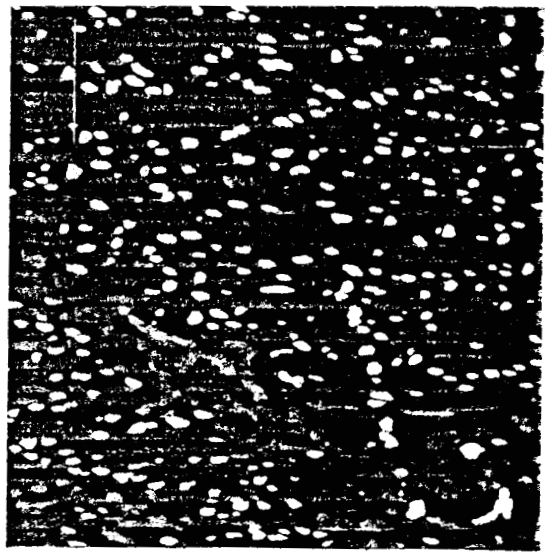

FIG. 5. 50-μm topographic AFM image of horizontally deposited poly(**I**) monolayer from an aqueous 1 mM $CdCl_2$ subphase on mica. Numerous micron scale crystallites (white dots) cover the surface.

parallel to the polydiacetylene backbone (15, 16). Each defined line feature was 10–20 nm wide, indicating that a set of 20–40 polymers created a single feature. The height contrast was ~0.2 nm. The origin of these features is not fully understood. It is possible that they arise from slightly different packing densities of groups of neighboring backbones. In any event, this topographic contrast clearly reveals the highly oriented nature of the backbones within each domain. In addition, we have obtained preliminary AFM images revealing molecular lattice resolution, similar to more detailed results of Lio *et al.* (12). With such highly oriented films, nanometer-scale structures can be readily and reproducibly imaged. The high quality of these films has allowed us to observe dramatic properties such as nanometer scale conversion from blue to red by mechanical stress (15) and strong friction anisotropy (16).

These results provide insight into the possible molecular orientation of diacetylene films as they convert from monomeric to blue- and red-phase polymer structures. The headgroup interactions and alkyldiyne chain stacking should dominate the film structure of the monomeric diacetylene Langmuir films. The ability of the amide headgroup of **II** to form intermolecular hydrogen-bonded structures (Fig. 7), similar to β-sheets in

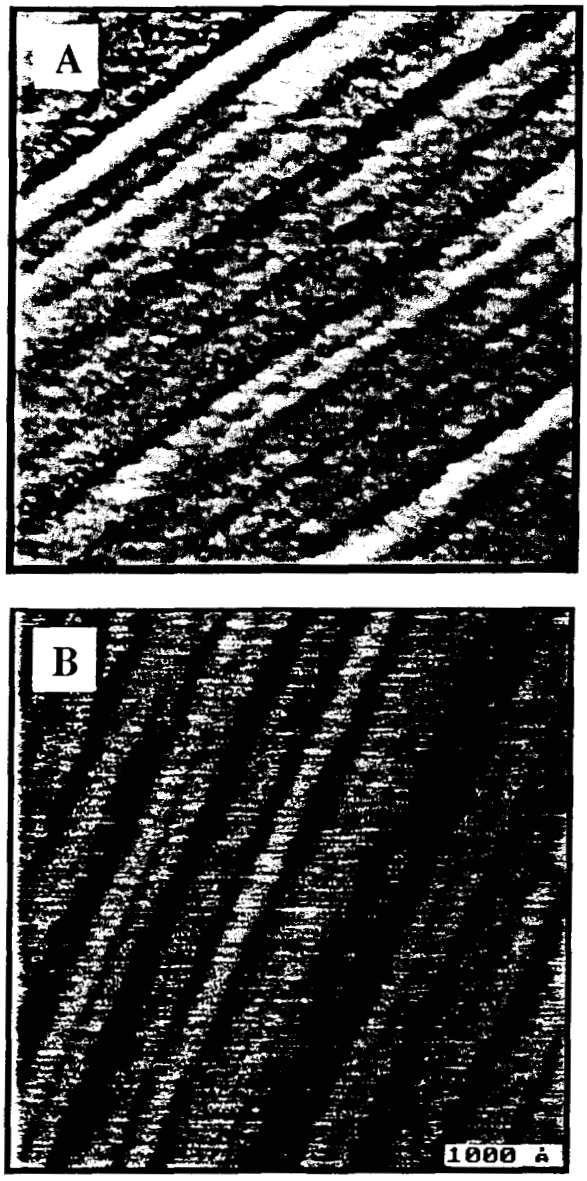

FIG. 6. High-resolution 1-μm-scale topographic AFM image of blue-phase poly(**I**) (A) and poly(**II**) (B) showing highly oriented film structure (on mica). The height contrast of the striations is 0.2 nm.

proteins, may explain the stability of this monolayer film on pure water. **I** films on a pure water subphase, on the other hand, are unstable as monolayers but stack favorably into trilayer structures. Carboxylic acid dimer formation may aid in stabilizing the structure (Fig. 7). Indeed, stable bilayer islands are commonly observed on top of the **I** trilayer.

The high registry of the diacetylene packing permits rapid topochemical polymerization of the diyne monomers to the ene-yne conjugation upon UV illumination, resulting in the blue-phase polydiacetylene. Little change in the amphiphile packing, and thus little reorientation of the alkyl side chains occurs, as evidenced by the minimal contraction of the film (Table 1). However, the hybridization change from sp to sp^2 for the terminal alkyne carbons creates a stress on the polymer as a result of the 180° to 120° bond angle conversion (see Fig. 7) (22). At low polymer conversion the conformational stress may be alleviated through the flexibility of neighboring monomeric or low molecular weight polydiacetylene chains. However, as the degree of polymerization of the polydiacetylene increases with UV illumination, the overall molecular stress in the film continues to increase. At some high degree of polymerization the film's original structure breaks down as the alkyl chains of the blue-phase

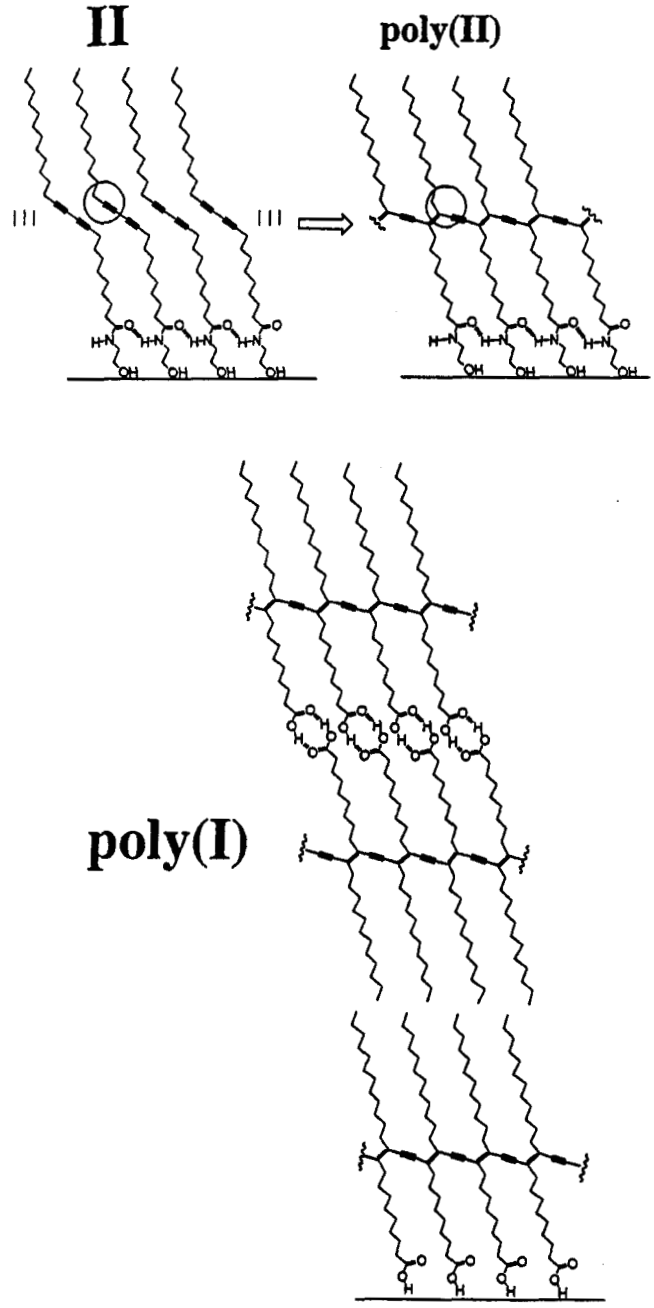

FIG. 7. Schematic of molecular orientation of **II** and its subsequent conversion to poly(**II**) upon UV irradiation (above). A hybridization change going from the diyne to ene-yne arrangement is circled to show the 180° to 120° bond angle conversion. A hydrogen-bonded network at the headgroup position is also drawn for the film of **II**. Below is a illustration of poly(**I**) in its trilayer form.

polymer reorganize to accommodate the bond angle conversion, yielding a closer packing (film contraction) and reorientation (vertical height enhancement) of the alkyl chains. This reorganization, although thermodynamically more stable, produces a loss of π conjugation and results in the red form of the polydiacetylene (13, 19, 23). We are currently investigating the alkyl side chain reorientation by coupling molecular modeling with experimental studies to further understand the color transitions and modes of actuation of these films.

CONCLUSION

Highly oriented, crystalline-like polydiacetylene mono- and trilayer films of **II** and **I**, respectively, have been prepared in both blue and red forms using a horizontal deposition technique from a pure water subphase. Due to the stiffness of the polymerized films, orientation of the substrate, and mild conditions of the deposition, we believe the features in the film to be identical to those formed on the air–water interface. AFM imaging showed nanometer-scale striations in the films that extended throughout crystalline-like domains that reached 100-μm. Through the observed contractions in the films on the air–water interface upon conversion from monomeric to blue phase and then to red-phase polydiacetylene, and AFM height measurements of those films, it appears that significant and spontaneous reorganization of the films occurs during UV illumination involving reorientation of alkyl chains. These molecularly flat films have allowed us to investigate chromatic transitions of polydiacetylene at the nanometer level.

ACKNOWLEDGMENTS

We thank Dr. Mary Crawford for the power measurement readings of the UV pen lamps, and Dr. Seema Singh for the AFM image of Fig. 5. R.W.C. acknowledges the support of the Natural Sciences and Engineering Research Council of Canada. Sandia is a multiprogram laboratory operated by Sandia Corporation, a Lockheed Martin Company, for the United States Department of Energy under Contract DE-AC04-94AL85000.

REFERENCES

1. Bloor, D., and Chance, R. R., "Polydiacetylenes," Nijhoff, Boston, 1985.
2. Wilson, T. E., and Bednarski, M. D., *Langmuir* **8,** 2361 (1992).
3. Kuriyama, K., Kikuchi, H., and Kajiyama, T., *Langmuir* **12,** 6468 (1996).
4. Charych, D. H., Nagy, J. O., Spevak, W., and Bednarski, M. D., *Science* **261,** 585 (1993).
5. Kim, T., Chan, K. C., and Crooks, R. M., *J. Am. Chem. Soc.* **119,** 189 (1997).
6. Bader, H., van Wagenen, R., Andrade, J. D., and Ringsdorf, H., *J. Colloid Interface Sci.* **101,** 246 (1984).
7. Charych, D., and Nagy, J. O., *Chem.- Tech.* **26,** 24 (1996).
8. Sarkar, A., Okada, S., Nakanishi, H., and Matsuda, H., *Macromolecules* **31,** 9174 (1998).
9. Litvin, A. L., Samuelson, L. A., Charych, D. H., Spevak, W., and Kaplan, D. L., *J. Phys. Chem.* **99,** 12065 (1995).
10. Rughooputh, S. D. D. V., Bloor, D., Phillips, D., Jankowiak, R., Schütz, L., and Bässler, H., *Chem. Phys.* **125,** 355 (1988).
11. Day, D., and Lando, J. B., *Macromolecules* **13,** 1483 (1980).
12. Lio, A., Reichert, A., Ahn, D. J., Nagy, J. O., Salmeron, M., and Charych, D. H., *Langmuir* **13,** 6524 (1997).
13. Saito, A., Urai, Y., and Itoh, K., *Langmuir* **12,** 3938 (1996).
14. Miyano, K., and Mori, A., *Thin Solid Films* **168,** 141 (1989).
15. Carpick, R. W., Sasaki, D. Y., and Burns, A. R., *Langmuir* **16,** 1270 (2000).
16. Carpick, R. W., Sasaki, D. Y., and Burns, A. R., *Tribology Lett.*, in press.
17. Marti, O., Ribi, H. O., Drake, B., Albrecht, T. R., Quate, C. F., and Hansma, P. K., *Science* **239,** 50 (1988).
18. Sheth, S. R., and Leckband, D. E., *Langmuir* **13,** 5652 (1997).
19. Collins, M., *J. Poly. Sci. B Polym. Phys.* **26,** 367 (1988).
20. Day, D., and Ringsdorf, H., *J. Polym. Sci. Poly. Lett.* **16,** 205 (1977).
21. Wilson, T. E., Spevak, W., Charych, D. H., and Bednarski, M. D., *Langmuir* **10,** 1512 (1994).
22. Menzel, H., Mowery, M. D., Cai, M., and Evans, C. E., *J. Phys. Chem. B* **102,** 9550 (1998).
23. Tomioka, Y., Tanaka, N., and Imazeki, S., *J. Chem. Phys.* **91,** 5694 (1989).

First Observation of Mechanochromism at the Nanometer Scale

R. W. Carpick, D. Y. Sasaki, and A. R. Burns*

Sandia National Laboratories, Nanomolecular Materials and Interfaces Department, Albuquerque, New Mexico 87185-1413.

Received June 3, 1999. In Final Form: September 9, 1999

A mechanically induced color transition ("mechanochromism") in poly(diacetylene) thin films has been generated at the nanometer scale using the tips of two different scanning probe microscopes. A blue-to-red chromatic transition in poly(diacetylene) molecular trilayer films, polymerized from 10,12-pentacosadiynoic acid (poly-PCDA), was found to result from shear forces acting between the tip and the poly-PCDA molecules, as independently observed with near-field scanning optical microscopy and atomic force microscopy (AFM). Red domains were identified by a fluorescence emission signature. Transformed regions as small as 30 nm in width were observed with AFM. The irreversibly transformed domains preferentially grow along the polymer backbone direction. Significant rearrangement of poly-PCDA bilayer segments is observed by AFM in transformed regions. The rearrangement of these segments appears to be a characteristic feature of the transition. To our knowledge, this is the first observation of nanometer-scale mechanochromism in any material.

Introduction

The ability of certain organic molecules to form densely packed and even self-organized films at surfaces and interfaces provides systems whose chemical, structural, and mechanical properties can be controlled for specific applications. For example, functionalized organic thin films can produce optical responses to specific molecular recognition events, thus providing molecular sensing capabilities.[1] The optical response of these films is often due to molecular rearrangements or stresses on the chromophoric element. A detailed understanding of the response of such molecules to applied stresses is necessary for further development of these unique sensing materials. Although scanning probe microscopy (SPM) has been previously used to examine the structure of a wide variety of organic films, we will discuss the first effort to induce color changes in an organic film with SPM probes.

The family of poly(diacetylene)s (PDAs) is of particular interest as these molecules exhibit strong optical absorption and fluorescence properties that can dramatically change with applied stress (*mechanochromism*).[2−4] PDAs exhibit chromatic transitions in response to other stimuli, including heat (*thermochromism*),[5,6] changes in chemical environment such as pH,[7,8] and binding of specific biological targets (*affinochromism / biochromism*).[1,9,10] The reversibility of this transition has been observed to depend on the specific PDA structure and the environmental stimulus. In general, the observed transition involves a significant shift in absorption from low- to high-energy bands of the visible spectrum; thus, the PDA appears to transform from a blue to a red color. In addition, the red form is highly fluorescent, while the blue form is not. As will be shown here, fluorescence intensity is a sensitive gauge of the color transition. This transition, along with

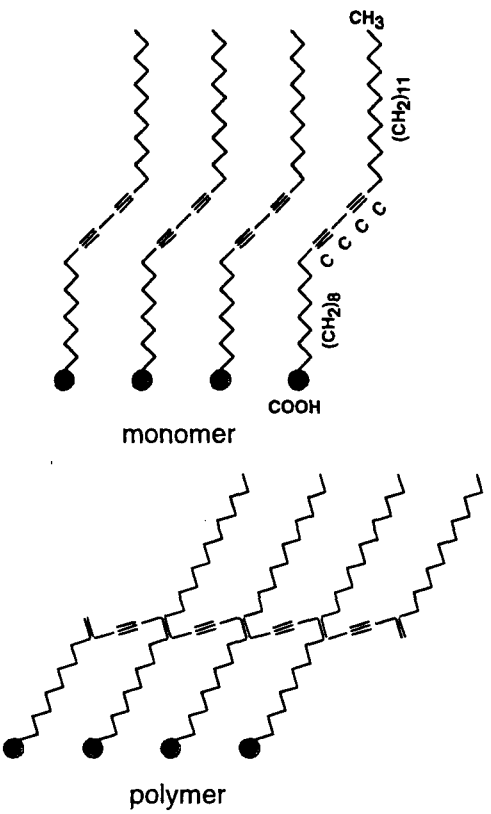

Figure 1. (a) Monomeric and (b) polymeric forms of PCDA. The linear π-conjugated backbones connect neighboring molecules and are oriented parallel to the substrate.

* Corresponding author. E-mail: aburns@sandia.gov. Tel: 505-844-9642. Fax: 505-844-5470.

(1) Charych, D. H.; Nagy, J. O.; Spevak, W.; Bednarski, M. D. *Science* **1993**, *261*, 585.
(2) Muller, H.; Eckhardt, C. J. *Mol. Cryst. Liq. Cryst.* **1978**, *45*, 313.
(3) Nallicheri, R. A.; Rubner, M. F. *Macromolecules* **1991**, *24*, 517.
(4) Tomioka, Y.; Tanaka, N.; Imazeki, S. *J. Chem. Phys.* **1989**, *91*, 5694.
(5) Wenzel, M.; Atkinson, G. H. *J. Am. Chem. Soc.* **1989**, *111*, 6123.
(6) Lio, A.; Reichert, A.; Ahn, D. J.; Nagy, J. O.; Salmeron, M.; Charych, D. H. *Langmuir* **1997**, *13*, 6524.
(7) Cheng, Q.; Stevens, R. C. *Langmuir* **1998**, *14*, 1974.
(8) Jonas, U.; Shah, K.; Norvez, S.; Charych, D. H. *J. Am. Chem. Soc.* **1999**, *121*, 4580.
(9) Reichert, A.; Nagy, J. O.; Spevak, W.; Charych, D. *J. Am. Chem. Soc.* **1995**, *117*, 829.
(10) Charych, D.; Cheng, Q.; Reichert, A.; Kuziemko, G.; Stroh, M.; Nagy, J. O.; Spevak, W.; Stevens, R. C. *Chem. Biol.* **1996**, *3*, 113.

10.1021/la990706a CCC: $19.00
Published on Web 02/01/2000

other properties, such as strong third-order nonlinear susceptibility[11] and unique photoconduction properties,[12] all attributed to the conjugated PDA backbone (Figure 1), have generated substantially wide interest in PDAs.

Mechanochromism has only been observed in a few instances at macroscopic scales. Müller and Eckhardt observed an irreversible transition in a PDA single crystal induced by compressive stress,[2] which resulted in coexisting blue and red phases. Nallicheri and Rubner[3] observed reversible mechanochromism for conjugated PDA chains embedded in a host elastomer that was subjected to tensile strain. Tomioka et al. induced reversible chromism by varying the lateral surface pressure of a PDA monolayer on the surface of water in a Langmuir–Blodgett trough,[4] with the red form present at higher (compressive) surface pressures. These macroscopic studies of mechanochromism have so far not examined molecular-level structural changes associated with the observed transitions.

The present experiments were conducted using the PDA formed from 10,12-pentacosadiynoic acid (PCDA) monomers (Figure 1). Topochemical polymerization of the monomers was accomplished through UV irradiation of the monomers in a Langmuir film.[13] Optical absorption occurs within the linear π-conjugated polymer backbone, which hosts delocalized electronic states. The exact mechanism(s) driving the various chromatic transitions are not fully understood. In general, it is believed that molecular conformational changes, such as side chain ordering and orientation, impart stresses that lead to different backbone conformations, thus changing the electronic states and the corresponding optical absorption.[6,14] It is also not established whether the blue-to-red transition is a continuous transition or a discrete transition between two states separated by an energy barrier. The factors governing the degree of reversibility of the transition are also not understood.

To better understand these chromatic transitions in general, and mechanochromism in particular, we have undertaken SPM studies of polymerized PCDA thin films. A SPM tip can be thought of as both an imaging probe and a localized stress actuator. With the appropriate tip structure and using low applied loads, the SPM tip forms a nanometer-scale single asperity contact point with a flat sample.[15] Depending on the specific SPM instrument (as described below), the tip can be used to measure the sample's topographic, frictional, and/or optical responses. For example, a near-field scanning optical microscopy (NSOM) probe has been recently utilized by Robinson et al.[16] as both an actuator and a spectroscopic tool to observe strain-induced optical emission shifts of quantum dot structures. Using these tools with PDA samples, we have obtained the first observation of mechanochromism at the nanometer scale.

Experimental Section

The details of our sample preparation will be described elsewhere.[17] A brief summary is given here. Both blue and red poly-PCDA films were prepared on a Langmuir trough

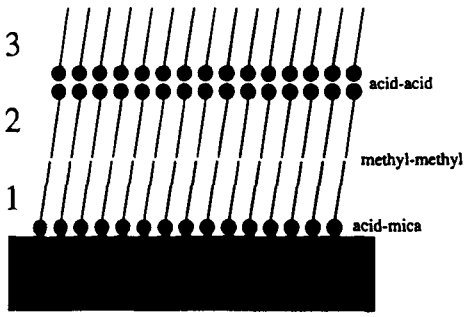

Figure 2. Trilayer packing of PCDA molecules. The circle represent the COOH headgroups which are expected to hydrogen bond to the mica substrate (mica–layer 1 interface) and each other (layer 2–layer 3 interface). Between layers 1 and 2 is a CH_3–CH_3 interface that is less strongly bonded through van der Waals' forces.

(Nima, Coventry, U.K.) that was situated on a vibration isolation table inside a class 100 clean room. The subphase was deionized water with a resistivity greater than 18 MΩ·cm (Barnstead Nanopure system, Dubuque, IA) held at a temperature of 15 ± 1 °C. Freshly cleaved muscovite mica substrates were immersed into the subphase prior to monolayer spreading. PCDA molecules (Farchan/GFS Chemicals, Powell, OH), which had been purified through a silica gel column, were spread onto the subphase in a 50% chloroform/benzene solution. On the pure water subphase the monolayer was unstable; however, as the monomer was compressed at a rate of 100 cm²/min (molar compression rate: 380 $m^2 s^{-1} mol^{-1}$ or 4 $Å^2 molec^{-1} min^{-1}$) to a pressure of 20 mN/m, a stable trilayer was produced (molecular area of ~8 Å²).[17,18] The Y-type configuration of these amphiphilic molecules results in the outermost surface layer consisting of hydrophobic methyl-terminated alkyl chains, as shown in Figure 2. All films were equilibrated for 20 min at 20 mN/m, prior to UV light exposure (254 nm) with a pair of Hg pen lamps (Oriel, Stratford, CT). Distinct methods were then used to transfer blue and red samples, as they exhibited different degrees of rigidity which will be discussed in detail elsewhere.[17] For the blue film, the mica substrate was seated horizontally approximately 1 mm below the water surface before spreading the molecules. The pen lamps, fixed 10 cm from the water surface, were switched on for 30 s producing a faintly visible, uniform blue film. The water level was lowered by slowly draining the trough, allowing the polymerized blue film to drape itself over the mica substrate. Vertical transfer was not possible for the blue film as it possessed significant rigidity which prevented film compression during vertical transfer attempts. For the red film, the mica substrate was held vertically below the water surface before spreading the molecules. The monomer film was exposed for 5 min with the UV lamps 5.5 cm above the water surface, producing a uniform red film, with a subtle textured appearance. We attribute the textured appearance to the presence of microscopic cracks in the film, as discussed further below. In contrast with the blue film, we believe the cracks allow compressibility of the red film during vertical transfer. The film was transferred to the mica substrate by drawing it upward at a rate of 10 cm/s while holding the trough pressure constant. Both samples were dried in clean room air and stored in a dark, nitrogen-purged container.

Samples were analyzed with several techniques. Microscopic (far-field) sample fluorescence was recorded using a Leitz optical fluorescence microscope equipped with a Xenon lamp and dichroic beam filters. The sample was illuminated with 520–550 nm polarized light, and emission wavelengths greater than 590 nm were passed to an intensified CCD camera, which captured the field of view for the images presented here. An atomic force microscope (AFM) (Nanoscope IIIA, Digital Instruments, Santa Barbara, CA) operating in contact mode with silicon nitride cantilevers was used to obtain topographic and friction force images. Measurements with the AFM were acquired

(11) Kobayashi, T. *Optoelectronics—Devices Technol.* **1993**, *8*, 309.
(12) Hoofman, R. J. O. M.; Siebbeles, L. D. A.; de Haas, M. P.; Hummel, A.; Bloor, D. *J. Chem. Phys.* **1998**, *109*, 1885.
(13) Mowery, M. D.; Menzel, H.; Cai, M.; Evans, C. E. *Langmuir* **1998**, *14*, 5594.
(14) Bloor, D.; Chance, R. R. *Polydiacetylenes: Synthesis, Structure, and Electronic Properties*; Martinus Nijhoff: Dordrecht, The Netherlands, 1985.
(15) Carpick, R. W.; Salmeron, M. *Chem. Rev.* **1997**, *97*, 1163.
(16) Robinson, H. D.; Muller, M. G.; Goldberg, B. B.; Merz, J. L. *Appl. Phys. Lett.* **1998**, *72*, 2081.
(17) Sasaki, D. Y.; Carpick, R. W.; Burns, A. R. Manuscript in preparation.
(18) Goettgens, B. M.; Tillmann, R. W.; Radmacher, M.; Gaub, H. E. *Langmuir* **1992**, *8*, 1768.

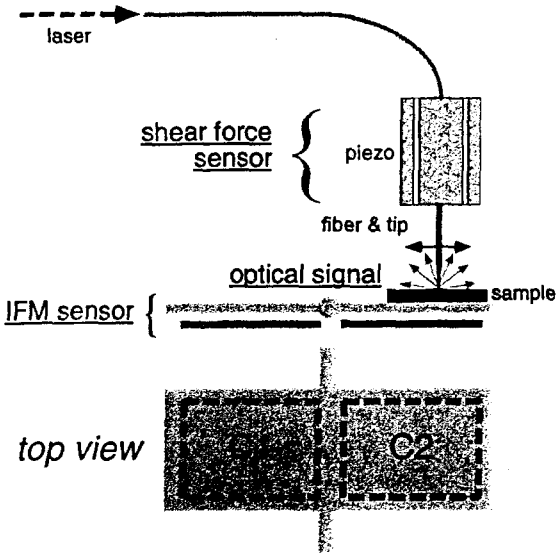

Figure 3. Schematic diagram of the NSOM/IFM instrument. The NSOM fiber is brought into contact with a sample resting on an IFM sensor. The sensor measures the attractive and repulsive normal forces between the tip and sample by maintaining an electrostatic balance of two capacitances C_1 and C_2, formed by the common plate and identical gold pads fixed on a glass substrate (not shown). Light is launched into the fiber and excites sample fluorescence in the near field. Light is collected in the far field above the sample by an objective (not shown).

under laboratory ambient conditions. The scan rate was 3 Hz (=lines/s).

A home-built NSOM integrated with an interfacial force microscope (IFM) sensor was used to obtain simultaneous optical, shear force, and normal force measurements at the nanometer scale (Figure 3). This instrument is described in more detail elsewhere.[19,20] The IFM is used here to determine the applied load during scanning, completely decoupled from the NSOM shear-force signal. Topographic feedback is accomplished using shear-force damping, as described below. The NSOM operates in reflection mode. Less than 0.5 mW of polarized 488 nm light from an Ar laser is launched into a single-mode fiber optic. The other end of the fiber is tapered by conventional fiber pulling[21] or chemical etching[22] and coated with ~80 nm Al. Scanning electron microscopy imaging confirms the tips are ~100 nm diameter or less. The fiber is mounted onto a small piezoelectric transducer that oscillates the fiber laterally for shear-force detection.[19,20] The fiber typically has a mechanical resonance at 25–50 kHz, depending on the free length (typically ~3 mm), a typical Q-factor of 100 (before contact), and a free lateral motion amplitude of typically 9 nm. Detection of fiber motion is accomplished nonoptically by monitoring induced voltages on the drive piezo.[23] The tip is brought close to the sample using a stepper motor. Final approach and topographic distance control is accomplished by a second piezo tube, upon which the sample and IFM force sensor are mounted. The fiber amplitude is attenuated upon interaction of the probe tip with the sample. Topographic images were obtained by rastering the tip across the sample while maintaining constant shear force damping (thus, contrast can occur due to true sample topography or higher friction[20]). A ×36 Schwarzschild objective (NA = 0.5) collects sample fluorescence concentric about the tip. Reflected 488 nm

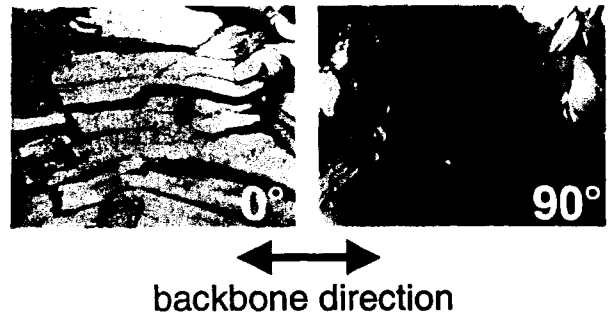

Figure 4. Fluorescence microscopy images (170 × 130 μm^2) of fully red PCDA at 0° and 90° polarization relative to the horizontal direction. At 0°, cracks are observed in the trilayer film. At 90°, emission from this single domain is largely extinguished, indicating a high degree of orientation of the polymer backbones.

light is attenuated with a holographic notch filter, and a 530 nm cutoff filter is used to eliminate signal due to Raman scattering in the fiber. The sample fluorescence is focused into a spectrometer (ISA/SPEX, Edison, NJ), and the signal is measured with a cooled photomultiplier tube and photon-counting electronics. The entire apparatus is enclosed and continuously purged with N_2 gas to eliminate capillary condensation between the tip and sample. The relative humidity was typically <5% for all experiments.

Sample Characterization. The optical absorption spectra of both the blue and red films are consistent with previously reported spectra.[6] Far-field fluorescence microscopy reveals that the red films are strongly fluorescent and organized into crystalline domains. The fluorescence images show extended cracks in the films that are roughly parallel. In Figure 4, the excitation light is polarized along the crack direction. The fluorescence emission is almost completely extinguished by rotating the polarization of the excitation light by 90°. Both the absorption and emission dipoles of PDA are known to be aligned along the backbone direction.[24–26] Thus, the domains we observe consist of highly oriented backbones, parallel to the cracks. Topographic AFM images are consistent with this, showing uniform terraces with roughly aligned cracks (Figure 5), similar to previous reports.[18,27] The cracks expose the mica substrate, as verified by the higher friction force measured within the cracks. The film height measured at these crack edges is ~9.0 ± 0.9 nm, corresponding to the height of a poly-PCDA trilayer with a nominal ~20° tilt of the molecule (the extended PCDA molecule is ~3.2 nm in length[6,28]). As mentioned previously, a trilayer structure is indicated by the pressure–area isotherms from the Langmuir trough. The tilt angle is similar to previous reports of Cd salts of the same molecule.[29] In addition, islands ~6.1 ± 0.6 nm in height are found on top of the trilayer. The height measurement indicates that the islands consist of an additional bilayer of poly-PCDA with the same tilt angle. The bilayers are likely stabilized by interfacial hydrogen-bonded ad dimers of the acid headgroups and thus present methyl groups to the tip as well. Indeed, there is no friction force contrast between the surface of the trilayer or the extra bilayer islands. The bilayers are likely produced during the monomer compression stage before polymerization and deposition.

Blue PCDA samples show only weak fluorescence, where this weak emission appears to be localized at film cracks, edges, and other defects. AFM imaging reveals large, uniform terraces, with a few film defects that expose the mica substrate (Figure 6). The trilayer film height is ~7.4 ± 0.8 nm, ~18% less than the red PCDA trilayer. This indicates that poly-PCDA molecules may be

(19) Burns, A. R.; Houston, J. E.; Carpick, R. W.; Michalske, T. A. *Phys. Rev. Lett.* **1999**, *82*, 1181.
(20) Burns, A. R.; Houston, J. E.; Carpick, R. W.; Michalske, T. A. *Langmuir* **1999**, *15*, 2922.
(21) Betzig, E.; Trautman, J. K.; Harris, T. D.; Weiner, J. S.; Kostelak, R. L. *Science* **1991**, *251*, 1468.
(22) Hoffmann, P.; Dutoit, B.; Salathe, R. P. *Ultramicroscopy* **1995**, *61*, 165.
(23) Barenz, J.; Hollricher, O.; Marti, O. *Rev. Sci. Instrum.* **1996**, *67*, 1912.
(24) Chance, R. R.; Patel, G. N.; Witt, J. D. *J. Chem. Phys.* **1979**, *71*, 206.
(25) Moers, M. H. P.; Gaub, H. E.; Vanhulst, N. F. *Langmuir* **1994**, *10*, 2774.
(26) Yamada, S.; Shimoyama, Y. *Jpn. J. Appl. Phys., Part 1* **1996**, *35*, 4480.
(27) Putman, C. A. J.; Hansma, H. G.; Gaub, H. E.; Hansma, P. K. *Langmuir* **1992**, *8*, 3014.
(28) Shelnutt, J. A. Personal communication.
(29) Lieser, G.; Tieke, B.; Wegner, G. *Thin Solid Films* **1980**, *68*, 77.

Figure 5. Topographic AFM image (50 × 50 μm^2) of fully red PCDA. The sample shows high coverage, with roughly parallel cracks. The cracks are oriented along the polymer backbone direction.

Figure 6. Topographic AFM image (50 × 50 μm^2) of blue PCDA. The sample also shows high coverage, with a few isolated holes in the film.

more tilted away from the surface normal in the blue phase (nominal tilt angle ~39°), and additionally the height may be reduced by an altered backbone conformation. The height difference is consistent with poly-PCDA trilayer measurements of Lio et al.,[6] where blue PCDA trilayers were 15% shorter than the red phase which was formed thermochromically. X-ray diffraction measurements of poly-PCDA multilayers also indicate the red phase (formed by UV irradiation) is substantially less tilted from the surface normal than the blue.[30] As with the red sample, bilayer islands atop the trilayer base are occasionally observed. High-resolution images on the terraces reveal large, extended arrays of parallel striations (see Figure 10), similar to

(30) Fischetti, R. F.; Filipkowski, M.; Garito, A. F.; Blasie, J. K. *Phys. Rev. B* **1988**, *37*, 4714.

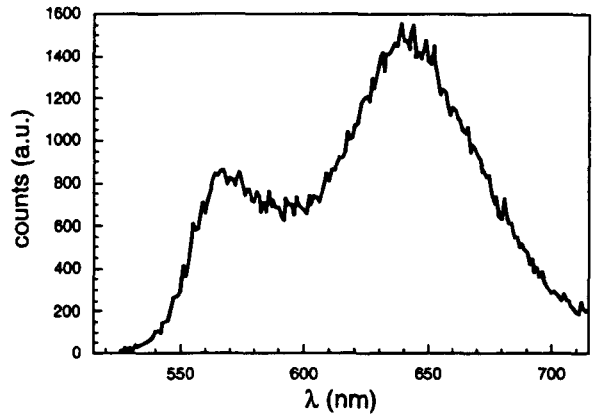

Figure 7. Near-field fluorescence spectrum of fully red PCDA, showing characteristic peaks at 640 and 560 nm.

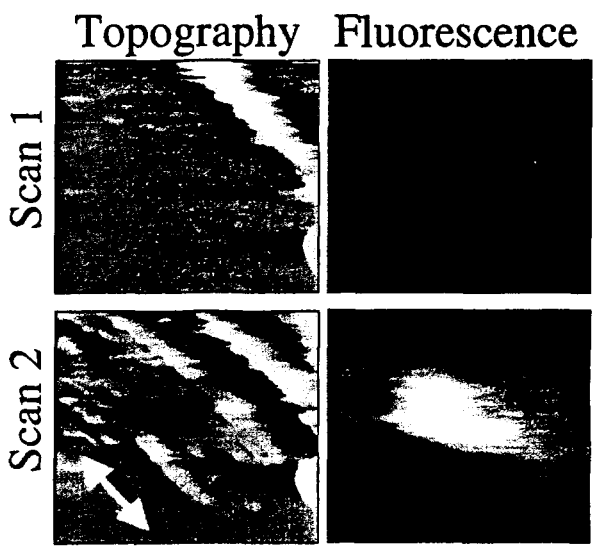

Figure 8. NSOM shear force topography (left) and simultaneous fluorescence (right) images acquired (2.4 × 2.4 μm^2) showing tip-induced mechanochromism. In the first scan (top), no fluorescence is seen over the flat PCDA region. In the subsequent scan, topographic changes are created, and fluorescence emission is produced within the imaging region. The topographic features display alignment along the polymer backbone direction (arrow).

previous reports.[6] The striations correspond to the backbone direction. This indicates that the backbones are also highly oriented within individual domains in the blue phase.

While the microstructural features of both the blue and red films involve cracks, extra bilayer islands, and other defects, we observe with both blue and red films that large, crystalline domains comprise a significant fraction of the sample. These domains are atomically flat and have a high degree of backbone ordering. We conclude overall that both blue and red film quality within these individual domains is extremely high at the molecular level. From the trilayer configuration of the films, as depicted in Figure 2, we assert that the acid–mica and acid–acid interfaces are more strongly bonded due to hydrogen bonding, while the methyl–methyl interface is less strongly bonded (with van der Waals' forces).

Results and Discussion

Tip-Induced Mechanochromism. Red PCDA samples were examined with the NSOM/IFM instrument and exhibited fairly uniform fluorescence, with no changes induced by tip–sample contact. Simultaneous shear-force topography and polarization-sensitive fluorescence images are consistent with those previously obtained for red films

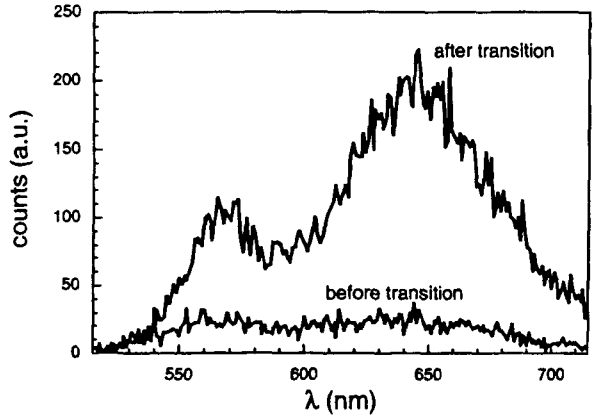

Figure 9. Near-field fluorescence spectrum of blue PCDA, before and after tip-induced mechanochromism. Before the transition, only a weak background is observed. The fluorescence spectrum after the transition shows the same characteristic peaks (at 640 and 560 nm) as fully red PCDA, formed through UV polymerization.

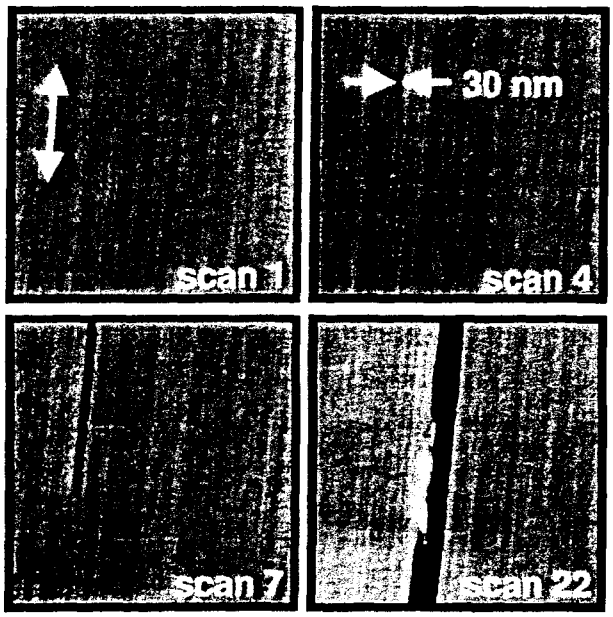

Figure 10. Series of 1 × 1 μm^2 topographic AFM images of blue PCDA showing the progressive growth of the tip-induced red domains. In the first scan, striations indicative of the polymer backbone direction are observed. By the fourth scan, a topographically distinct (i.e. lower) region, only 30 nm wide, appears. This region continues to grow in subsequent scans.

using transmission-mode NSOMs.[25,31] A typical near-field fluorescence spectrum is shown in Figure 7. The spectral features, a large peak at ~640 nm and a smaller peak at ~560 nm, are consistent with previous reports of red PDA fluorescence.[32] Note that the 530 nm cutoff filter attenuates the high-energy tail.

Blue PCDA samples were investigated with the NSOM/IFM instrument. Figure 8 shows simultaneous 2.4 × 2.4 μm^2 shear force topography and fluorescence images, obtained with the monochromator set at 640 nm. The shear-force damping was set to a constant value of 15% for a ~9 nm free amplitude. The dither direction is aligned with the vertical axis of the image. In scan 1, the shear force topography is essentially flat, with identifying defective features on the right side of the image. The fluorescence image shows only an extremely weak and uniform noise background characteristic of blue films (Figure 9).

Upon the imaging of the same region a second time, dramatic local changes occur. The arrow in Figure 8, scan 2, indicates the polymer backbone direction, as identified by other images within the same poly-PCDA domain which show striations aligned along that direction (the preexisting defect is also oriented along this direction and may correspond to a step or crack in the film). The shear-force topography displays features, *of apparent* high topography, that consist of stripes along the backbone direction. The fluorescence image shows a distinct, localized response that coincides with the topographic features. A fluorescence spectrum obtained over this region reveals the spectral fingerprint of red PCDA (Figure 9). The fluorescence region grows larger with subsequent imaging. This effect was reproduced multiple times with this tip and sample, as well as with a second NSOM tip and a second blue PCDA sample. In general, when this transition is observed, the fluorescent regions grow gradually with each image acquired. We postulate that the transition takes place during the image acquisition itself, in the case of Figure 8. The example in Figure 8 represents one of the largest changes between subsequent images that we observed. Simultaneous normal-force measurements with the IFM while under shear-force feedback reveal that this transition can occur with either negative or positive applied loads. Typically, applied loads were in the range of −20 to +20 nN, where the minimum possible load (or "adhesion force") was in the range of −30 to −70 nN. The slow imaging speed required to collect NSOM fluorescence images combined with drift of the IFM sensor prevented us from performing a detailed correlation of domain growth rate and normal load at this time.

Unfortunately, the spatial resolution of the fluorescence image in Figure 9 is lower than expected given the ~100 nm tip aperture. This resolution degradation was due to scattering of the exciting 488 nm light in the mica substrate. Mica provides an ideal flat substrate for excellent film quality. Since the film quality was of utmost importance, we therefore settled with less-than-optimal lateral resolution for collection of fluorescence images.

The blue-to-red transition was then investigated with the AFM. For AFM measurements, applied loads were in the range of −20 to +10 nN, where the minimum possible load (or "adhesion force") was in the range of −5 to −40 nN. The scan speed was 3 μm/s. Figure 10 shows excerpts from a series of topographic images (1 × 1 μm^2) where a distinct region progressively grows due to scanning. Backbone-related striations are seen in the images. The region, initially only 30 nm wide,[33] preferentially grows along the backbone direction but also grows, more slowly, perpendicular to the backbone direction. The topographic details of this transformed region are discussed further below. To verify that this was indeed the same transition observed in the NSOM/IFM experiments, a large area was patterned by repeated scanning. Figure 11a,b respectively shows the initial and final 10 × 10 μm^2 topographic images. Several defects, such as film cracks (dark) and extra bilayer islands atop the trilayer (bright), are seen. Figure 11c shows the same region viewed under the far-field fluorescence microscope. Characteristic red

(31) Kramer, A.; Hartmann, T.; Eschrich, R.; Guckenberger, R. *Ultramicroscopy* **1998**, *71*, 123.
(32) Olmsted, J.; Strand, M. *J. Phys. Chem.* **1983**, *87*, 4790.

(33) The 30 nm width is likely limited by the contact area between the tip and sample. A smaller tip may be capable of producing a transformed region even smaller in size.

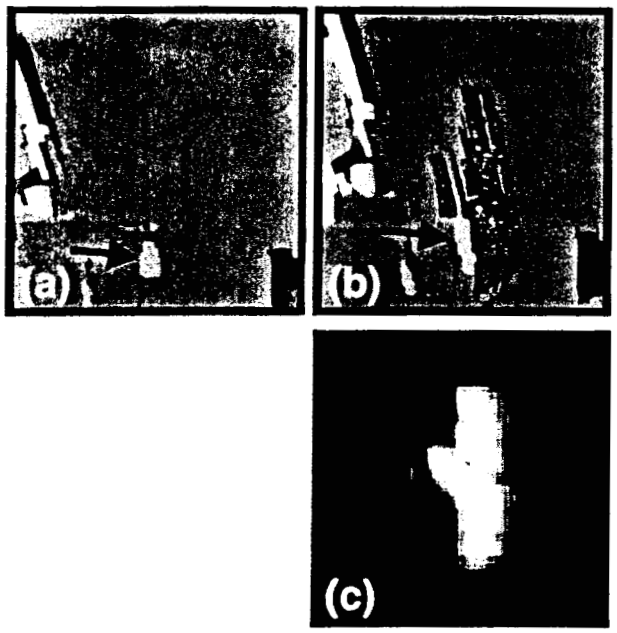

Figure 11. 10 × 10 μm^2 topographic AFM images showing tip-induced patterning of red PCDA domains. (a) Initial image of a blue film. (b) Final image with a patterned red region. The backbones are oriented in roughly the vertical direction. The patterning was formed by multiple, high-load 1 × 1 μm^2 scans within the patterned region. The black arrow indicates a bilayer island that has grown in size after the patterning. (c) Far-field fluorescence microscope image of the same region. Characteristic red PCDA fluorescence is localized within the patterned region.

PCDA fluorescence is localized within the patterned region. The fluorescence persists for at least 30 days, indicating that the transition is irreversible. Two animations of the color transition, each composed of a series of AFM topographic images, can be viewed at http://www.sandia.gov/surface_science/nsom/nsom.htm. These movies illustrate the anisotropic growth of the domains and the structural changes that accompany the transition.

We have observed that heating blue PCDA samples to ~60 °C also causes an irreversible blue-to-red transition (thermochromism).[6] This raises the possibility that SPM tips are locally heating the PCDA during scanning, thus causing the observed transition.[34-36] However, AFM tips are not actively heated, and the transition occurs for NSOM tips even without the laser excitation present. Local heating arising from friction between the tip and PCDA cannot account for the transition, as phonons excited by tip–sample contacts are in general predicted to rapidly propagate away from the contact zone.[37] In other words, the tip and sample act as large thermal baths for the contact. Significant heating of the contact zone is therefore unfeasible.

Observations of several transitions with both NSOM/IFM and AFM reveal the following properties:

(1) Although transitions are observed in apparently defect-free regions, defects in the film such as pinholes and crack edges assist significantly in the initial formation and growth of the red domains.

(2) The transition does not proceed without sliding contact occurring between the tip and sample; i.e., *shear forces are required*. The transition is always initiated and grows within the imaging region (where tip–sample sliding contact occurs). Engagement of AFM force–distance profiles, where the normal load is varied without allowing lateral motion of the tip, does not contribute to the domain formation or growth.

(3) The growth of the red domains is strongly anisotropic, with preferential growth along the backbone direction. Furthermore, red domains will often extend outside the imaging region. This indicates *that the transition propagates along the backbone direction* beyond the region where stress has been applied.

(4) As verified with the AFM, the *growth proceeds most rapidly when the sliding (fast scan) direction is perpendicular to the backbone direction*.[38] In most cases, growth will not proceed at all when the fast scan direction is parallel to the backbone direction.

(5) Nucleation and growth of the red domains occurs at negative (adhesive) loads, but the *growth proceeds faster at larger loads*. Note that finite shear forces persist even at negative loads in an adhesive contact.[19,20,39,40] Imaging at very low, negative loads in the absence of significant adhesion effectively provides a method of imaging the sample without promoting further growth.

(6) The rate of growth varies between samples, and even within a single sample, suggesting that the transition rate is highly dependent on sample preparation conditions (such as UV exposure), local defect density, and the film/substrate interface. This variation makes it difficult to quantify the exact load dependence of the growth without a large number of further experiments. However, it is clear that shear forces perpendicular to the backbone are required.

Role of Topographic Structural Changes. As mentioned previously, the red PCDA film formed by UV exposure is taller than the blue PCDA film by ~18% (9.0 ± 0.9 nm vs 7.4 ± 0.8 nm). However, the red regions formed by tip-induced mechanochromism generally exhibit *lower* topography, such as in Figure 10. These regions also typically exhibit higher friction and substantial corrugation (Figure 12a). The depth of the lower regions varies but is generally observed to be 4.3 ± 0.3 nm below the trilayer. This suggests that material is removed during the transformation process, or it is severely compressed. Note that the blue trilayer film has a height of 7.4 ± 0.8 nm; therefore, the film has not been completely removed from this region. Indeed, high-resolution images within these lower regions reveal the familiar backbone-related structure, verifying that poly-PCDA remains (Figure 12a). Also, within the transformed regions, strands with height 2.6 ± 0.3 nm above the lowest region are frequently observed (solid arrow, Figure 12b) and are correlated with higher friction. One possibility is that these features are COOH-terminated strands, namely remains of layer 2 with exposed COOH headgroups, where layer 3 has been removed. Although most of the transformed region is lower than the surrounding trilayer, it occasionally includes small regions that are higher than the surrounding trilayer

(34) Kavaldjiev, D. I.; Toledo-Crow, R.; Vaez-Iravani, M. *Appl. Phys. Lett.* **1995**, *67*, 2771.
(35) Stahelin, M.; Bopp, M. A.; Tarrach, G.; Meixner, A. J.; Zschokke-Granacher, I. *Appl. Phys. Lett.* **1996**, *68*, 2603.
(36) La Rosa, A. H.; Yakobson, B. I.; Hallen, H. D. *Appl. Phys. Lett.* **1995**, *67*, 2597.
(37) Perry, M. D.; Harrison, J. A. *J. Phys. Chem.* **1995**, *99*, 9960.
(38) The applied shear forces in NSOM are more complicated than in AFM. Dithering of the fiber exerts oscillatory shear forces at 25–35 kHz during imaging, roughly along the vertical direction of Figure 8. Rastering of the tip exerts additional shear forces at a few hertz along the "fast-scan" direction, which is the horizontal direction of Figure 8.
(39) Cohen, S. R.; Neubauer, G.; McClelland, G. M. *J. Vac. Sci. Technol. A* **1990**, *8*, 3449.
(40) Carpick, R. W.; Agraït, N.; Ogletree, D. F.; Salmeron, M. *J. Vac. Sci. Technol. B* **1996**, *14*, 1289.

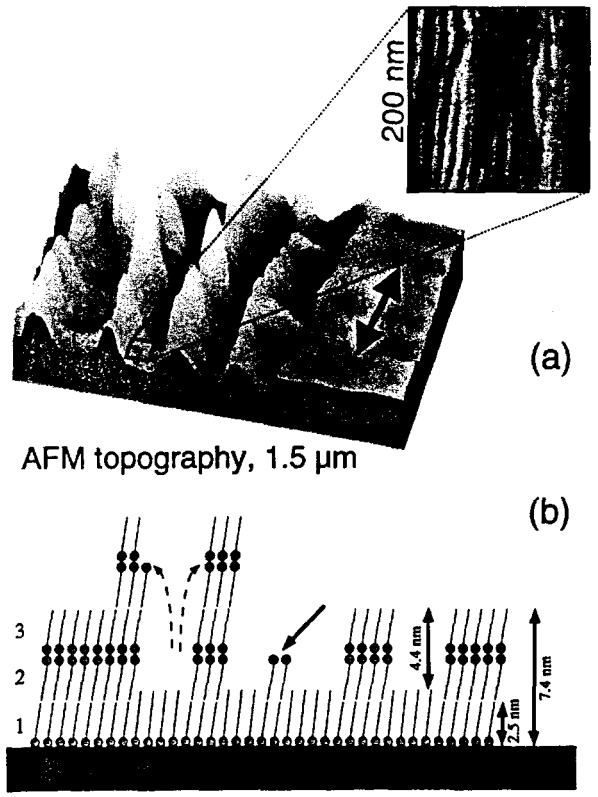

Figure 12. (a) 1.5 × 1.5 μm^2 topographic AFM image at the boundary of a tip-induced red PCDA domain. The significant corrugation is aligned along the backbone direction (arrow) and corresponds to bilayer "valleys" and possibly bilayer "bumps". At the bottom of the "valleys" an oriented PCDA monolayer remains, as seen from the high-resolution 200 × 200 nm^2 image where the typical backbone striations are observed. (b) Sketch of the observed molecular rearrangement, where bilayer strands (layers 2 and 3) have been displaced and relocated on top of the original trilayer. The solid arrow indicates exposed COOH groups from layer 2.

(see Figure 12a). The heights of such areas are quite variable but are typically 5.5 ± 0.6 nm higher than the surrounding trilayer. This is consistent with the height of a PCDA bilayer segment of either the blue or red form. Indeed, in Figure 11b it is apparent that a bilayer island has grown significantly in size after the scanning procedure. Therefore, significant rearrangement of PCDA bilayer segments occurs during the transformation.

These AFM measurements at first appear to contradict the NSOM shear-force topography image in Figure 8, where the transformed region appears *higher* than the surroundings. However, topographic contrast reversal has been previously reported for other materials examined with NSOM,[41] as the shear-force topography mode is highly sensitive to friction forces and structural effects. With our samples, highly corrugated regions with exposed COOH-terminated strands will produce higher friction than CH_3-terminated strands, as could other defects in the region, thus leading to regions of higher *apparent* topography. This has been recently observed in a comparison between CH_3 and COOH-terminated thiol films.[19,20] This effect will depend on the amount of COOH-terminated strands present, as well as the applied load, and the NSOM tip structure and composition. Indeed, we have observed other transformed regions with NSOM that possess *lower* apparent topography. We propose that the NSOM and

(41) Durkan, C.; Shvets, I. V. *J. Appl. Phys.* **1996**, *79*, 1219.

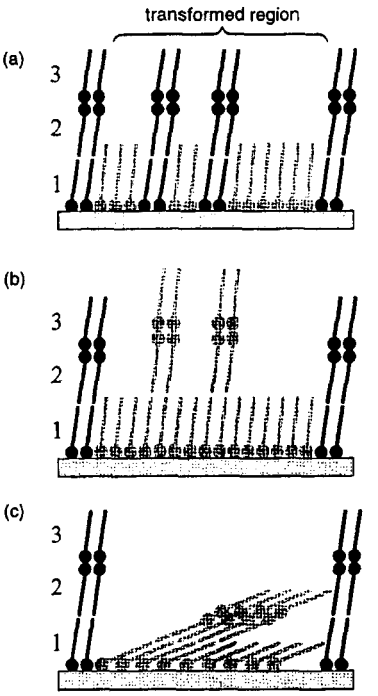

Figure 13. Proposed configurations of red (dashed lines) and blue (solid lines) components after the transition. (a) Layers 2 and 3 are removed, and layer 1 is transformed to the red state. (b) Shear forces convert molecules to the red form and, independently, rearrange some of them. (c) PCDA molecules to adopt a heavily tilted or compressed configuration due to shear and compressive forces.

AFM transitions produce essentially the same topographic structural changes despite the differences in *apparent* topography, and we refrain from using the apparent topography in NSOM shear force images as an indication of true topography.

From these results, we can propose three distinct processes for the mechanically induced transition:

(1) Shear forces between the tip and sample displace segments of the topmost bilayer (layers 2 and 3). The underlying monolayer (layer 1) then adopts the red configuration as a result of its altered environment (with no molecules above it any longer) or by the subsequent application of shear forces during scanning. This is illustrated in Figure 13a. If we assume that the remaining monolayer (layer 1) has been converted to the red form and possesses one-third of the height of the UV-formed red trilayer (9.0 nm), then a depth of 4.4 nm is expected ($7.4 - \frac{1}{3} \cdot 9.0 = 4.4$). This is consistent with the observed depth. Note that the removal of a bilayer of blue PCDA (layers 2 and 3), with no change in the height of the remaining monolayer (layer 1), would produce a depth of 4.9 nm ($\frac{2}{3} \cdot 7.4 = 4.9$), which is inconsistent with the results.

(2) Shear forces between the tip and sample directly distort the molecular conformation from the blue to the red state. The rearrangement of bilayer segments is an independent side effect. In other words, all or most of the molecules in the affected region adopt the red configuration (Figure 13c).

(3) Shear and compressive forces cause PCDA molecules to adopt a heavily tilted or compressed conformation that is lower in height than the surrounding trilayer. This distortion alters the backbone configuration, producing the red phase (Figure 13c).

Process 1 is consistent with our observations, particularly the measured height differences between the mono-

layer and the surrounding blue trilayer with AFM. It is also consistent with the observation that step edges and pinhole defects in the film assist in the transition, as such vacancies allow the instigation of molecular displacement via lateral motion. Obviously, this displacement would be significantly restricted in a defect-free region. Process 2 is not supported by the consistently observed correlation between molecular displacement and the blue to red transition, nor does it explain the observed depth of the transformed regions. Process 3 requires severe distortion of the PCDA molecules. In the simplistic diagram of Figure 13c, we are omitting related processes such as bending of alkyl chains, interdigitation, and a mixture of different tilt angles. If such distortions occurs, it would mean that there are multiple conformations that produce red PCDA. While we cannot rule out such possibilities, process 1 appears to be the most likely. How the remaining monolayer is converted to the red form remains to be explained and is discussed below.

It has been suggested that the red phase involves alkyl side chain entanglement and disorder.[42,43] However, recent evidence suggests otherwise. AFM images that resolved the atomic lattice of blue and red PCDA trilayers were obtained by Lio et al. They observed that the red phase, formed thermochromically, displayed a *higher* degree of ordering of the alkyl side chains. In the red phase, the chains formed a close-packed hexagonal arrangement, whereas, in the blue phase, a partially disordered arrangement was observed. Preliminary high-resolution AFM results suggest that our UV-formed red films exist in a highly ordered arrangement. Furthermore, FTIR data of Lio et al.[6] and ^{13}C NMR data of Tanaka et al.[44] suggest that some of the tilted side chains rotate toward the surface normal in the red phase. Such a rotation is consistent with the observed height increase of the red phase and would impart stress to the polymer backbone. In particular, it could lead to rotation about the C−C bond of the polymer backbone, thus changing the planarity of the backbone (Figure 14). Theoretical calculations indicate that a rotation of only 5° about this bond dramatically changes the π-orbital overlap[45] (shown schematically in Figure 14), causing a significant blue-shift of the absorption spectrum. In general, deformation modes other than bond rotations such as backbone bending and stretching, or combinations thereof, could also be involved. While not definitive, the observed shear force dependence of the transition suggests that bond rotation occurs.

In the absence of the alkyl side chains, there would be a monotonic change in the energy of the polymer backbone as the C−C bond angle changes.[45,46] The torsional mobility of the polymer backbone is restricted by alkyl side chain packing and H-bonding of the headgroups.[46] The irreversibility of the transition we observe indicates the greater stability of the red phase compared to the blue. The competing factors of backbone stress, side chain orientation and spacing, and headgroup H-bonding may lead to two distinct phases separated by an energy barrier—a metastable blue phase and a more stable red phase. The energy to overcome this barrier could be provided by the tip. The applied shear stress assists in rotating and deforming the methyl-terminated alkyl side chains into the more stable red configuration. Note that this requires the shear force to be applied perpendicular to the polymer backbone; indeed we observe that shear forces perpendicular to the backbone are most efficient in generating the transition. Alternately, the removal of the uppermost bilayer (layers 2 and 3, Figure 2) may change the stresses acting on the monolayer (layer 1, Figure 2), thus allowing it to transform to the red phase. We are unable to suggest a mechanism by which this transition occurs in this case. In either event, it would clearly be advantageous to study a stable PDA *monolayer*, to reduce the complications associated with analyzing substantial molecular displacement. Studies of stable PDA monolayers are currently underway in our laboratory.

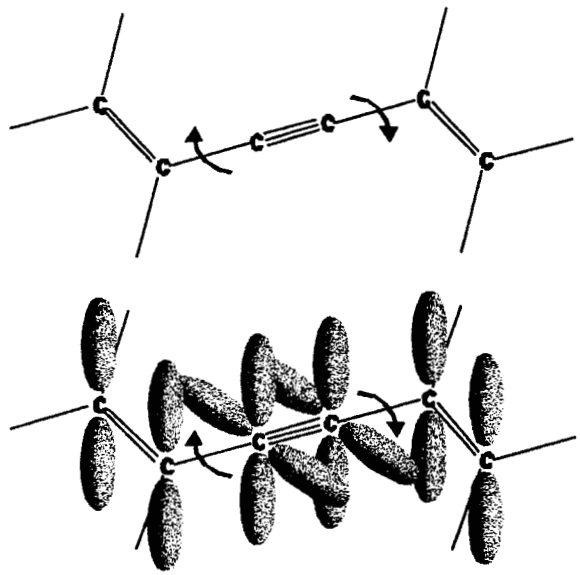

Figure 14. Schematic diagram of the molecular orbitals in the π-conjugated PCDA backbone in the planar configuration. Energy levels are affected by the overlap of these orbitals. This overlap is altered by rotation about one of the C−C bonds in the backbone. The red phase may consist of a nonplanar backbone configuration in conjunction with rotated and/or distorted alkyl side chains.

Summary

For the first time, the blue-to-red chromatic transition of a trilayer poly(diacetylene) thin film has been induced using a nanometer-scale probe tip. Shear forces between the tip and poly-PCDA molecules in the blue phase create nanometer-scale red domains that preferentially nucleate at film defects and propagate along the polymer backbone. The transition is irreversible and appears to be discrete. Significant displacement of the poly-PCDA molecules is observed within the red domains. Removal of the uppermost bilayer appears to be correlated with the transition, where the remaining monolayer exists in the red phase. The transition is reproducibly observed with both AFM and NSOM probe tips. The rate of domain formation increases with applied load and hence with higher shear forces and is favored when shear forces are applied perpendicular to the backbones. The shear-force-induced transition is consistent with models that invoke side-chain rotation about the conjugated backbone. Future work will focus on quantifying the shear forces and loads required to cause this transition for both trilayer and monolayer PDA films, as well as molecular dynamics simulations of the molecular conformation in both the blue and red phases. We expect that these efforts will allow us to precisely correlate molecular conformational changes with color transitions in these fascinating materials.

(42) Saito, A.; Urai, Y.; Itoh, K. *Langmuir* **1996**, *12*, 3938.
(43) Mino, N.; Tamura, H.; Ogawa, K. *Langmuir* **1991**, *7*, 2336.
(44) Tanaka, H.; Gomez, M. A.; Tonelli, A. E.; Thakur, M. *Macromolecules* **1989**, *22*, 1208.
(45) Orchard, B. J.; Tripathy, S. K. *Macromolecules* **1986**, *19*, 1844.
(46) Dobrosavljevic, V.; Stratt, R. M. *Phys. Rev. B* **1987**, *35*, 2781.

Acknowledgment. We gratefully acknowledge S. Singh, who assisted with PCDA film preparation and analysis and provided useful discussions. We acknowledge useful discussions with D. H. Charych, U. Jonas, J. Houston, and T. Michalske. R.W.C. acknowledges the support of the Natural Sciences and Engineering Research Council of Canada. Sandia is a multiprogram laboratory operated by Sandia Corp., a Lockheed Martin Co., for the United States Department of Energy under Contract DE-AC04-94AL85000.

LA990706A

Shear-induced mechanochromism in polydiacetylene monolayers

A.R. Burns [a,*], R.W. Carpick [a,**], D.Y. Sasaki [a], J.A. Shelnutt [a,***] and R. Haddad [b]

[a] *Sandia National Laboratories, MS 1413, Albuquerque, NM 87185-1413, USA*
E-mail: aburns@sandia.gov
[b] *Department of Chemical Engineering, University of New Mexico, Albuquerque, NM 87131, USA*

We use atomic force microscopy to actuate and characterize the nanoscale "mechanochromism" of polydiacetylene monolayers on atomically-flat silicon oxide substrates. We find explicit evidence that the irreversible blue-to-red transformation is caused by shear forces exerted normal to the polydiacetylene polymer backbone. The anisotropic probe-induced transformation is characterized by a significant change in the tilt orientation of the side chains with respect to the surface normal. We discuss preliminary molecular dynamics simulations and electronic structure calculations on twelve-unit polydiacetylene oligomers that allow us to correlate the transformation with bond-angle changes in the conjugated polymer backbone.

KEY WORDS: atomic force microscopy; friction force microscopy; friction anisotropy; shear force microscopy; nanotribology; polydiacetylenes; LB films; molecular mechanics; conjugated polymers

1. Introduction

As evidenced by other articles in this issue, organic films of ordered, densely-packed molecules have been used extensively as model lubricants to study the structural, mechanical, and chemical aspects of adhesion and tribology. In most cases, these films are monolayers of simple alkanes, of variable chain length and tail group chemistry, that are created either by Langmuir–Blodgett (LB) [1] or self-assembly techniques [1,2]. We have been working on another class of organic thin films that are also composed of densely-packed alkane chains; each chain, however, has an integral diacetylene unit (figure 1(A)). The distinguishing feature of these films is that the molecules may be cross-linked via UV photochemistry in a one-dimensional fashion to form highly-ordered arrays of long polydiacetylene (PDA) polymers (figure 1 (B) and (C)). These films have been the subject of many years of research [3] because the cross-linking produces a conjugated backbone that exhibits a chromatic response to elevated temperature, solvents, and stress. Mechanically-induced color changes, or "mechanochromism" [4], offers an intriguing potential use in tribology as an optical sensor of contact, friction, and adhesion. Thus our motivation in this paper, and that of a previous study of PDA trilayers [5], is to understand what molecular changes (e.g., disordering, re-orientation) are involved in the friction-induced mechanochromism of PDA monolayers. To accomplish this, we use scanning probe microscopy to both actuate and characterize the structural changes of the PDA films. Since these are unusual films, we will first discuss some of their salient features.

In figure 1, we show the basic structure of a PDA monolayer that is created on a LB trough and transferred to a solid substrate. An ordered monomer phase (B) is formed and then polymerized (C) with UV light. The linear conjugated backbone is parallel to the LB subphase and retains this geometry when transferred to the substrate surface (D). Thus it is bound to the substrate via an interaction with the (hydroxyl) head groups on the lower set of side chains, while the upper set of side chains and methyl tail groups becomes the "interface" with probe tips, analytes, solvents, etc. Using optical and atomic force microscopy (AFM), we have shown that the polymer backbones align in highly parallel arrays in domains exceeding 100 μm^2 [5–7]. The lengths of

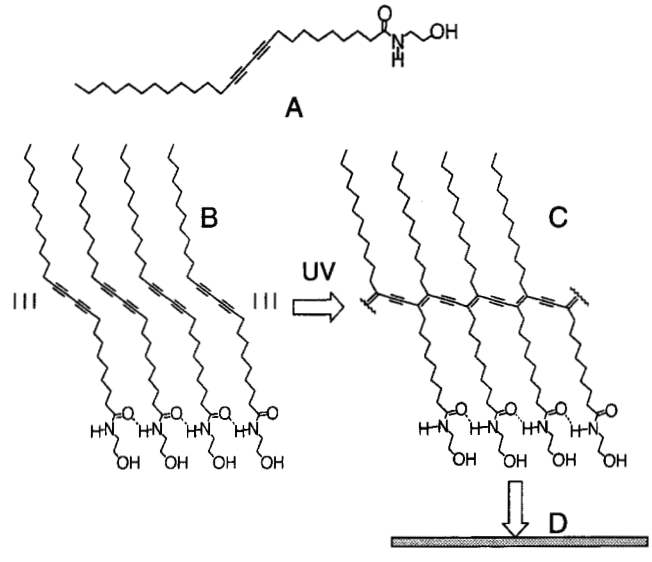

Figure 1. (A) Diacetylene monomer N-(2-ethanol)-10,12-pentacosadinamide. (B) Ordering of monomers under 20 mN/m pressure on LB trough, followed by UV polymerization into (C) polydiacetylene (PDA). (D) The PDA monolayer is horizontally transferred (head groups down) to a hydrophilic SiO_2 substrate.

* To whom correspondence should be addressed.
** Current address: Department of Engineering Physics, University of Wisconsin-Madison, 1500 Engineering Dr., Madison, WI 53706-1687, USA.
*** Current address: Department of Chemistry, University of New Mexico, Albuquerque, NM 87131, USA.

1023-8883/01/0300-0089$19.50/0

the side chains and the chemistry of the head and tail groups can be modified much in the same manner as for the model lubricant alkanethiols or silanes [7–11]. In this paper, we use a hydrophilic silicon oxide substrate because, like mica, it is atomically flat and interacts with the transferred film via hydrogen bonding. Unlike metallic substrates, the thick thermally-grown oxide layer (80 nm) of the silicon substrate prevents quenching of the optical excitations. The weaker hydrogen-bonding, relative to the strong covalent bonding of thiol linkages to gold [11], allows for greater molecular motion about the backbone (discussed below), yet is sufficient for robust, good quality films. Mica offers the same qualities as the silicon oxide, along with possible ionic bonding to K^+ impurities.

The intense optical absorption characteristic of PDA, and of conjugated polymers in general [12–14], is caused by the excitation of π electrons in the extended linear backbone. Both absorption and fluorescence (if any) in the visible region tend to be highly polarized along the backbone direction. We have shown that the large domains of crystalline alignment exhibit strong polarization extinction [5,7,15]. The blue-shift in the absorption spectra which characterizes the thermally-, chemically-, or stress-induced chromatic transition of PDA from the "blue" form to the "red" form is shown in figure 2. A very important feature of these PDA films is that the red form exhibits intense fluorescence (see dotted curve in figure 2), whereas the blue form does not. *Thus we are able to use fluorescence as an optical signature of the mechanochromism, thermochromism [6], etc.* The fluorescence can be detected simultaneously by using a near field scanning optical microscope (NSOM) [5] or verified subsequent to AFM actuation with a conventional optical microscope. The NSOM is ideally the best tool because it can actuate and detect the fluorescence; however, AFM offers far superior topographical lateral and height resolution. Since the latter is more critical for determining the structural changes associated with the PDA mechanochromism we have taken that approach in this article.

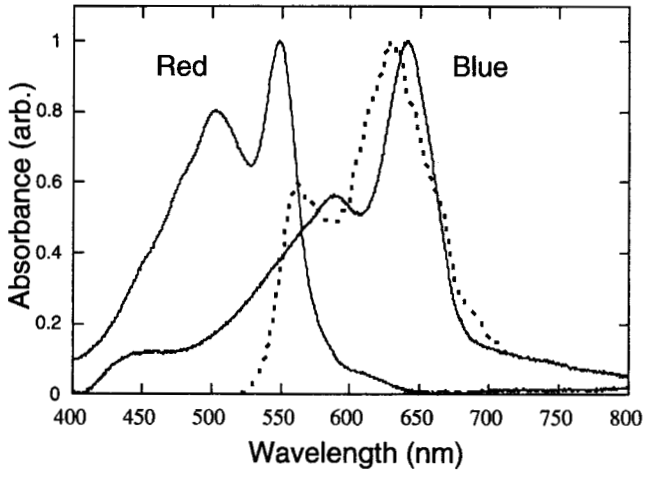

Figure 2. Visible absorption spectra of "blue" and "red" form PDA trilayer films; (- - -) is the fluorescence spectrum of the red form. The blue form does not fluoresce.

The blue-shift of the absorption in going from the blue to the red form is not fully understood, but is generally associated with "strain" imposed onto the conjugated backbone by the side chains [16]. As depicted in the highly schematic figure 3, the blue form is thought to be in the planar all-*trans* geometry, where the side chains are in the same plane as the backbone. This geometry permits extended, continuous π overlap or "conjugation length" [17–20]. Out-of-plane conformations in the side chains disrupt the π overlap which shortens the conjugation length and blue-shifts the absorption spectrum to that of the red form (figure 3). Note that out-of-plane rotation of the side chains requires possible rupture and reformation of the surface bond; thus strong covalent bonding to the substrate may hinder this rotation. The exact correlation between the conformational geometry and the electronic structure is not known. We address this problem by using a molecular dynamics (MD) simulation followed by electronic structure calculations. In this preliminary effort, we use twelve repeating unit energy-minimized oligomers of PDA on which we perform the MD. The resulting conformational changes in the backbone, particularly dihedral angles induced by side chain movement, are then correlated with the calculated electronic structure and absorption spectra. In this way, we are able to estimate minimum conformational changes for color shifts.

In our earlier study of mechanochromism in PDA [5], we presented results consistent with the notion of side chain rotation out of the backbone plane. However, that study was restricted to *trilayers*, since LB monolayers of the 10,12-pentacosadiynoic acid monomer precursor are not stable on a pure water subphase. We found that the shear-induced blue-to-red transformations were complicated by the removal of the top bilayer, revealing a seemingly "flattened" monolayer underneath. Thus molecular-scale aspects of conformation changes in the transformation were obscured by the trilayer geometry. It became clear that stable *monolayer* films were required to simplify characterization of the transformation. Since then, we have been able to produce stable monolayers by synthesizing the monomer N-(2-ethanol)-10,12-pentacosadinamide [7] (figure 1(A)). The monolayer stability is due to inter-chain H-bonding at

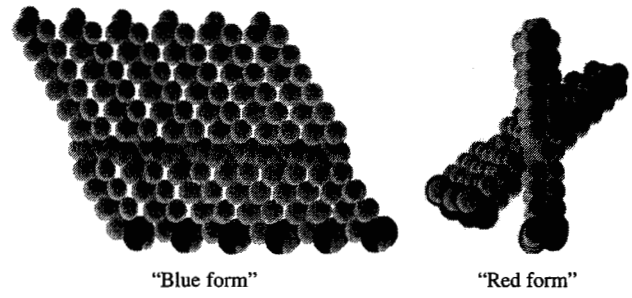

Figure 3. Highly schematic model for the blue and red PDA forms. The planar "blue" form at left has unbroken π-electron overlap and a full conjugation length. At right, the out-of-plane side chain rotation has broken the π-electron overlap in the "red" form, reducing the conjugation length.

the head groups. In this report, we thus describe evidence of side chain rotation actuated by AFM probe tips.

2. Methods

2.1. Sample preparation

Si substrates with 80 nm thick thermally-grown oxide were cleaned in organic solvents followed by a 50/50 mixture of 30% H_2O_2 and concentrated H_2SO_4 for 20 min at 100 °C, then immediately rinsed and stored in pure water before transfer to the LB trough. AFM images indicated very little observable contamination and verified that the substrates were extremely flat, with <2 Å RMS roughness. Just prior to monolayer spreading, the substrates were removed from water storage and completely immersed into the trough subphase, minimizing exposure to air. The Si substrate was seated horizontally approximately 1 mm below the subphase surface.

PDA monolayers were prepared via UV polymerization on the LB trough that rests on a vibration isolation table inside a class 100 clean room. The pure water subphase had a resistivity greater than 18 MΩ cm and was held at a temperature of 15 ± 1 °C. The monomer N-(2-ethanol)-10,12-pentacosadinamide (structure (A) in figure 1) was synthesized as described elsewhere [7] and dissolved in 50% chloroform/benzene for dropwise spreading on the subphase. All films were equilibrated for 20 min at 20 mN/m, prior to UV light exposure from a pair of Hg pen lamps whose output is dominated by the 254 and 365 nm lines. To produce a uniform blue film, the pen lamps were fixed 15 cm from the compressed monolayer (23 μW/cm^2) and switched on for 30 s. Horizontal transfer of the blue films was accomplished by slowly lowering the polymerized film onto the parallel Si substrate by draining the trough. Samples were dried in clean room air and stored in a dark, nitrogen-purged container. More details may be found in [7].

2.2. Atomic force microscopy, fluorescence microscopy

The AFM (Multimode Nanoscope IIIA, Digital Instruments) was operated in contact mode under ambient conditions with a single silicon nitride cantilever and tip. We used the nominal force constant of 0.06 N/m for the calculated loads. More scanning details are discussed in section 3.1. To verify that the PDA blue form was converted into the fluorescent red form, samples were removed from the AFM and placed under a Leitz fluorescence microscope that used 520–550 nm excitation and a 590 nm long-pass filter. An example of this method is shown in figure 4.

2.3. Molecular dynamics and quantum calculations

The molecular mechanics (MM) and molecular dynamics (MD) simulations were performed with PolyGraf software (Version 3.21) using a Dreiding II force field for atomic interactions. The dielectric constant was set to 2.64, and charges were assigned using the charge equilibration method. A canonical MD simulation using the Hoover formalism was then setup for a total run time of 500 ps with the temperature set at 300 K. Following the MM and MD calculations, the electronic properties of the conjugated backbone in its various configurations at selected intervals (e.g., 80, 100, and 128 ps) were calculated using ZINDO/S semi-empirical methods on the HyperChem 5.02 software package.

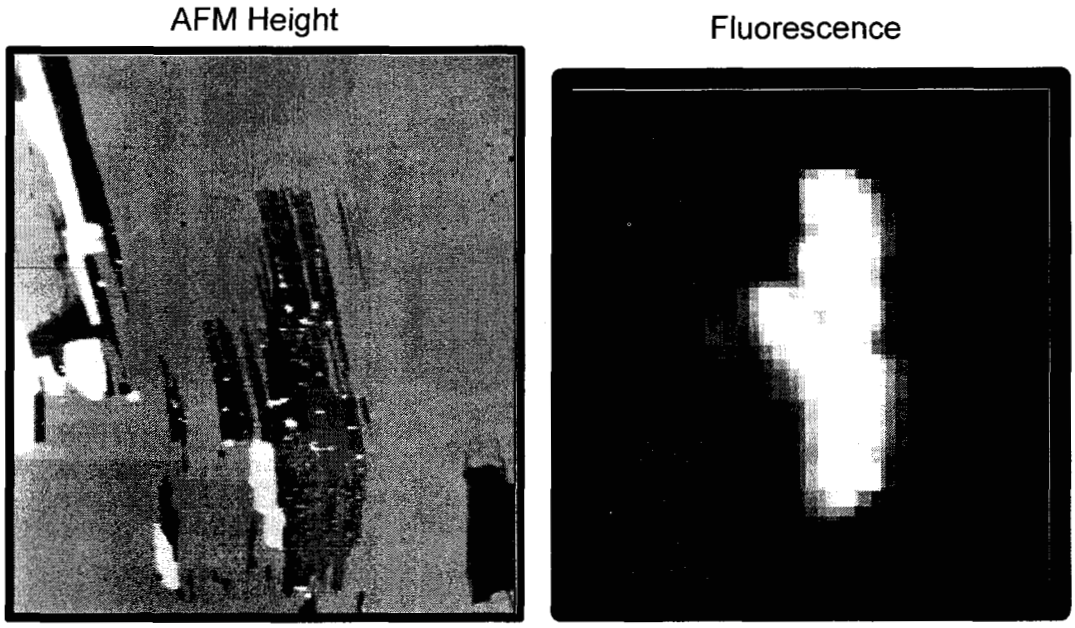

Figure 4. Left side, 10 × 10 μm^2 topographic AFM image showing tip-induced conversion of the blue form into the fluorescent red form of PDA. Note that the red region appears lower than the surrounding blue region. Right side, fluorescence microscope image of same region. From [5].

3. Results

3.1. AFM-induced mechanochromism of PDA monolayer

In this section, we present AFM images that are representative of the mechanically-induced blue-to-red transformation of the PDA monolayer. They provide us with fairly detailed structural information concerning the transformed regions, how they differ from the initial blue regions, and insight into how the "mechanochromism" takes place. In all cases, the transformation is irreversible, even after several weeks. Other than the transformation, we saw no evidence for monolayer instability or AFM-induced damage to the films.

We show in figure 5 the 1×1 μm^2 height and friction AFM images of an initially blue PDA monolayer (near a bare silicon oxide defect) that was in the process of being transformed into a red region. The transformation only occurred with sliding contact between the tip and sample, and took place during repeated scanning (>30 scans) at an estimated load of 6 nN and scan rate of 4.5 Hz. Imaging at very low loads (0 to −20 nN) and a 3 Hz rate, in the absence of significant adhesion, allows us to image the sample without inducing further transformation. The rate of growth of the red areas proceeds faster at larger loads; however, variation from sample to sample and even within one sample makes it difficult to quantify the exact load dependence of the transformation rate.

The transformed (red) regions, particularly in the friction image, reveal the backbone direction (indicated by the arrows) via striations that may be due to uneven packing density of the individual backbones [15]. Note that the scan direction is almost normal to the backbone direction in the upper region, which appears to have transformed to a greater extent (probably faster) than the lower region of the image. In most cases, the transformation proceeds most rapidly when the sliding (fast scan) direction is perpendicular to the backbone direction. Usually, it will not proceed at all when the fast scan direction is parallel to the backbone direction. Thus, *shear forces are required.* These observations are consistent with the shear-force anisotropy that was observed to be a function of chain orientation (highest forces being perpendicular to chain direction) for PDA monolayers on mica [15] and gold [21]. We note a factor of three in the ratio between high and low friction forces (for sliding perpendicular and parallel to the backbones, respectively). Unfortunately, our cantilever in the present work was not calibrated for quantitative shear force measurement. However, we do not expect the shear forces to differ appreciably from the AFM results reported by Mowery et al. [21], for PDA monolayers on gold, where the anisotropic shear forces were in the range 10–35 nN for loads below 20 nN.

Defects in the blue film such as the bare SiO_2 area assist significantly in the initial formation and growth of the red domains. The red regions appear to nucleate at the edge of the hole. In general, we find the growth of the red domains is strongly anisotropic, with preferential growth along the backbone direction. Furthermore, we find that the transformation may propagate along the backbone direction *beyond* the region where shear stress has been applied.

From the molecular modeling calculations (below) we estimate that the head-to-tail distance of the all-*trans* PDA (figure 1) is approximately 31.7 Å. AFM measurements under light imaging loads (0 to −20 nN) determined a blue-form PDA film thickness of 27 ± 3 Å. Thus the nominal molecular tilt angle of the blue film is $30° \pm 10°$, which is consistent with previously reported values of multilayer films [22,23]. The blue regions in figure 6 are 22 ± 2 Å thick ($45° \pm 5°$ nominal tilt) and the transformed red regions are 9 ± 0.9 Å

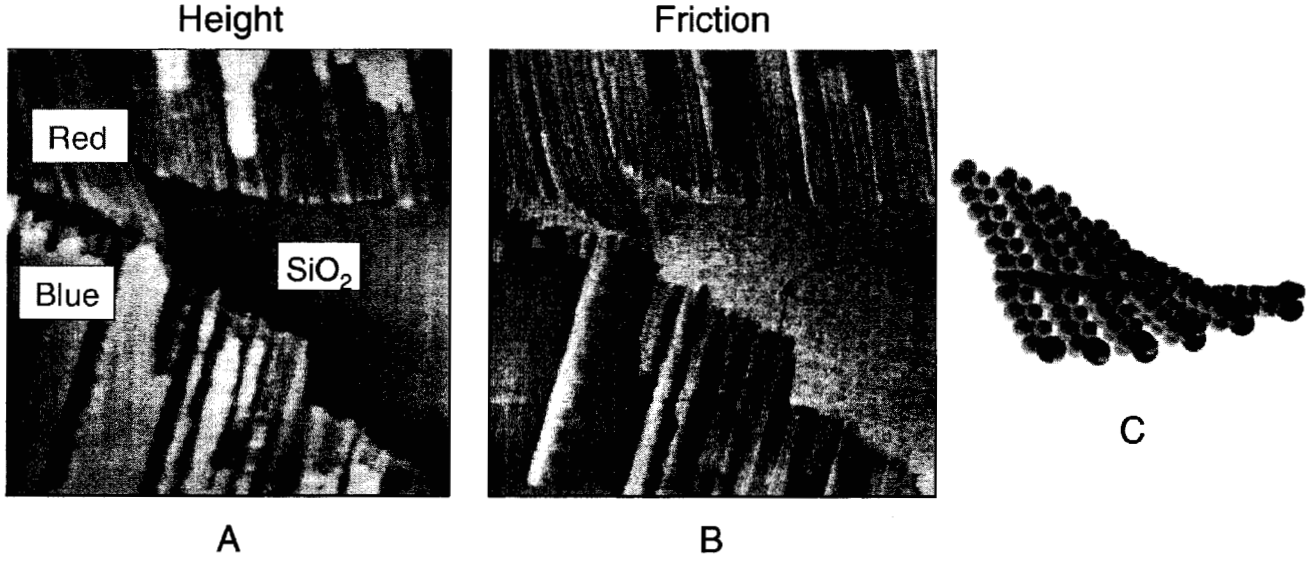

Figure 5. Height (A) and friction (B) images (1×1 μm^2) of region that was transformed under AFM shear forces. Arrows indicate backbone directions. The fast scan direction is along the x-axis. The original blue (brightest in (A), darkest in (B)) and transformed red regions are labeled as well as the bare substrate (darkest in (A), brightest in (B)). The heights of the blue and red areas relative to the substrate are 22 ± 2 and 9 ± 0.9 Å, respectively. (C) Schematic representation of blue-to-red transformation.

thick (74° ± 2° nominal tilt). *Thus it appears that the side chains are being pushed towards the substrate by the tip as it scans perpendicular to the backbone direction.* We depict this schematically in figure 6(C). It is important to note that the morphology of the mechanically-transformed red region appears to be different from the closely-packed, upright morphology of thermally-transformed red multilayer films [22] or photochromic red monolayers made on the LB trough with excessive UV exposure [7,15]. However, all three red forms have identical fluorescence spectra and comparable emission intensities. This leads us to conclude that neither the overall polymer orientation with respect to the substrate nor the packing density significantly influence the optical properties of the red films. Instead, we believe that it is the local strain on the backbone by the (re-oriented) side chains that is the important aspect.

The friction in the red transformed regions increases up to 100% relative to the blue regions. Moreover, the lowest red PDA regions have the highest friction. Thus the friction appears to correlate directly with the compression or re-orientation of the side chains towards the surface. Much of the friction in the transformed regions is most likely due to increased disorder of both the side chains and the backbone packing. However, the re-orientation will also expose the side chain methylene ($-CH_2-$) groups and the conjugated backbone. Since these have a higher surface energy than the methyl (CH_3) tail groups [24], it is likely that a component of the higher friction is due to an increased adhesive interaction with the tip.

Since the AFM tip causes a re-orientation of the PDA side chains in the manner described above, more steric freedom is needed to accommodate the increased area per molecule. This is a primary reason why the transformation is facilitated near bare spots and defects. This can be seen in figure 6, where the backbone direction is parallel to the edge of the hole and almost perpendicular to the scan direction. Both aspects readily facilitated the conversion; we see growth of the red area along the backbone direction and perpendicular to it. The 1×1 μm^2 height and friction images were acquired *during* the transformation, thus they are "stills" from

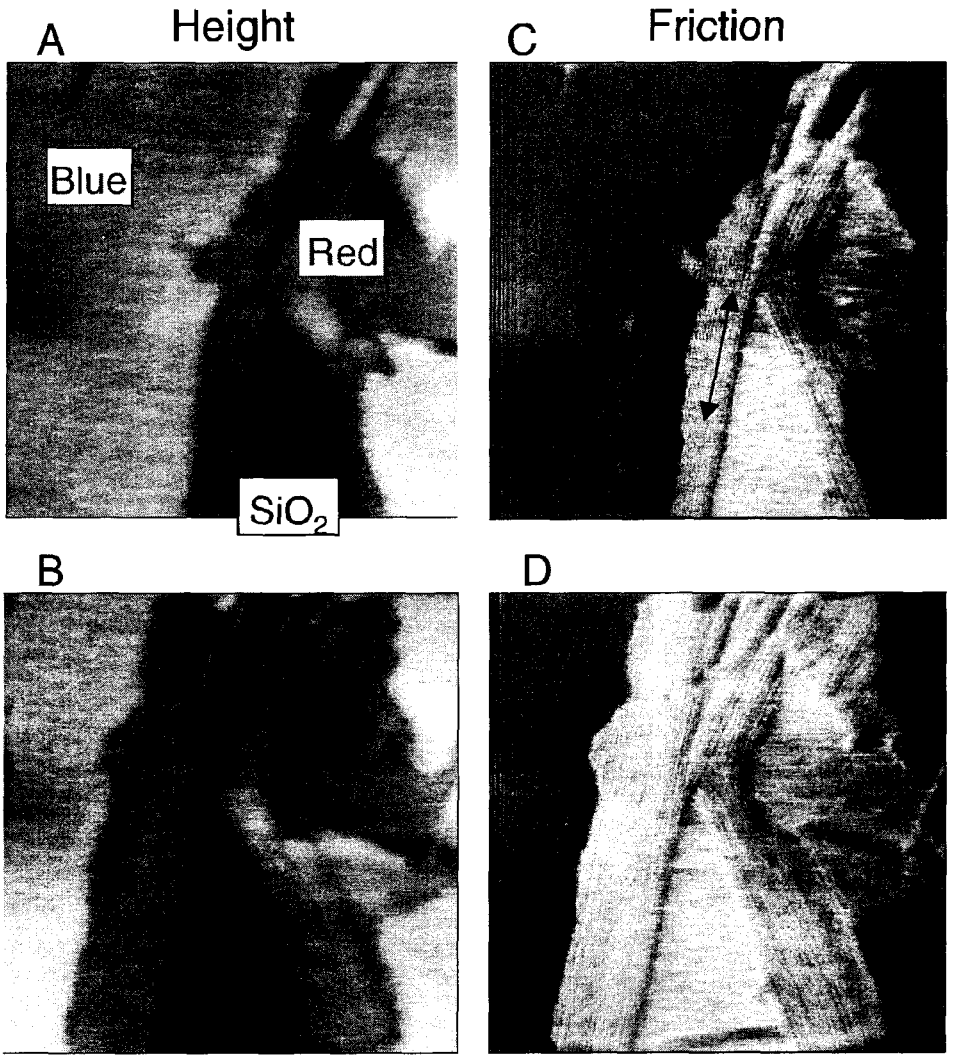

Figure 6. Consecutive height and friction images (1×1 μm^2) acquired *during* blue-to-red transformation by AFM shear forces. (C) and (D) were acquired 28 frames after (A) and (B) at scan rate of 4.5 Hz. The arrow indicates backbone direction and the blue, red and substrate areas are marked. See text for details.

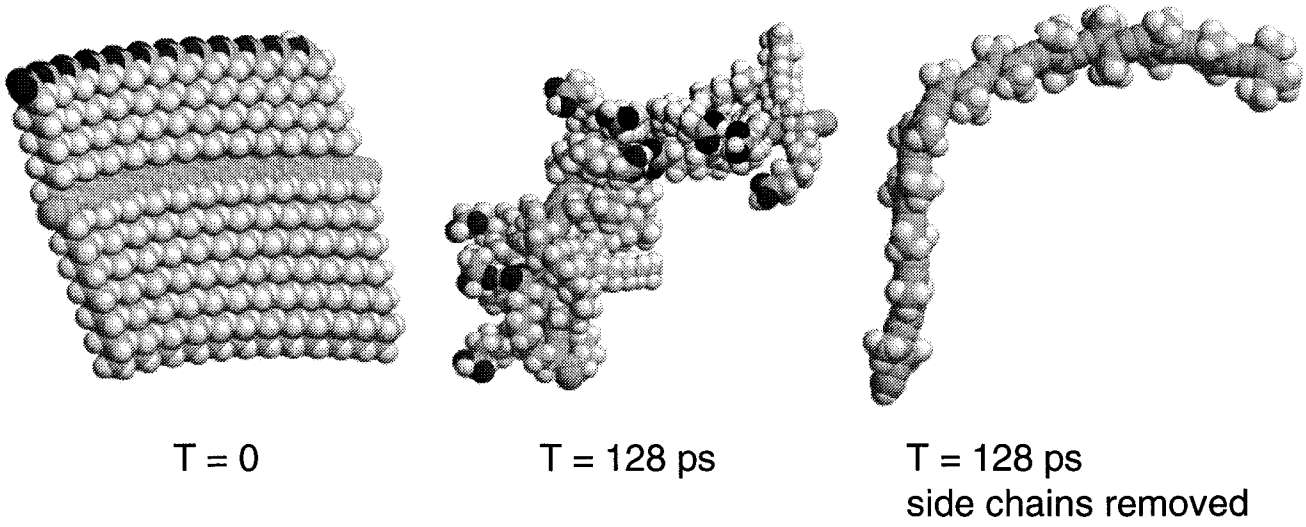

Figure 7. Left part, twelve-unit planar PDA oligomer ("blue" form) minimized by molecular mechanics (note head groups are on top) prior to MD simulation. Middle part, same oligomer after 128 ps of the MD simulation. Right part, same 128 ps structure with side chains "pruned" for quantum calculations. The clipping takes place *after* the simulation and is used to simply the quantum calculations.

a long sequence of images: (A) and (C) under a 6 nN load and scan rate of 4.5 Hz, while (B) and (D) were acquired 28 frames later under an increased load of 17 nN. The transformation rate was observed to increase with higher load, but eventually decreased (at the same higher load) as the red region progressed farther from the bare substrate. Thus the side chains were now sterically hindered from re-orienting at the same rate. Once again, the friction contrast is substantial between the red and blue regions.

3.2. Molecular mechanics and electronic structure calculations

The results presented above clearly indicate that the shear forces experienced by AFM tip are due to an interaction with the side chains that alters their orientation with respect to the original plane of the all-*trans* "blue" form. Out-of-plane rotations of the side chains will disrupt the π-orbital overlap or "conjugation length," causing a blue shift of the absorption. One of the primary motivations in using the PDA monolayers is the potential use of its mechanochromism as an optical transducer of disordering, film defects, or shear forces. In this section, we briefly discuss our initial efforts to use MD and electronic structure calculations to determine quantitatively what the minimum angle changes are that result in the absorption shifts.

Two oligomers with differing headgroups were examined in the MD simulations. The first one was terminated with the carboxyl head groups of 10,12-pentacosadiynoic acid, while the other was terminated with the amide head groups of N-(2-ethanol)-10,12-pentacosadinamide (shown in figure 1(A)). The latter is expected to exhibit hydrogen bonding between head groups. Each all-*trans* PDA oligomer was made twelve units long (i.e., twelve sets of side-chains above and below the backbone), and minimized by molecular mechanics where it remained planar and ordered. This is shown at left in figure 7. During the 500 ps time scale of the 300 K MD simulation, the side chains of the oligomers became highly disordered and the backbones developed bends due to out-plane side chain rotations (see middle of figure 7). These thermal fluctuations of the isolated oligomers are expected, whereas in a close-packed film, the polymers would be more stabilized by their neighbors. However, for the present purposes, the fluctuations allow us to quantitatively sample backbone geometries and corresponding electronic structures for various conformations.

Structural analysis was performed on the molecular geometries at fixed intervals (<0.25 ps) during the 500 ps simulation. For the structure at each time interval, eleven dihedral angles (between the twelve units in the chain) were calculated along the backbone. The dihedral angles were measured from one C=C double bond to the next, as shown below:

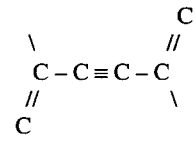

In the dihedral angles reported, the origin (0°) is set at what is traditionally defined as 180° since this is the starting (planar) configuration. This convention makes it easier to look at the deviations from planarity. The "average dihedral angle" is used as an index of overall deviation from planarity in the oligomer. The sign of the angles is unimportant, hence the average uses the absolute value.

In figure 8, we show the average dihedral angle vs. MD simulation time for the two oligomers with differing head groups. In both oligomers we see significant deviations from planarity early on in the simulation. The upper curve (A) is for the oligomer made from 10,12-pentacosadiynoic acid, which does not make stable PDA monolayers. The lower curve (B) is for the oligomer based on N-(2-ethanol)-10,12-pentacosadinamide, that does make stable PDA monolay-

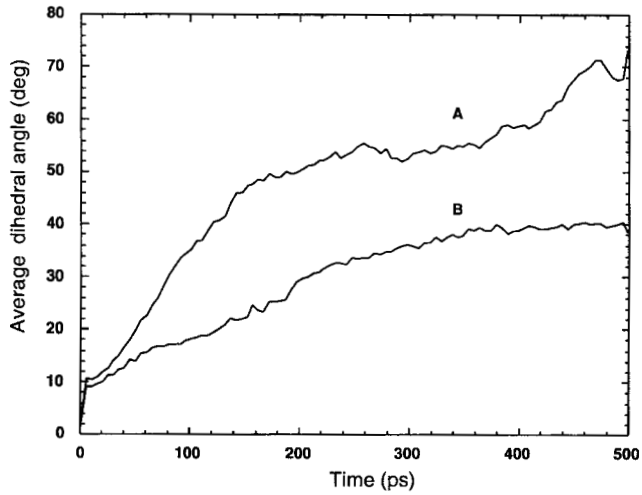

Figure 8. Calculated average dihedral angles vs. time from the molecular mechanics and dynamics simulation at 300 K. Curve (A) is for the twelve-unit oligomer with the COOH head group, and curve (B) is for the amide head group shown in figure 1(A) (see text).

ers. We see evidence of hydrogen bonding between the amide head groups in the smaller average dihedral angles at each time interval relative to the simulation for COOH head groups. Thus the hydrogen bonding not only stabilizes the monolayer on the LB trough, but it also tends to counteract out-of-plane side chain rotation.

After the MD simulation, some geometries (e.g., at 0, 80 and 200 ps), were selected for the quantum calculations on the conjugated backbone. To considerably shorten the time required for these calculations, all side groups were "clipped" off, leaving methyl groups in their place. Hydrogens added to the methyl carbons were minimized using molecular mechanics while holding the backbone and methyl carbon positions fixed. A bent and clipped oligomer is shown at right in figure 7. In figure 9, we show the calculated absorption spectra of oligomers selected from curve (A) of figure 8. (Once the oligomers are clipped it makes no difference which molecule was used for the quantum calculations. Curve (A) offers a bigger range of dihedral angles than curve (B).) For visualization purposes, the absorption spectra are generated from summing Lorentzian curves of oscillator strengths about the highest-occupied to lowest-unoccupied singlet transitions. Hence, the line shapes and widths are arbitrary. We also make no assignments concerning symmetry, so many of the transitions may be weakly allowed. Regardless, the important information presented here is the *blue-shift* in the spectra due the change in backbone π-orbital energies during the molecular dynamics simulation. One can see in figure 9 that there is a definite blue-shift with increasing average dihedral angle (values taken from curve (A) of figure 8). We also see that there is a rapid shift from $t = 0$ to 80 ps, followed by relatively no change after 200 ps. It is important to note that these spectra are instantaneous "snap shots" rather than averages, thus there can be large fluctuations in line position with time (e.g., see spectra at 200 ps).

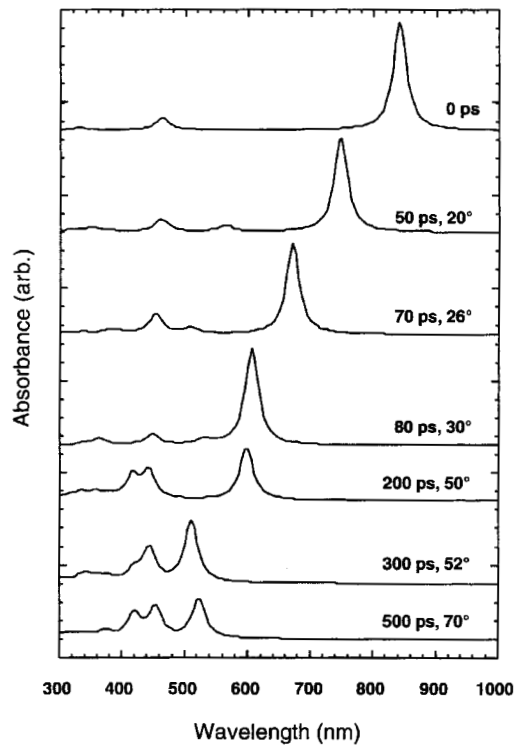

Figure 9. Absorption spectra from the quantum calculations for clipped oligomers at various times during the MD simulation. The arbitrary Lorentzian line shapes and widths are for visual purposes only. Also shown is the average dihedral angle from curve (A) of figure 8 for the oligomer at the specified time.

The blue-shifts in the spectra are caused by dihedral rotations of the side chains that break the π-orbital overlap and shorten the conjugation length. Two important questions arise: What critical angle is required to break conjugation in a way that shifts the absorption spectrum? What is the maximum conjugation length during the simulation for that critical angle? We try to answer these questions by using the index "conjugation length," which for a certain critical angle γ, we define as the longest backbone length (within the whole twelve-unit oligomer) that is not "broken" by an angle greater (absolute value) than γ. The results are shown in figure 10 for a few selected γ. We see that for $t < 5$ ps in the MD simulation there are some $<5°$ dihedral rotations. The conjugation (backbone) length between these $<5°$ rotations drops from the initial twelve units to four, followed by a gradual change to two units over the next 200 ps. However, if we compare this index to the spectral shifts in figure 9, we see that those shifts clearly have a different time dependence and must have required $\gamma \gg 5°$. *Thus we can rule out very small dihedral angles from our analysis.* In contrast, for $\gamma < 80°$, there is essentially no change in the conjugation length before 50 ps, yet we see significant spectral shifts in figure 9 before 50 ps. Thus we conclude that the conjugation is broken for dihedral angles smaller than 80°. (γ greater than 90° will tend to "re-form" conjugation as they approach 180°, and perhaps theoretically should not be counted as "breaking" the conjugation. In our computations, however, this effect was neglected since our dynamics

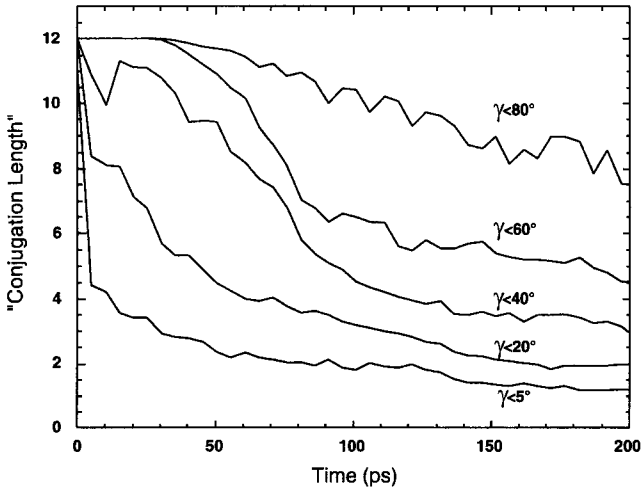

Figure 10. "Conjugation length" of oligomer vs. time during the MD simulation. The length, which for a certain critical angle γ, measures the longest backbone length (within the whole twelve-unit oligomer) present that is not "broken" by an angle greater (absolute value) than γ.

simulation did not go on for long enough for it to become significant.) For $20° < \gamma < 60°$, the analysis becomes some less obvious. If we assume that the shift is roughly linear from 0 to 80 ps, and rapidly levels off after $t = 80$ ps, then the "best fits" appear for critical angles γ in the range 40°–60°, and that the conjugation length for the "red form" is less than six units.

We conclude this section by noting that we can use the above analysis as a rough guide to morphological *changes* are required to observe mechanochromism. For the isolated twelve-unit oligomer, those average changes are 40°–60° side chain rotations at least once every six units. Clearly, a more detailed analysis is required, including longer oligomers, nearest-neighbor interactions, and substrate effects. However, we can conclude that very *small* changes in the blue form morphology are insufficient for mechanochromism, which is consistent with the AFM results discussed above, and consistent with the 18 kcal/mol activation energy required for trilayer thermochromism [6].

4. Conclusions

We have used AFM to actuate and characterize the "mechanochromism" of PDA monolayers on silicon oxide substrates. The blue-to-red transformation was analyzed in detail and found to be dependent on the shear forces exerted on the pendant side chains. Those shear forces perpendicular to the backbone direction were most effective in the transformation, which was also facilitated by defects and neighboring areas of bare substrate. Overall, the transformation was the result of significant side chain rotation towards the substrate. We presented preliminary modeling results on isolated twelve-chain oligomers that will help us correlate the molecular structure changes such as side chain rotation with the color changes of the PDA films. So far, we find that dihedral angle deviations from the blue planar form must be in the range of 40°–60°, every six units, in order to see shifts in the absorption spectra that compare with those observed experimentally. The irreversible nature of the chromatic conversion is somewhat limiting in its potential use as an *in situ* optical sensor. However, recent successes in reversibility in modified PDA vesicles [10] may lead to much more versatile and functional organic thin films.

Acknowledgement

RWC acknowledges the support of the Natural Sciences and Engineering Research Council of Canada. Sandia is a multiprogram laboratory operated by Sandia Corporation, a Lockheed Martin Company, for the United States Department of Energy under Contract DE-AC04-94AL85000.

References

[1] A. Ulman, *Introduction to Ultrathin Organic Films from Langmuir–Blodgett to Self-Assembly* (Academic Press, New York, 1991).
[2] L.H. Dubois and R.G. Nuzzo, Annu. Rev. Phys. Chem. 43 (1992) 437.
[3] D. Bloor and R.R. Chance, *Polydiacetylenes: Synthesis, Structure, and Electronic Properties* (Nijhoff, Dordrecht, 1985).
[4] R.A. Nallicheri and M.F. Rubner, Macromolecules 24 (1991) 517.
[5] R.W. Carpick, D.Y. Sasaki and A.R. Burns, Langmuir 16 (2000) 1270.
[6] R.W. Carpick, T.M. Mayer, D.Y. Sasaki and A.R. Burns, Langmuir 16 (2000) 4639.
[7] D.Y. Sasaki, R.W. Carpick and A.R. Burns, J. Colloid Interface Sci. (2000), in press.
[8] D.H. Charych, J.O. Nagy, W. Spevak and M.D. Bednarski, Science 261 (1993) 585.
[9] S. Okada, S. Peng, W. Spevak and D. Charych, Acc. Chem. Res. 31 (1998) 229.
[10] U. Jonas, K. Shah, S. Norvez and D.H. Charych, J. Am. Chem. Soc. 121 (1999) 4580.
[11] M.D. Mowery and C.E. Evans, J. Phys. Chem. B 101 (1997) 8513.
[12] Z.G. Soos, D.S. Galvao and S. Etemad, Adv. Mater. 6 (1994) 280.
[13] F. Garnier, Acc. Chem. Res. 32 (1999) 209.
[14] J.-L. Bredas, J. Cornil, D. Beljohnne, D.A. Dos Santos and Z. Shuai, Acc. Chem. Res. 32 (1999) 267.
[15] R.W. Carpick, D.Y. Sasaki and A.R. Burns, Tribol. Lett. 7 (1999) 79.
[16] H. Eckhardt, D.S. Boudreaux and R.R. Chance, J. Chem. Phys. 85 (1986) 4116.
[17] K.S. Schweizer, J. Chem. Phys. 85 (1985) 1156.
[18] K.S. Schweizer, J. Chem. Phys. 85 (1985) 1176.
[19] V. Dobrosavljevic and R.M. Stratt, Phys. Rev. B 35 (1987) 2781.
[20] G. Rossi, R.R. Chance and R. Silbey, J. Chem. Phys. 90 (1989) 7594.
[21] M.D. Mowery, S. Kopta, D.F. Ogletree, M. Salmeron and C.E. Evans, Langmuir 15 (1999) 5118.
[22] A. Lio, A. Reichert, D.J. Ahn, J.O. Nagy, M. Salmeron and D.H. Charych, Langmuir 13 (1997) 6524.
[23] R.F. Fischetti, M. Filipkowski, A.F. Garito and J.K. Blasie, Phys. Rev. B 37 (1988) 4714.
[24] J.N. Israelachvili, *Intermolecular and Surface Forces* (Academic Press, London, 1992).

Large friction anisotropy of a polydiacetylene monolayer

R.W. Carpick [a], D.Y. Sasaki [b] and A.R. Burns [a,*]

[a] *Sandia National Laboratories, Surface and Interface Sciences, Albuquerque, NM 87185-1413, USA*
E-mail: aburns@sandia.gov

[b] *Sandia National Laboratories, Organic Materials Aging and Reliability, Albuquerque, NM 87185-1407, USA*

Friction force microscopy measurements of a polydiacetylene monolayer film reveal a 300% friction anisotropy that is correlated with the film structure. The film consists of a monolayer of the red form of N-(2-ethanol)-10,12-pentacosadiynamide, prepared on a Langmuir trough and deposited on a mica substrate. As confirmed by atomic force microscopy and fluorescence microscopy, the monolayer consists of domains of linearly oriented conjugated backbones with pendant hydrocarbon side chains above and below the backbones. Maximum friction occurs when the sliding direction is perpendicular to the backbones. We propose that this effect is due to anisotropic film stiffness, which is a result of anisotropic side chain packing and/or anisotropic stiffness of the backbone itself. Friction anisotropy is therefore a sensitive, optically-independent indicator of polymer backbone direction and monolayer structural properties.

Keywords: atomic force microscopy, friction force microscopy, friction anisotropy, friction asymmetry, nanotribology, polydiacetylene, LB films, directional dependence, fluorescence

1. Introduction

Recent fundamental studies of friction at the atomic or molecular level have revealed behavior distinct from common macroscopic experience [1], such as violation of Amonton's Law [2], adhesion hysteresis [3], and dependence upon sliding velocity [4] and direction [5–13]. The dependence of friction upon sliding direction arises from structural properties of the materials in contact. As such, friction measurements can reveal specific structural properties, such as molecular or crystallographic orientation, which may not be seen in topographic images. Such experiments can then elucidate how friction is fundamentally related to these structural properties. Furthermore, anisotropic friction forces can be exploited for the purpose of nanofabrication [9] by providing preferred pathways for interfacial sliding of nanocomponents.

Friction anisotropy refers to the variation of friction with the relative orientation angle between sliding surfaces, or with the sliding direction itself. For example, Hirano and Shinjo [5] observed frictional anisotropy between bare mica surfaces in a surface forces apparatus. In one experiment, they fixed the sliding direction and varied the relative orientation of the crystallographic axes (the misfit angle) of the opposing surfaces, observing maximum friction when the axes were aligned (commensurate). In another experiment, they fixed the crystal axes in the aligned orientation while the sliding direction was varied, observing lowest friction when the sliding direction coincided with the primitive vectors of the surfaces. Using the atomic force microscope (AFM), Sheehan and Lieber [9] demonstrated that MoO_3 islands on a MoS_2 substrate could be displaced by the AFM tip, but only along preferred directions that were determined by the given alignment of the MoO_3 and MoS_2 crystal axes. In these two cases, friction anisotropy was correlated with the relative crystallographic orientation of the sliding interface. Friction anisotropy has also been observed between AFM tips and surfaces with molecular groups tilted with respect to the surface normal, such as ferroelectric materials [7,8] and lipid monolayers [11]. In addition, these groups also observed *friction asymmetry*, which refers to a change in friction when the sliding direction is changed by 180° (i.e. from back to forth).

In this study, we examine friction anisotropy of a polydiacetylene monolayer film, polymerized from the monomer N-(2-ethanol)-10,12-pentacosadiynamide (PCEA). In general, ordered diacetylene molecular layers can be formed by Langmuir–Blodgett (LB) techniques [14,15] or self-assembly [16–18]. The molecular film consists of pendant methylene side chains attached to either side of a polymerized diacetylene backbone that is oriented parallel to the substrate. A PCEA monolayer is illustrated in figure 1. Polydiacetylenes are an important class of organic materials as they exhibit strong optical absorption that is altered by thermal annealing [19,20], mechanical stress [21–23], or chemical and biological attachment [24–26]. These transitions are correlated with changes in molecular conformation that are not fully understood [14]. Recently we have observed a mechanically-induced color transition in polydiacetylene at the nanometer-scale using scanning probe microscopy [27].

2. Experimental

Details of our sample preparation will be described elsewhere [27,28]. Briefly, the diacetylene amphiphile N-(2-ethanol)-10,12-pentacosadiynamide (PCEA) was prepared by coupling ethanolamine with 10,12-pentacosadiynoyl chloride in tetrahydrofuran and triethylamine. The acid

* To whom correspondence should be addressed.

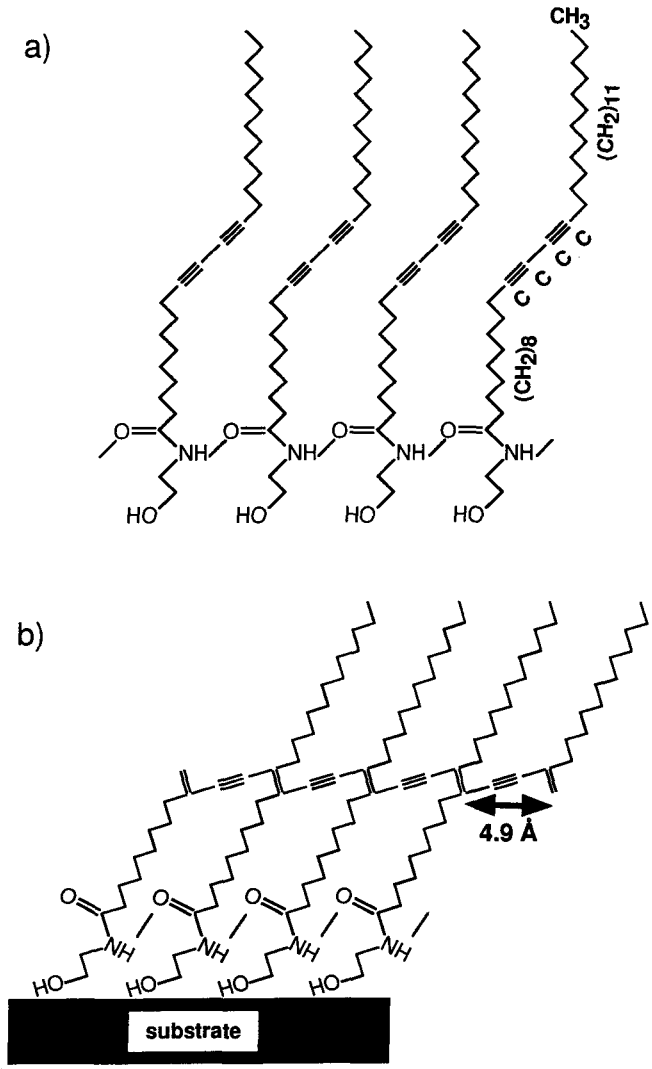

Figure 1. (a) PCEA monomer and (b) polymer showing the ethanol-amine head group bound to the substrate. Dotted lines represent possible hydrogen bonding interactions. The polymer backbone repeat unit of polydiacetylene is expected to be 4.9 Å.

chloride was prepared from 10,12-pentacosadiynoic acid (Farchan/GFS Chemicals, Powell, OH) using oxalyl chloride in methylene chloride. PCEA was isolated by flash column chromatography on silica gel (25% ethylacetate/hexanes, $R_f = 0.23$). Although the product was pure white immediately after isolation, upon standing in the freezer for a day the crystals became tinted with a blue color.

Langmuir monolayers of the PCEA amphiphile were prepared and polymerized by UV light on the water surface. The circular Langmuir trough (Nima, Coventry, UK) was situated on a vibration isolated table inside a class 100 clean room. The subphase used was deionized water with a resistivity of > 18 MΩ cm (Barnstead Nanopure system, Dubuque, IA) kept at a temperature of 15 ± 0.2 °C. Freshly-cleaved muscovite mica were situated horizontally 1–2 mm below the water surface prior to monolayer spreading. A 50% chloroform/benzene solution of PCEA was prepared and run through a 0.2 micron filter to remove small traces of red polymer in solution prior to deposition on the water surface. The monolayer was compressed at a rate of 100 cm^2/min to a pressure of 20 mN/m, corresponding to a molecular area of ca. 20 $Å^2$/molecule. Unlike 10,12-pentacosadiynoic acid films, which form trilayers under identical conditions, the PCEA formed a stable monolayer with a collapse pressure of ca. 35 mN/m. All films were equilibrated for 20–30 min at 20 mN/m, prior to UV light exposure (254 nm) with a pair of Hg pen lamps (Oriel, Stratford, CT) spaced 8 cm apart. The lamps were situated 10 cm above the monolayer and the exposure time was 30 s. The polymerized monolayer was deposited on the underlying mica by slowly lowering the water level in the trough by aspirating water away. The mica substrate was then taken out of the trough using forceps and allowed to dry in clean room air and then stored in a dark, nitrogen-purged container. Figure 1 shows the proper orientation of the monolayer to the mica substrate with the hydrophilic head group oriented to the interface and the hydrophobic tails pointed away.

Microscopic sample fluorescence was recorded using a Leitz optical fluorescence microscope equipped with dichroic beam filters and polarized white light from a xenon lamp. A CCD camera was used to capture the field of view for the images presented here. A Nanoscope IIIA atomic force microscope (AFM) (Digital Instruments, Santa Barbara, CA) operating in contact mode was used to obtain topographic and friction force images. Measurements with the AFM were acquired under laboratory ambient conditions. The scan rate was 3 Hz (= lines/s) unless otherwise noted. A single silicon nitride cantilever (Digital Instruments, Santa Barbara, CA) with a nominal normal force constant of 0.06 N/m was used for all measurements. Friction measurements were obtained in conventional fashion by scanning the cantilever perpendicular to its long axis at constant load while recording lateral-force-induced twisting, and then calculating the difference between "trace" and "retrace" scans ("friction loop width"). Because of the inherent difficulty in calibrating the lateral force response of AFM cantilevers [29], lateral forces are reported in raw units (signal volts). The results presented in this paper refer to *relative* quantitative changes in friction forces.

It is crucial to ensure that the AFM probe tip is not geometrically anisotropic, otherwise tip-induced friction anisotropy may result, providing misleading results. To characterize the tip geometry, we used "inverse imaging" [2,29] by scanning the tip at the lowest possible load over a substrate consisting of a microfabricated array of silicon tips with a <10 nm curvature radius (NT-MDT, Moscow, Russia). The high resolution contact mode image then represents a convolution of this small feature with the AFM tip. Since the AFM tip has significantly larger curvature than 10 nm, the observed profile is dominated by features of the AFM tip. Several members of the nanotip array are compared to verify that the observed profile is reproducible and not affected by anomalous features of a particular nanotip. We emphasize that the *majority* of AFM tips we

characterized possessed anisotropic shapes, double tips and other unsuitable structures. The AFM tip selected for this study consisted of a single, symmetric protrusion within the measurement error. Specifically, we measured orthogonal cross-sections of the last 2 nm of the tip, giving effective curvature radii of 27 ± 3 nm and 32 ± 4 nm. While it is possible that this method may not uncover small anisotropic AFM tip features at the atomic scale, this method allows us to avoid grossly anisotropic tips. To our knowledge, this is the only study of friction anisotropy where the AFM probe tip was characterized in this fashion.

3. Results

3.1. Polarized fluorescence microscopy

Polarized fluorescence microscopy reveals that the PCEA film is strongly fluorescent and organized into crystalline domains (figure 2). The domains range in size from 10–100 μm and possess irregularly-shaped boundaries. Furthermore, the film coverage is nearly complete, indicating that a high quality film is produced on the trough, and is not seriously disrupted by the transfer process. The fluorescence intensity of each domain varies as the incident polarization angle is changed, and can be almost completely extinguished. Both the absorption and emission dipole of polydiacetylene is known to be aligned along the backbone direction [30–32]. Thus, the polymer backbones are highly oriented within individual domains. Fluorescence intensity variations within the domains are observed in the form of linear striations. The direction of these striations coincides with the polarization angle that produces maximum fluorescence. Therefore, the striations reveal the backbone direction within each domain. The striations may be produced by variations of the film density, which will be discussed further below.

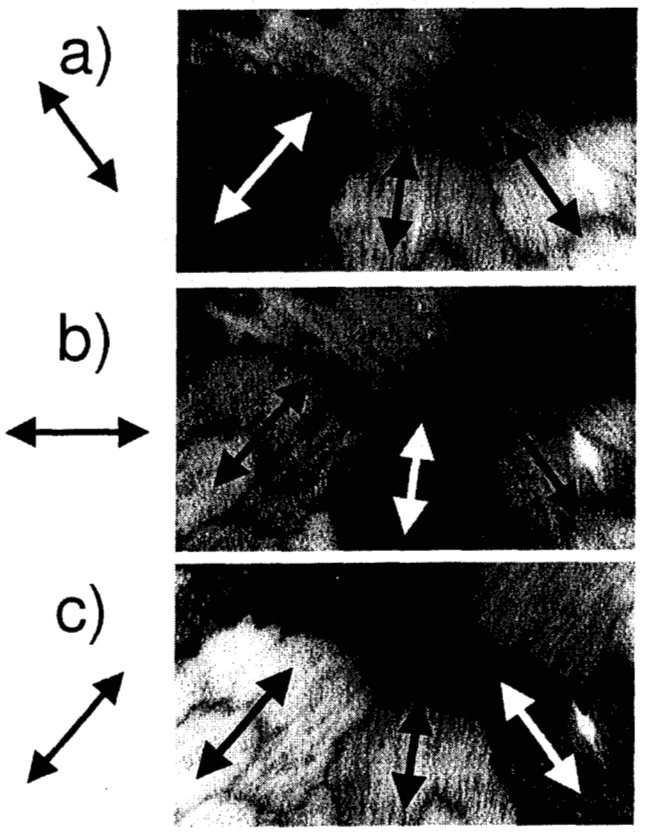

Figure 2. 170×100 μm^2 polarized fluorescence microscopy images. The arrows on the left represent the polarization direction, which is roughly (a) $-45°$, (b) $0°$ and (c) $+45°$. The polymer backbone direction of three domains is indicated by the other arrows. High fluorescence occurs when the polarization is aligned with backbone direction, and is dramatically reduced when the polarization is nearly orthogonal to the backbone direction (white arrows).

3.2. Friction anisotropy

AFM images (figure 3) reveal film structure that is consistent with the fluorescence microscopy. The 50×50 μm^2 friction image reveals the individual domains, as the friction force varies substantially from one domain to the next, and is nearly uniform within each domain. The topographic image reveals a flat film with some material, 2–4 nm high, situated at a significant fraction of the domain boundaries. Occasionally a small crack in the film revealing the mica substrate is found. This allows measurement of the film height, which we observe to be 2.3 ± 0.3 nm, corresponding to a monolayer with an average tilt of $\sim 30°$. Topographic and friction images (500×500 nm^2) within a single domain reveal parallel striations of varying width and uniform direction (figure 4), similar to previous reports [20,33]. The total height variation between these striations is ~ 2 Å. These striations are clearly associated with the direction of the underlying polymer backbone, and allow us to accurately determine the relative angle between the sliding direction and the backbone direction. Herein this angle will be referred to as the "domain orientation", where $\pm 90°$ ($0°$) represents scanning perpendicular (parallel) to the backbone orientation.

Friction was measured as a function of angle for 14 separate domains with a range of orientations (figure 5). At least three measurements were acquired on different regions of each domain. The values plotted represent the average of the difference between trace and retrace 1×1 μm^2 lateral force images. Friction is lowest when sliding parallel to the backbones, and maximal when sliding perpendicular, representing an increase of $\sim 300\%$. For all measurements, zero externally-applied load was used. The adhesion force, determined from force–distance curves on every domain, was measured to be 35 ± 7 nN, and had no correlation with domain orientation.

3.3. Friction asymmetry

We also attempted to observe friction asymmetry, which could possibly be induced by the molecular tilt of the pendant methylene side chains [11]. Friction asymmetry is manifested by an offset of the friction loop from zero

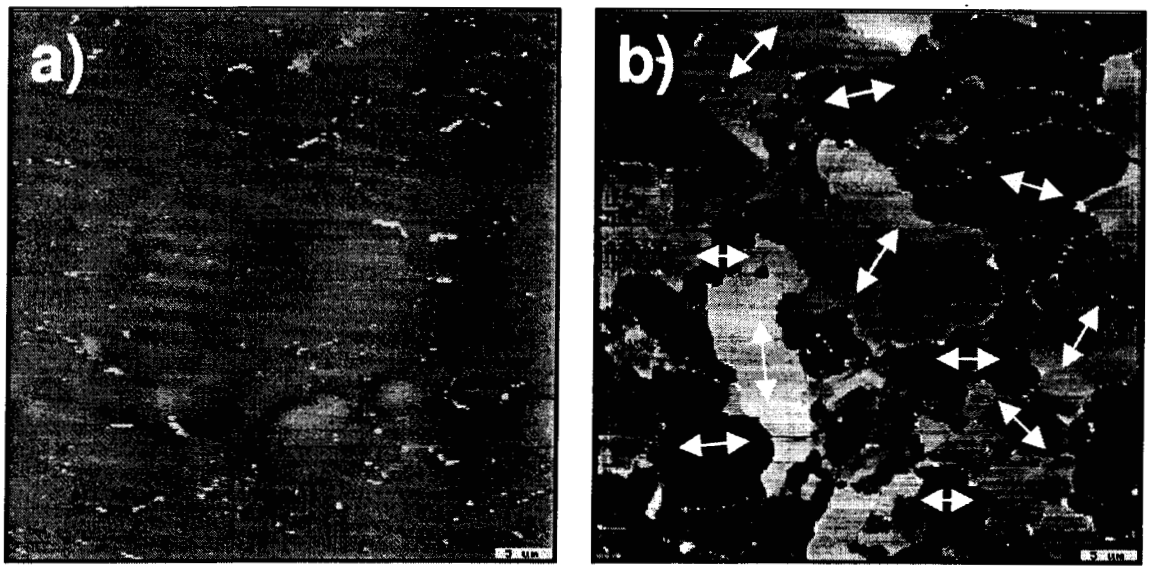

Figure 3. $50 \times 50\ \mu m^2$ AFM images of the PCEA monolayer. (a) Topography. (b) Friction. The topography is flat to within 2–3 Å, with the exception of some material piled up at a fraction of the domain boundaries. The friction image reveals the different domains. The white arrows indicate the domain orientation, determined from higher resolution images like those in figure 4.

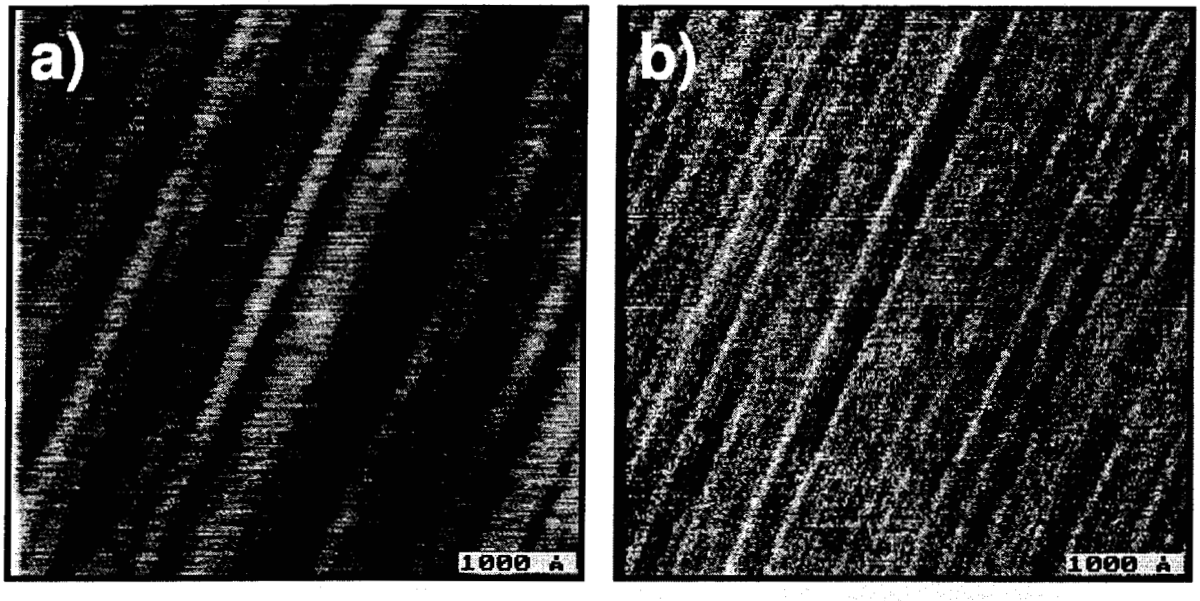

Figure 4. $500 \times 500\ nm^2$ images within a single domain. (a) Topography. (b) Friction. Linear striations are observed, which reveal the backbone orientation. The topography image displays ~ 2 Å height variations between different striations. There is some variation in the friction signal as well, but the friction force is uniform to within $\sim 10\%$.

force [7,8,11]. However, the friction loop may be offset by instrumental artifacts such as misalignment of the deflection sensing components. If friction asymmetry is maximal for a particular domain orientation, it should be minimal for an orthogonal orientation [11]. Thus, we looked for a relative change in the center of the friction loop between neighboring domains with orthogonal orientations. As shown in figure 6, no effect is observed. However, there is significant spatial fluctuation in the lateral force signal. This fluctuation is an inherent property of the film, due to the striations described in figure 4, and obscures the observation of friction asymmetry below 10% of the maximum friction signal.

4. Discussion

4.1. Friction anisotropy

The observed friction anisotropy is clearly associated with the polymer backbone direction, as independently verified with topographic AFM images and polarized fluorescence microscopy. The angular dependence of the friction force F_f (figure 5) can be simply modeled by the following equation:

$$F_f = F_1 + F_2|\sin\theta|, \tag{1}$$

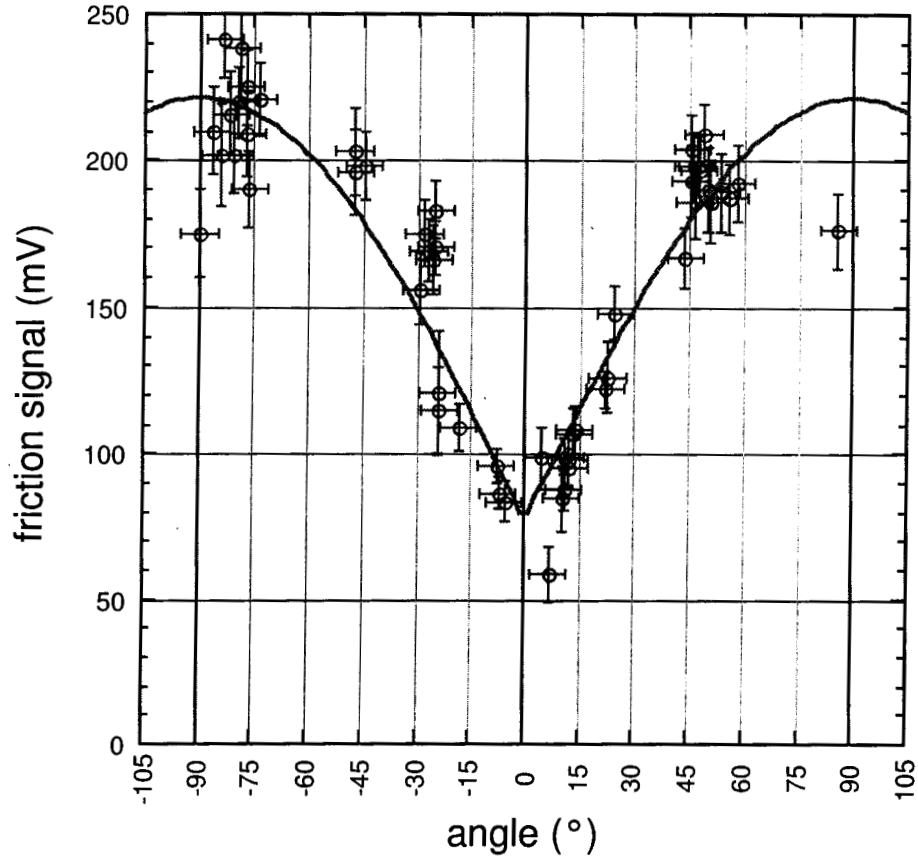

Figure 5. Friction force (raw signal units) vs. angle. 0° indicates sliding parallel to the backbone direction. Friction is calculated by taking the difference between trace and retrace images (1 × 1 μm^2, 256 × 256 pixels) on single domains. The edges of the image were excluded so as to only sample the sliding portion of the measurement. Each measurement represents the average value of approximately 40,000 pixels. The standard deviation is used for the friction error bars. The solid line represents the fit of equation (1) to the data.

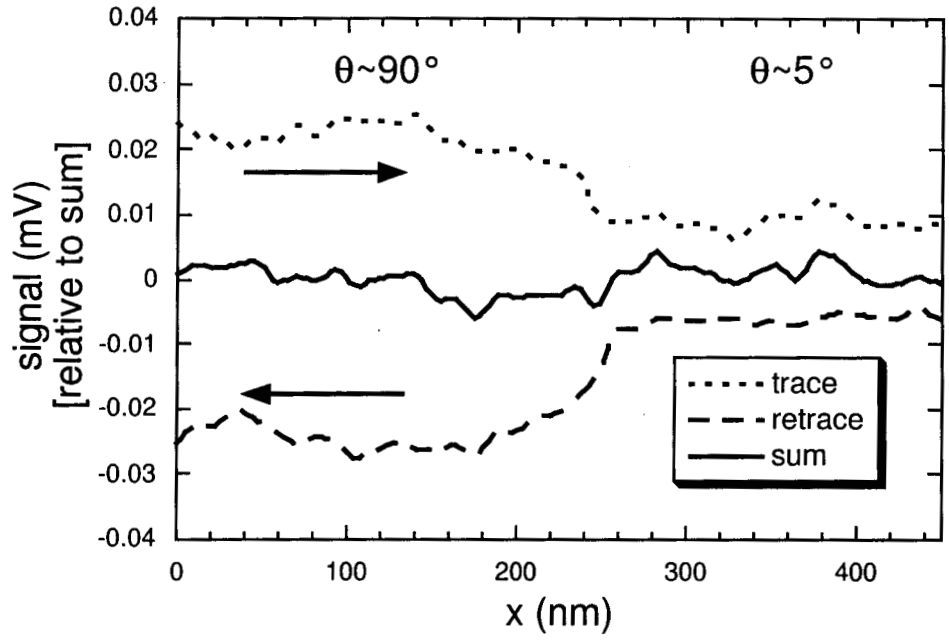

Figure 6. Lateral force trace, retrace, and the sum of the trace and retrace signals over two orthogonal domains. Although the loop width (i.e. friction force) varies greatly between the two domains, the sum is nearly constant. This indicates that there is no observable friction asymmetry on either of these domains. However, there is a $\sim 10\%$ spatial variation in the friction signals, rendering the observation of a small asymmetry effect difficult.

where θ represents the domain orientation. F_1 represents the angle-independent contribution to friction and can be thought of as an intrinsic friction force between the film and the tip. F_2 represents an additional contribution to friction that arises when there is a component of sliding motion perpendicular to the polymer backbone direction. The origin of this force is discussed below. The absolute value is used to ensure that this contribution is positive. Equation (1) provides a consistent fit to the data as shown in figure 5, giving $F_1 = 77$ mV and $F_2 = 144$ mV. Thus, according to the fit, the total friction anisotropy is

$$F_{\max} = \frac{F_1 + F_2}{F_1} = 2.9.$$

We propose that this effect is due to anisotropic lateral film stiffness caused by anisotropic packing and/or ordering of the alkyl side chains as well as the anisotropic stiffness of the polymer backbone itself. Along the backbone direction, the extended conjugated polymer bonds provide a rigid link between alkyl chains, and impose a regular spacing of 4.9 Å (figure 1) [15]. This spacing simultaneously satisfies the bond lengths of the polymer backbone as well as the equilibrium van der Waals' spacing of the alkyl chains with an appropriate tilt angle (figure 1). Indeed, we observe regular stick–slip friction with ~ 5 Å periodicity along the backbone direction for these films. However, the spacing between alkyl chains linked to *neighboring* backbones is determined by weaker interchain van der Waals' forces and possibly by the spacing of the head groups which are bonded to the mica substrate. The head groups are not necessarily uniformly spaced in the direction perpendicular to the backbones and may be influenced by the substrate lattice. In other words, the lack of covalent bonding between neighboring polymer chains allows some freedom in their spacing. Indeed, Lio et al. observed such anisotropic spacing in atomic lattice-resolved images of a similar polydiacetylene thin film [20,33]. In fact, variations in film density could explain the film height contrast observed in figure 4(a). Both the tilt angle and gauche defect population of films of alkyl chains are affected by packing density [34–36]. Regions with different density are therefore likely to exhibit height variations due to different tilt angles of the alkyl chains and/or increased number of gauche defects. However, as seen in figure 4, friction is not correlated with the local height of these individual regions. Rather, the reduced packing density and lack of covalent bonding perpendicular to the backbone direction leads to higher friction when sliding along this direction, as discussed below.

Several observations with AFM have indicated that lower packing density and/or increased disorder of monolayer hydrocarbon films leads to increased friction [37–40]. It is proposed that a lower packing density provides increased freedom to displace molecules during sliding (low lateral stiffness), possibly by increasing the contact area and also providing more channels for energy dissipation. For our system, we propose that there is high lateral stiffness when sliding the tip along the backbone direction, as the molecules are densely packed and rigidly linked in this direction and have little freedom to be displaced. Thus a minimum friction force is expected. However, any component of motion perpendicular to the chains could lead to increased molecular displacement and correspondingly increased friction. According to this model, the increase in friction should be proportional to the vector component of the sliding direction perpendicular to the backbone direction. This is precisely the model proposed in equation (1), and is clearly consistent with the data in figure 5. Further measurements, specifically lateral stiffness measurements [41] are required to verify this hypothesis. We can only state at this point that this proposed model is consistent with both our observations and the existing examples in the literature.

4.2. Friction asymmetry

As previously mentioned, friction asymmetry has been observed to be induced by the tilt of molecular groups from the surface normal, although it is a relatively subtle effect. Bluhm et al. [7,8] observed friction asymmetry with a ferroelectric material, triglycine sulfate, which corresponded to $\sim 4\%$ of the total friction force. Liley et al. [11] observed friction asymmetry of a thiolipid Langmuir–Blodgett monolayer of $\sim 15\%$ of the friction force. The thiolipid monolayer consists of domains with alkyl chains uniformly tilted with respect to the surface normal. The alkyl chains, with which the tip interacts, are linked to each other by a complex head group that is bound to the substrate. Asymmetry was observed when scanning the AFM tip back and forth along the tilt direction of the alkyl chains. We believe that the alkyl chains in our monolayer film are tilted with respect to the surface normal, as indicated by film height measurements, and consistent with other structural studies of polydiacetylene thin films [20,42]. This tilt could perhaps cause friction asymmetry, but spatial fluctuations of the friction force, as discussed above, obscure this effect if it is present. It is not known if friction asymmetry is a universal effect; despite a vast number of AFM studies of ordered alkanethiol monolayers [1], whose alkyl chains are uniformly tilted at $\sim 30°$ with respect to the surface normal, no friction asymmetry has yet been reported.

5. Conclusion

Monolayer films of PCEA exhibit strong friction anisotropy of $\sim 300\%$. This effect may allow this system to be used for nanofabrication, as the film provides a substrate with a single preferred sliding direction within a given domain, and the direction can be remotely determined using optical microscopy. Friction is highest when scanning perpendicular to the polymer backbone direction. We propose that this effect results from anisotropic film stiffness. Further measurements of the directional dependence of film stiffness are needed to verify this hypothesis.

Acknowledgement

We acknowledge useful discussions with M. Crawford, D.H. Charych, U. Jonas, J.E. Houston and T.A. Michalske. RWC acknowledges the support of the Natural Sciences and Engineering Research Council of Canada. Sandia is a multiprogram laboratory operated by Sandia Corporation, a Lockheed Martin Company, for the United States Department of Energy under Contract DE-AC04-94AL85000.

References

[1] R.W. Carpick and M. Salmeron, Chem. Rev. 97 (1997) 1163.
[2] R.W. Carpick, N. Agraït, D.F. Ogletree and M. Salmeron, J. Vac. Sci. Technol. B 14 (1996) 1289.
[3] H. Yoshizawa, Y.-L. Chen and J. Israelachvili, Wear 168 (1993) 161.
[4] T. Bouhacina, J.P. Aimé, S. Gauthier, D. Michel and V. Heroguez, Phys. Rev. B 56 (1997) 7694.
[5] M. Hirano, K. Shinjo, R. Kaneko and Y. Murata, Phys. Rev. Lett. 67 (1991) 2642.
[6] R.M. Overney, H. Takano, M. Fujihira, W. Paulus and H. Ringsdorf, Phys. Rev. Lett. 72 (1994) 3546.
[7] H. Bluhm, U.D. Schwarz, K.P. Meyer and R. Wiesendanger, Appl. Phys. A 61 (1995) 525.
[8] U.D. Schwarz, H. Bluhm, H. Hölscher, W. Allers and R. Wiesendanger, in: *Physics of Sliding Friction*, eds. B.N.J. Persson and E. Tosatti (Kluwer, 1996), p. 369.
[9] P.E. Sheehan and C.M. Lieber, Science 272 (1996) 1158.
[10] U. Gehlert, J.Y. Fang and C.M. Knobler, J. Phys. Chem. B 102 (1998) 2614.
[11] M. Liley, D. Gourdon, D. Stamou, U. Meseth, T.M. Fischer, C. Lautz, H. Stahlberg, H. Vogel, N.A. Burnham and C. Duschl, Science 280 (1998) 273.
[12] R. Pearce and G.J. Vancso, Polymer 39 (1998) 6743.
[13] A. Artsyukhovich, L.D. Broekman and M. Salmeron, Langmuir 15 (1999) 2217.
[14] D. Bloor and R.R. Chance, in: *Polydiacetylenes: Synthesis, Structure, and Electronic Properties*, eds. D. Bloor and R.R. Chance (Martinus Nijhoff, Dordrecht, 1985).
[15] A. Ulman, in: *Introduction to Ultrathin Organic Films from Langmuir–Blodgett to Self-Assembly* (Academic Press, 1991) pp. 182–191 and references therein.
[16] D.N. Batchelder, S.D. Evans, T.L. Freeman, L. Haussling, H. Ringsdorf and H. Wolf, J. Am. Chem. Soc. 116 (1994) 1050.
[17] T. Kim and R.M. Crooks, Tetrahedron Lett. 35 (1994) 9501.
[18] M.D. Mowery and C.E. Evans, Tetrahedron Lett. 38 (1997) 11.
[19] M. Wenzel and G.H. Atkinson, J. Am. Chem. Soc. 111 (1989) 6123.
[20] A. Lio, A. Reichert, D.J. Ahn, J.O. Nagy, M. Salmeron and D.H. Charych, Langmuir 13 (1997) 6524.
[21] H. Muller and C.J. Eckhardt, Mol. Cryst. Liq. Cryst. 45 (1978) 313.
[22] Y. Tomioka, N. Tanaka and S. Imazeki, J. Chem. Phys. 91 (1989) 5694.
[23] R.A. Nallicheri and M.F. Rubner, Macromolecules 24 (1991) 517.
[24] D.H. Charych, J.O. Nagy, W. Spevak and M.D. Bednarski, Science 261 (1993) 585.
[25] A. Reichert, J.O. Nagy, W. Spevak and D. Charych, J. Am. Chem. Soc. 117 (1995) 829.
[26] D. Charych, Q. Cheng, A. Reichert, G. Kuziemko, M. Stroh, J.O. Nagy, W. Spevak and R.C. Stevens, Chemistry & Biology 3 (1996) 113.
[27] R.W. Carpick, D.Y. Sasaki and A.R. Burns, Langmuir (1999), submitted.
[28] D.Y. Sasaki, R.W. Carpick and A.R. Burns, in preparation (1999).
[29] D.F. Ogletree, R.W. Carpick and M. Salmeron, Rev. Sci. Instrum. 67 (1996) 3298.
[30] R.R. Chance, G.N. Patel and J.D. Witt, J. Chem. Phys. 71 (1979) 206.
[31] M.H.P. Moers, H.E. Gaub and N.F. Vanhulst, Langmuir 10 (1994) 2774.
[32] S. Yamada and Y. Shimoyama, Jpn. J. Appl. Phys. 1, Regul. Pap. 35 (1996) 4480.
[33] A. Lio, A. Reichert, J.O. Nagy, M. Salmeron and D.H. Charych, J. Vac. Sci. Technol. B 14 (1996) 1481.
[34] M.D. Porter, T.B. Bright, D.L. Allara and C.E.D. Chidsey, J. Am. Chem. Soc. 109 (1987) 3559.
[35] M.A. Bryant and J.E. Pemberton, J. Am. Chem. Soc. 113 (1991) 8284.
[36] P. Fenter, P. Eisenberger and K.S. Liang, Phys. Rev. Lett. 70 (1993) 2447.
[37] A. Lio, D.H. Charych and M. Salmeron, J. Phys. Chem. B 101 (1997) 3800.
[38] M.T. McDermott, J.-B.D. Green and M.D. Porter, Langmuir 13 (1997) 2505.
[39] J.D. Kiely, J.E. Houston, J.A. Mulder, R.P. Hsung and X.Y. Zhu, Tribol. Lett. 7 (1999) 103.
[40] J.D. Kiely, N.D. Shinn and J.E. Houston, Langmuir (1999), in preparation.
[41] R.W. Carpick, D.F. Ogletree and M. Salmeron, Appl. Phys. Lett. 70 (1997) 1548.
[42] M.D. Mowery, H. Menzel, M. Cai and C.E. Evans, Langmuir 14 (1998) 5594.

Spectroscopic Ellipsometry and Fluorescence Study of Thermochromism in an Ultrathin Poly(diacetylene) Film: Reversibility and Transition Kinetics

R. W. Carpick,[†,‡] T. M. Mayer,[§] D. Y. Sasaki,[†] and A. R. Burns*,[†]

Biomolecular Materials and Interfaces Department, Sandia National Laboratories, Albuquerque, New Mexico 87185-1413, and Chemical Processing Science Department, Sandia National Laboratories, Albuquerque, New Mexico 87185-0601

Received December 2, 1999. In Final Form: February 18, 2000

We have investigated the thermochromic transition of an ultrathin poly(diacetylene) film. The Langmuir film is composed of three layers of polymerized 10,12-pentacosadiynoic acid [$CH_3(CH_2)_{11}C{\equiv}CC{\equiv}C(CH_2)_8$-COOH] (poly-PCDA) organized into crystalline domains on a silicon substrate. Spectroscopic ellipsometry and fluorescence intensity measurements are obtained with in situ temperature control. Poly-PCDA films exhibit a reversible thermal transition between the initial blue form and an intermediate "purple" form that exists only at elevated temperature (between 303 and 333 K), followed by an irreversible transition to the red form after annealing above 320 K. We propose that the purple form is thermally distorted blue poly-PCDA and may represent a transitional configuration in the irreversible conversion to red. This hypothesis is supported by the appearance of unique features in the absorption spectra for each form as derived from the ellipsometry measurements. Significant fluorescence emission occurs only with the red form and is reduced at elevated temperatures while the absorption remains unchanged. Reduced emission is likely related to thermal fluctuations of the hydrocarbon side chains. Time-resolved fluorescence measurements of the irreversible transition have been performed. Using a first-order kinetic analysis of these measurements, we deduce an energy barrier of 17.6 ± 1.1 kcal mol^{-1} between the blue and red forms.

Introduction

Ultrathin organic films, prepared through methods such as Langmuir deposition or self-assembly,[1,2] offer the possibility of tailoring the optical, mechanical, and chemical properties of surfaces at the molecular scale. Such control of surface properties is required to implement micro- and nanoscale sensors, actuators, and computational devices. Materials that change in response to external stimuli are especially important for such applications. Poly(diacetylene)s (PDAs)[3] merit particular interest as these molecules exhibit strong optical absorption and fluorescence emission that change dramatically with various stimuli, namely, UV absorption (*photochromism*),[4–7] heat (*thermochromism*),[8–10] and applied stress (*mechanochromism*),[7,11–13] changes in chemical environment such as pH,[14,15] and binding of specific chemical or biological targets to functionalized PDA side chains (*affinochromism / biochromism*).[16–18] Chromatic transitions in PDA can even be studied at the nanometer scale, as we have recently observed and controlled mechanochromism by locally applying shear stresses with scanning probe microscope tips.[7] PDA chromatic transitions, along with other properties such as high third-order nonlinear susceptibility,[19] unique photoconduction characteristics,[20] and strong nanometer-scale friction anisotropy,[21] render PDA an extremely interesting material to study with many potential applications.

Optical absorption in PDAs occurs via a π-to-π^* absorption within the linear π-conjugated polymer backbone.[3] In general, PDA chromatic transitions involve a significant shift in absorption from low- to high-energy bands of the visible spectrum; thus the PDA appears to transform from a blue to a red color. The mechanism driving these transitions is not understood in detail. It is believed that molecular conformational changes, such as side chain

* Corresponding author. Tel: 505-844-9642. Fax: 505-844-5470. E-mail: aburns@sandia.gov.

† Biomolecular Materials and Interfaces Department, Sandia National Laboratories.

‡ Current address: Department of Engineering Physics, University of Wisconsin—Madison, 1500 Engineering Dr., Madison, WI 53706-1687.

§ Chemical Processing Science Department, Sandia National Laboratories.

(1) Ulman, A. *Introduction to Ultrathin Organic Films from Langmuir–Blodgett to Self-Assembly*; Academic Press: New York, 1991.
(2) Schwartz, D. K. *Surf. Sci. Rep.* **1997**, *27*, 245–334.
(3) Bloor, D.; Chance, R. R. *Polydiacetylenes: Synthesis, Structure, and Electronic Properties*; Martinus Nijhoff: Dordrecht, 1985.
(4) Day, D.; Hub, H. H.; Ringsdorf, H. *Isr. J. Chem.* **1979**, *18*, 325–329.
(5) Tieke, B.; Lieser, G.; Wegner, G. *J. Polym. Sci., Part A: Polym. Chem., Ed.* **1979**, *17*, 1631–1644.
(6) Olmsted, J.; Strand, M. *J. Phys. Chem.* **1983**, *87*, 4790–2.
(7) Carpick, R. W.; Sasaki, D. Y.; Burns, A. R. *Langmuir* **2000**, *16*, 1270–1278.
(8) Wenzel, M.; Atkinson, G. H. *J. Am. Chem. Soc.* **1989**, *111*, 6123–6127.
(9) Lio, A.; Reichert, A.; Ahn, D. J.; Nagy, J. O.; Salmeron, M.; Charych, D. H. *Langmuir* **1997**, *13*, 6524–6532.
(10) Chance, R. R.; Baughman, R. H.; Muller, H.; Eckhardt, C. J. *J. of Chem. Phys.* **1977**, *67*, 3616–18.
(11) Muller, H.; Eckhardt, C. J. *Mol. Cryst. Liquid Cryst.* **1978**, *45*, 313–18.
(12) Nallicheri, R. A.; Rubner, M. F. *Macromolecules* **1991**, *24*, 517–525.
(13) Tomioka, Y.; Tanaka, N.; Imazeki, S. *J. Chem. Phys.* **1989**, *91*, 5694–700.
(14) Cheng, Q.; Stevens, R. C. *Langmuir* **1998**, *14*, 1974–1976.
(15) Jonas, U.; Shah, K.; Norvez, S.; Charych, D. H. *J. Am. Chem. Soc.* **1999**, *121*, 4580–4588.
(16) Charych, D. H.; Nagy, J. O.; Spevak, W.; Bednarski, M. D. *Science* **1993**, *261*, 585–588.
(17) Reichert, A.; Nagy, J. O.; Spevak, W.; Charych, D. *J. Am. Chem. Soc.* **1995**, *117*, 829–830.
(18) Charych, D.; Cheng, Q.; Reichert, A.; Kuziemko, G.; Stroh, M.; Nagy, J. O.; Spevak, W.; Stevens, R. C. *Chem. Biol.* **1996**, *3*, 113–120.
(19) Kobayashi, T. *Optoelectron.—Devices Technol.* **1993**, *8*, 309–32.
(20) Hoofman, R. J. O. M.; Siebbeles, L. D. A.; de Haas, M. P.; Hummel, A.; Bloor, D. *J. Chem. Phys.* **1998**, *109*, 1885–93.
(21) Carpick, R. W.; Sasaki, D. Y.; Burns, A. R. *Tribol. Lett.* **1999**, *7*, 79–85.

10.1021/la991580k CCC: $19.00
Published on Web 04/07/2000

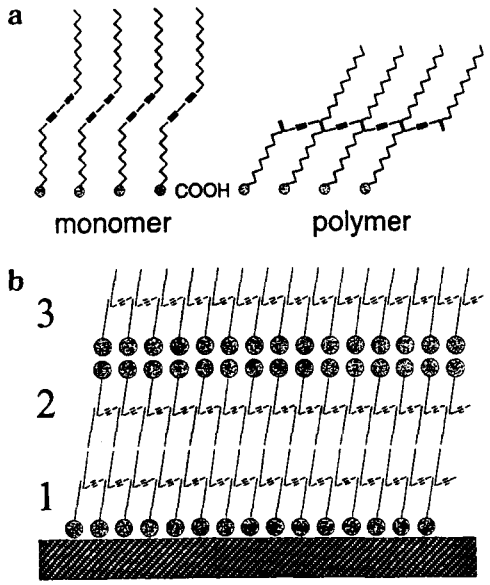

Figure 1. (a) Sketch of the monomeric and polymeric form of PCDA molecules. The polymerized form possesses extended linearly conjugated backbones that link the molecules together. The hydrocarbon side chains comprise a large fraction of the molecular structure. (b) Simplified sketch of the trilayer stacking of PCDA molecules. The circles represent the COOH headgroups which are expected to hydrogen bond to the silicon substrate (silicon–layer 1 interface) or with each other (layer 2–layer 3 interface). The polymer backbones (thick lines), which lie parallel to the surface, are aligned in all three layers within a given domain of the film.

packing, ordering, and orientation, impart stresses to the polymer backbone that alter its conformation, thus changing the electronic states and the corresponding optical absorption.[3,9] It is not fully established whether the blue-to-red transitions are continuous transitions or discrete transitions between two or more forms. The factors governing the degree of reversibility of the transitions are also not fully understood.

Our studies of mechanochromism and mechanical properties of ultrathin PDA films[7,21] have prompted us to study thermochromism of the same films to determine the underlying and unifying features of these chromatic transitions. Recent studies of thermochromism in thicker multilayer PDA films have indicated that there is some degree of reversibility to the transition[22–24] involving an intermediate form of the PDA.

The present experiments were conducted using the PDA formed from 10,12-pentacosadiynoic acid [$CH_3(CH_2)_{11}C{\equiv}CC{\equiv}C(CH_2)_8COOH$] (PCDA) monomers ordered on a Langmuir trough (Figure 1a). Our goal was to optimize the film quality. Thus, we avoided the use of metal ion salts in the subphase (e.g., Cd^{2+}), as we have observed that these generate precipitates on the film.[25] We prepared films consisting of three molecular layers of PCDA, which is the minimum number of layers that can be stabilized on the trough under these conditions.[7,25] Topochemical polymerization was accomplished through UV irradiation of the trilayer on the Langmuir trough.[26] The polymerized PCDA (poly-PCDA) films are then transferred to atomically flat silicon substrates. Since the opaque substrates preclude performing absorption spectroscopy, we employ spectroscopic ellipsometry and fluorescence intensity measurements to investigate changes upon annealing in the absorption spectrum and fluorescence emission.

Experimental Section

Preparation of Trilayer Poly-PCDA Films. The details of our sample preparation will be described elsewhere.[25] Briefly, both blue and red poly-PCDA films were prepared via UV polymerization on a Langmuir trough (Nima, Coventry, U.K.). The trough was situated on a vibration-isolation table inside a class 100 clean room. The subphase was deionized water with a resistivity greater than 18 MΩ cm (Barnstead Nanopure system, Dubuque, IA) held at a temperature of 15 ± 1 °C. Si substrates with either native or thermally grown oxide were cleaned in organic solvents followed by a 50/50 mixture of H_2O_2 and 30% H_2SO_4 for 20 min at 100 °C and then immediately rinsed and stored in subphase-quality water before transfer to the Langmuir trough. This rendered the substrates hydrophilic and clean, as high-resolution atomic force microscope (AFM) images obtained in air shortly after rinsing indicated very little observable contamination. From AFM measurements we also verified that the substrates were extremely flat, with <0.2 nm root mean square roughness. Just prior to monolayer spreading, the substrates were removed from water storage and completely immersed into the subphase, minimizing exposure to clean room air. The Si substrate was seated horizontally approximately 1 mm below the water surface before spreading the molecules.

PCDA molecules (Farchan/GFS Chemicals, Powell, OH) that had been purified through a silica gel column were spread onto the subphase in a 50% chloroform/benzene solution. On the pure water subphase the monolayer was unstable. However, as the monomer was compressed at a rate of 100 $cm^2\ min^{-1}$ (molar compression rate 380 $m^2\ s^{-1}\ mol^{-1}$ or 4 $Å^2\ molecule^{-1}\ min^{-1}$) to a pressure of 20 mN m^{-1}, a stable trilayer was produced (molecular area of ~8 $Å^2$ for three layers).[25,27] The film possesses the Y-type configuration, which is common for these amphiphilic molecules, as shown in Figure 1b. All films were equilibrated for 20 min at 20 mN m^{-1}, prior to UV light exposure from a pair of Hg pen lamps (Oriel, Stratford, CT). To produce a blue film, the pen lamps were fixed 10 cm from the water surface and switched on for 30 s. This produced a faintly visible, uniform blue film. Red films were produced by using extended UV exposure. In this case, the pen lamps were fixed at 6 cm from the water surface and switched on for 5 min. This produced a clearly visible red film.

In either case, the water level was then lowered by slowly draining the trough, allowing the polymerized film to drape itself over the substrate. Samples were dried in clean room air and stored in a dark, nitrogen-purged container. A sample that is converted from blue to red by UV irradiation is referred to as a "photochromic" red sample; a sample converted from blue to red thermally is referred to as a "thermochromic" red sample.

Spectroscopic Ellipsometry Measurements. A variable angle spectroscopic ellipsometer (J. A. Woollam Co., Lincoln, NE) was employed for ellipsometric studies. Ellipsometry[28] measures the ratio of the complex reflection coefficients, r, of the p and s polarization components of a beam of polarized light reflected from a surface in terms of two angles, Ψ and Δ, where

$$r^p/r^s = \tan \psi e^{i\Delta} \qquad (1)$$

In eq 1, tan Ψ and Δ are the ratio of the magnitudes and the phase difference between the p and s reflection coefficients, respectively. The reflection coefficients are related to physical characteristics of the sample, such as index of refraction, film thickness, etc., through the Fresnel equations. To extract these sample characteristics, we must construct an optical model of

(22) Mino, N.; Tamura, H.; Ogawa, K. *Langmuir* **1991**, *7*, 2336–2341.
(23) Deckert, A. A.; Fallon, L.; Kiernan, L.; Cashin, C.; Perrone, A.; Encalarde, T. *Langmuir* **1994**, *10*, 1948–1954.
(24) Deckert, A. A.; Horne, J. C.; Valentine, B.; Kiernan, L.; Fallon, L. *Langmuir* **1995**, *11*, 643–649.
(25) Sasaki, D. Y.; Carpick, R. W.; Burns, A. R. Submitted for publication in *J. Colloid Interface Sci.*
(26) Mowery, M. D.; Menzel, H.; Cai, M.; Evans, C. E. *Langmuir* **1998**, *14*, 5594–5602.
(27) Goettgens, B. M.; Tillmann, R. W.; Radmacher, M.; Gaub, H. E. *Langmuir* **1992**, *8*, 1768–1774.
(28) Azzam, R. M. A.; Bashara, N. M. *Ellipsometry and Polarized Light*; North-Holland: Amsterdam, 1987.

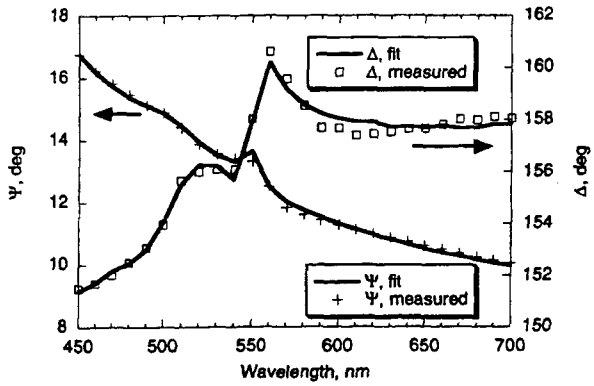

Figure 2. Spectroscopic ellipsometric measurement of photochromic red poly-PCDA trilayer film. Angle of incidence is 70°. Fit to the data is obtained using a Lorentz oscillator model for the poly-PCDA complex index of refraction.

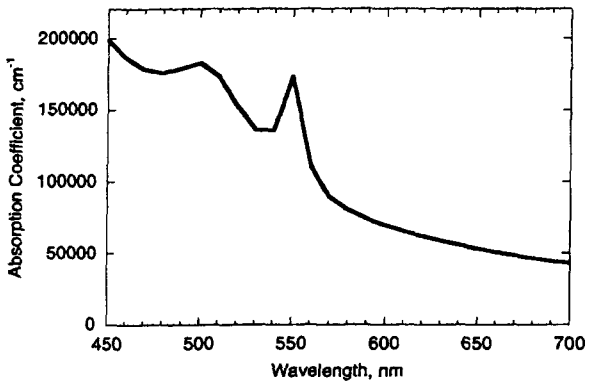

Figure 3. Absorption coefficient for photochromic red poly-PCDA film determined from ellipsometric measurements of Figure 2.

the sample, calculate Ψ and Δ for the model, and then fit the model to the experimental results. For the present case of a thin film of poly-PCDA on a Si substrate with a native oxide, we employ a model in which the well-known optical properties of the substrate are used, and the thickness of the film is determined from AFM measurements. We then extract the complex index of refraction of the film as a function of wavelength. The imaginary part of the index (the extinction coefficient, k) of the film is related to the absorption coefficient, α, via

$$\alpha = 4\pi k/\lambda \qquad (2)$$

As an example of such a measurement, Figure 2 shows ellipsometric data from a photochromic red poly-PCDA trilayer film at room temperature from 450 to 700 nm, measured at 70° angle of incidence. Also shown in the figure are fits to the data using a Lorentz oscillator parametrization of the complex index of refraction (see Appendix). The absorption coefficient, α, extracted from this fit (Figure 3) shows a major absorption feature at 550 nm, with a smaller feature at 500 nm. The blue film shows a major absorption feature at 640 nm (Figure 4). These spectra are consistent with previous absorption studies of various PDA films.[9,22-24]

Sample temperature during the measurements is controlled with a small home-built heat/cool stage with an operating range of 270–370 K. A thermoelectric element is attached to the bottom of a copper block (12 × 12 × 4 mm). By use of thermally conductive paste, the sample is attached on top of the copper block to provide uniform sample heating. A solid-state temperature sensor is embedded in the block for temperature readout and regulation using a control unit (Wavelength Electronics, Bozeman, MT). After any change in temperature, the stage was allowed to equilibrate for approximately 1 min before measurement. Once equilibrated, the temperature was stable to within ±0.5°. Ellipsometric measurements are made at fixed temperatures

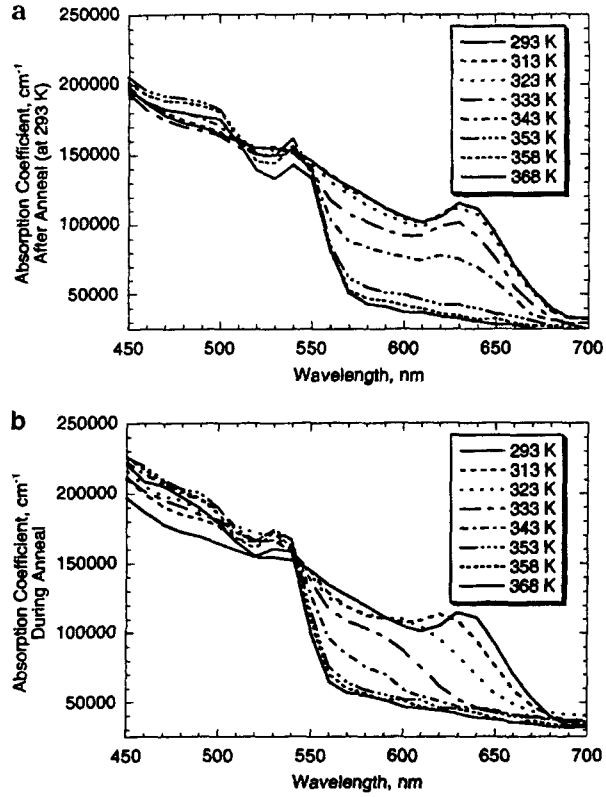

Figure 4. (a) Absorption spectra determined from ellipsometric measurements obtained *at room temperature*, after annealing to the indicated temperatures. The sample is initially a blue poly-PCDA film. Spectra at several temperatures are omitted for clarity. (b) The corresponding absorption spectra obtained *while annealing* at the indicated temperatures.

over the wavelength range 400–700 nm. A series of annealing and quenching steps were carried out, as described in more detail below. The total time at any given annealing temperature was approximately 2 min.

Microscopic Fluorescence Intensity Measurements at Fixed Temperatures. Microscopic sample fluorescence was recorded using a Leitz optical fluorescence microscope equipped with a xenon lamp and dichroic beam filters. The sample was illuminated with 520–550 nm light, and emission wavelengths greater than 590 nm were passed to an intensified CCD camera and digitized. The field of view was 170 × 130 μm^2. Temperature was controlled with the same heat/cool stage used for the ellipsometry measurements. As with those measurements, the stage was equilibrated for approximately 1 min before measurement after any temperature change, and the total time at any given annealing temperature was approximately 2 min, as with the ellipsometric measurements. Throughout a given series of measurements, the same region of the sample was observed at several different fixed temperatures. Therefore, any observed changes in fluorescence intensity are due to annealing and not to spatial inhomogeneity of the sample. For each measurement, 16 frames were averaged together and the total fluorescence intensity of the image was calculated. This method allows highly accurate, but relatively slow, measurements of fluorescence intensity.

Time-Resolved Fluorescence Intensity Measurements. To obtain time-resolved measurements of the thermal transition, an optical platform incorporating a CCD spectrometer with fiber optic collection was set up to measure fluorescence spectra. The temperature was controlled with the same heat/cool stage used for the previous measurements. Poly-PCDA fluorescence was recorded using a fiber-optic-coupled spectrometer (Ocean Optics, Inc., Dunedin, FL), interfaced to a PC using LabView (National Instruments, Austin, TX) data acquisition control. Fluorescence spectra were acquired continuously with a 250 ms integration

time per spectrum. A 550 nm cutoff filter was inserted in the collection path to reduce capturing the excitation light from the blue LED source. Each spectrum was integrated between 585 and 720 nm to completely avoid including any of the remaining excitation light. To carry out the experiment, a background measurement was conducted with the stage at room temperature and a fresh blue sample in place. The sample was then removed, and thermally conducting paste was applied to the stage, which was then allowed to equilibrate at the desired elevated temperature. The underside of the sample was also coated with thermally conducting paste. Data acquisition was then started, and the sample was quickly placed in firm contact with the stage. We calculate that the sample equilibrates with the heater within a few milliseconds, while the conversion from blue to red occurs at an substantially slower rate. Therefore, we assert that the experiment is essentially isothermal. Each measurement is performed on a fresh sample cut from the same substrate. Several measurements are obtained at each temperature over the observable range.

Initial Film Characterization

The poly-PCDA film quality is nearly identical to films we produced on mica substrates that are described in substantial detail elsewhere.[7,25] To summarize, AFM images confirm that both blue and photochromic red films are organized into uniform, atomically flat crystalline domains up to 100 μm in size. The film covers >90% of the substrate. High-resolution images within the domains reveal large, extended arrays of parallel striations, similar to previous reports.[9] The striations correspond to the backbone direction. This indicates that the backbones are highly oriented within individual domains. Between and within some domains are cracks which expose the substrate, allowing film height measurements that confirm that the film is indeed a trilayer. The photochromic red film is observed to be ~15% taller than the blue film, which is due to the reduced degree of tilt of the molecules.[7,9,29] In addition, islands are occasionally found on top of the trilayer. AFM height measurements indicate that the islands are an additional bilayer of poly-PCDA. The bilayers are likely stabilized by interfacial hydrogen-bonded ad-dimers of the acid headgroups (as in Figure 1b, between layers 2 and 3). We believe that the bilayers are produced during the monomer compression stage before polymerization and deposition. The bilayer islands cover less than 10% of the underlying trilayer film. Thus, to a good approximation the average film thickness of the trilayer height is 7.4 ± 0.8 nm for the blue film and 9.0 ± 0.9 nm for the photochromic red film.

Strong fluorescence emission is observed from photochromic red films, as well as from thermochromic red films as discussed in the next section. In general, fluorescence emission from PDAs is polarized along the backbone direction.[30-32] Using polarized fluorescence microscopy, we can extinguish the emission from a given trilayer domain by analyzing the emission at 90° to the backbone direction.[7] This confirms that the conjugated backbones within each domain are highly ordered and that there is structural registry between the three layers of both photochromic and thermochromic red films. In other words, the backbones are oriented along the same direction in all three layers within a domain. Thus, the crystallinity of the domains exists not only parallel to the substrate but also normal to it as well. This is a particular advantage of using a single-transfer film. It is not established, and not likely, that thicker multilayer Langmuir–Blodgett films formed by multiple dips exhibit such structural registry normal to the substrate.[2] This may significantly affect the phase transformation behavior. In addition, these ultrathin films are attractive materials since they can be end-functionalized to provide colorimetric detection of molecules that bind to the functional group.[16-18]

Results

To investigate the thermochromic transition of the poly-PCDA film, we obtained ellipsometry and fluorescence measurements on a film initially prepared in the blue form. For both sets of measurements, the temperature was varied as follows. The sample was annealed at a fixed temperature, and the measurement (ellipsometric or fluorescence) was acquired at that temperature. The sample was then quenched to 293 K, where a room-temperature measurement was acquired. The sample was then annealed at a temperature 5 deg higher than the previous anneal, and the next measurement was acquired. The sample was then quenched to room-temperature again, and so on. The first anneal temperature was 303 K, and the final anneal temperature was 368 K. In this way we can determine the extent of reversibility after annealing at each temperature and follow the progressive conversion from the blue to red forms of a single region of a given sample.

Shown in Figure 4 are absorption spectra derived from the ellipsometry measurements. Figure 4a shows the *room temperature* absorption after annealing to the indicated temperature. Figure 4b shows the absorption obtained *at* the annealing temperature. Note that the absorption features of the final thermochromic red film are not as pronounced as those for the photochromic red film shown in Figure 3. The room-temperature spectra demonstrate that the major absorption feature of the blue form at 640 nm disappears and the red-form absorption features at 550 and 500 nm appear as the annealing temperature increases. At intermediate annealing temperatures, the 640 nm feature appears to shift to a shorter wavelength, resulting in an apparent new broad absorption feature at 600 nm. This feature is only observed at elevated temperatures (Figure 4b) and is not present in measurements made at room temperature either before or after annealing (Figure 4a). Furthermore it is only observed upon annealing a film originally in the blue form. Material exhibiting this absorption feature we call the "purple" form of the material. Deckert et al.[23,24] have postulated the existence of an intermediate "purple" form based on kinetic aspects of the transition from blue to red.

We would like to know the temperature at which the blue-to-red transition takes place, as well as the relative concentrations of blue and red form that exist at room temperature after each annealing temperature. To do this we assume that the sample consists solely of blue form at the start of the annealing study and solely of the thermochromic red form after annealing to 368 K. Then considering the film to be made up of a mixture of blue and red forms *at room temperature* after each annealing cycle, we construct an effective index of refraction for the film using the Bruggeman effective medium approximation (EMA).[33,34] This procedure is commonly used to

(29) Fischetti, R. F.; Filipkowski, M.; Garito, A. F.; Blasie, J. K. *Phys. Rev. B* **1988**, *37*, 4714–26.
(30) Chance, R. R.; Patel, G. N.; Witt, J. D. *J. Chem. Phys.* **1979**, *71*, 206–11.
(31) Moers, M. H. P.; Gaub, H. E.; Vanhulst, N. F. *Langmuir* **1994**, *10*, 2774–2777.
(32) Yamada, S.; Shimoyama, Y. *Jpn. J. Appl. Phys.* **1996**, *35*, 4480–4485.
(33) Aspnes, D. E.; Theeten, J. B.; Hottier, F. *Phys. Rev. B* **1979**, *20*, 3292.
(34) Tompkins, H. *A Users Guide to Ellipsometry*; Academic Press: San Diego, CA, 1993.

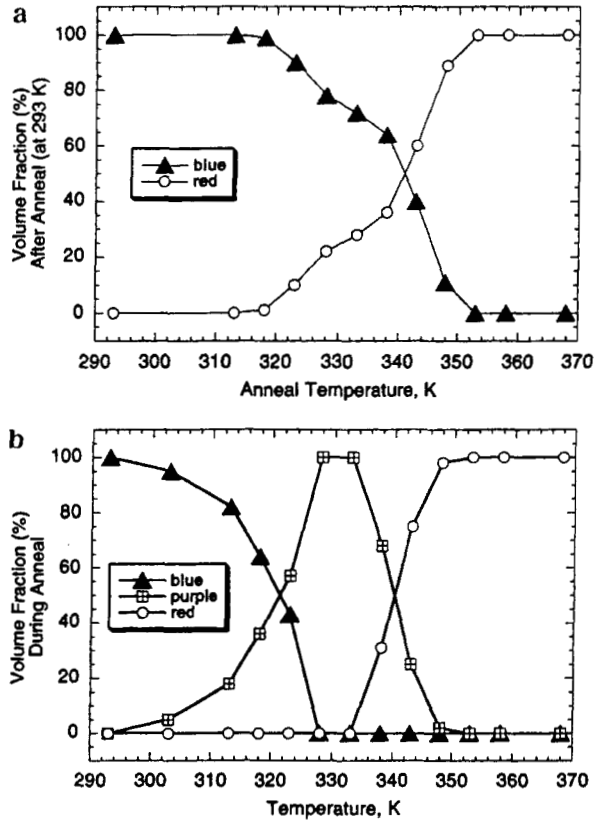

Figure 5. (a) Volume fractions of blue and thermochromic red form poly-PCDA in the film at room temperature after annealing to the indicated temperature. (b) "Effective" volume fractions of blue, purple, and red form poly-PCDA in the film at the anneal temperature. It is implicitly assumed that the film entirely consists of the purple form at 333 K; this plot is meant to illustrate the temperature ranges over which each form is created or lost.

analyze multicomponent materials and, when fit to the experimental data, yields the volume fractions of the constituent materials in the film (see Appendix). Applying this two-component model provides good fits to all of the spectra of Figure 4a. The resulting volume fractions are shown in Figure 5a. Starting at about 320 K, a significant fraction of the blue form is converted to red, with near complete conversion after annealing to 353 K. We do not observe any reversion from red back to blue. Annealing a film initially in the red form does not produce any of the blue form.

Absorption spectra derived *at* each annealing temperature between 320 and 350 K (Figure 4b) indicate the shift of the blue absorption feature to the "purple form". Assuming this to be a distinct form of the poly-PCDA, and that all blue form has been converted to purple at 328 K (where the purple feature is maximized), we apply a three-component EMA analysis (see Appendix) to the ellipsometric spectra of Figure 4b. This gives the volume fractions of blue, purple, and red forms *at the annealing temperatures*. The result is shown in Figure 5b. While the assumptions underlying this analysis are not completely rigorous, it allows us to illustrate the temperatures at which each form is created, and the pathways for conversion of the material from blue to red. Examination of Figure 5 shows that the purple form reverts primarily to blue after quenching to room temperature, with approximately 30% converting to red after annealing to 330–340 K and then quenching to room temperature. It is very likely that the ratio of red to blue material formed

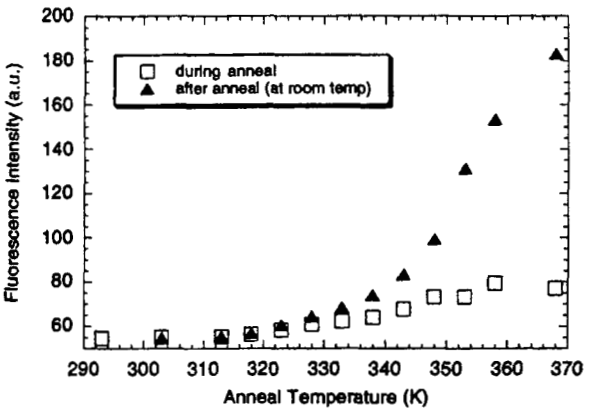

Figure 6. Fluorescence emission intensity vs temperature for a sample initially in the blue form: open squares, intensity *at* the annealing temperature; closed triangles, intensity at room temperature *after* annealing to the indicated temperature. Substantial emission does not occur until the sample is annealed above 320 K, corresponding to the onset of the formation of red poly-PCDA observed with spectroscopic ellipsometry.

at each annealing increment depends on the length of time the sample was held at the annealing temperature. However, this was not investigated in the present study.

Microscopic fluorescence intensity measurements made on a sample taken from the same film confirm the transition to the red form that is observed in the ellipsometric measurements. Figure 6 displays total fluorescence intensity for an initially blue sample, both during annealing and after quenching to room temperature. Initially, the blue sample displays almost no fluorescence. Fluorescence is also very low at temperatures where the purple form exists (313–343 K). Strong fluorescence begins to appear in the room-temperature measurements after the sample is annealed above 320 K. This coincides with the appearance of the red form in the ellipsometric data of Figure 5a. We have reported the room-temperature fluorescence spectrum elsewhere.[7] It consists of a large peak at 640 nm and a smaller peak at 560 nm. While the ellipsometric absorption data indicate that conversion to the red form was complete above 353 K, the fluorescence emission further increases between the final two experimental annealing cycles at 363 and 368 K. Thus, the fluorescence intensity may be more sensitive to the structure of the film than the absorption. This effect may also partially result from somewhat different heating and cooling rates in the two measurements.

The fluorescence intensity of thermochromic red films is strongly diminished at elevated temperatures. As seen in Figure 6, substantial fluorescence from the red form at room temperature (solid triangles) is reduced when the sample is being annealed (open squares). To completely separate this effect from fluorescence changes occurring due to the blue-to-red transition, we obtained microscopic fluorescence intensity measurements on a photochromic red film using the same series of anneal and quenching steps. Figure 7 shows that fluorescence is also strongly reduced at elevated temperatures for the photochromic red film. Yet, according to the ellipsometric measurements, these films maintain their characteristic red absorption spectrum at elevated temperatures. This effect is reversible, as the fluorescence emission recovers after quenching to room temperature. Furthermore, as seen in Figure 7, *cooling* the sample below room temperature leads to an *increase* in fluorescence emission. Thus, fluorescence emission for red films has a completely reversible and distinct temperature dependence.

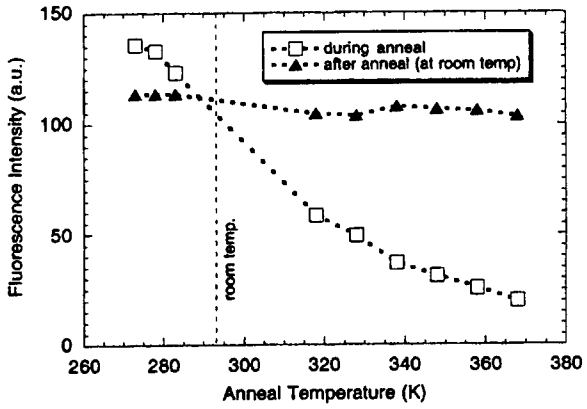

Figure 7. Fluorescence emission intensity vs temperature for a sample initially in the red form: open squares, intensity *at* the annealing temperature; closed triangles, intensity at room temperature *after* annealing to the indicated temperature. The emission at room temperature is unaffected by the annealing cycles. Increased temperature reduces fluorescence emission, and cooling below room temperature increases fluorescence emission.

Discussion

Initial and Final Conversion to the Red Form. The observed threshold anneal temperatures of ~320 K to initiate creation of red poly-PCDA, and 353 K to establish nearly complete conversion to the red form, is similar to previous studies of other poly-PCDA films. Comparisons with these studies are somewhat complicated by the fact that the film properties (e.g., number of layers, use of interlayer divalent ions) and the thermal treatments differ from ours. Deckert et al. studied thermochromism of a 30-layer Cd^{2+} salt of poly-PCDA formed by the Langmuir–Blodgett technique on both sides of a hydrophobic glass slide.[23] Absorption spectroscopy was performed as a function of temperature, and similar thermochromic effects were observed, although with some differences that will be discussed below. They observed that changes in the optical absorption spectrum of their poly-PCDA films were fully reversible up to 317 K. Complete conversion to the red form occurred at ~355 K, with only a small recovery of the blue form upon returning to room temperature. Mino et al.[22] studied 25-layer Ca^{2+} salts of poly-PCDA on quartz and observed full reversibility up to 323 K. After annealing to 343 K, the film was largely converted to the red form, but there was some recovery of the blue form absorption features upon cooling. Absorption spectra were not reported for higher anneal temperatures. Lio et al. studied a trilayer film of poly-PCDA formed on glass substrates modified with a hydrophobic coating[9] and measured absorption spectra at room temperature only, after a series of annealing cycles. They observed very little change in the absorption spectrum at room temperature after annealing to 323 K. The film showed partial conversion to the red form after annealing to 343 K, and complete conversion to red poly-PCDA was observed after annealing to 363 K. The films of Lio et al. were not fully blue to begin with, as absorption features indicated a partial presence of the red form in the film, presumably formed by photochromism during the initial polymerization step. Collectively, these studies, along with ours, indicate that the optical properties of poly-PCDA films can be reversibly altered by heating to approximately 320 K. Overall this change is far less profound than the changes that occur with full conversion to the red form, which occurs at ~353 K in our film.

Intermediate Purple Form. The purple form appears over the temperature range of 313–343 K, and its appearance at these elevated temperatures is primarily associated with the disappearance of the blue form. Inspection of Figures 4b and 5b show that the purple absorption feature reaches its maximum intensity at about 330 K, while the blue absorption at 640 nm has largely disappeared. However, upon quenching to room temperature the blue form reappears and is still the predominant component of the film. We see no evidence for existence of the purple form at room temperature after any annealing step, as the two-component (red and blue) model provides good fits to all the room-temperature ellipsometry results (Figure 4a). As seen in Figure 4b, the peak of the purple form absorption shifts to shorter wavelength as the temperature increases, and there does not appear to be an isosbestic point associated with the disappearance of blue form and appearance of purple. Since the purple form exists only at elevated temperature, it appears not to be a stable or metastable form of the material, which is interconvertible with the blue form.

These results lead us to propose that the purple form is a thermally distorted configuration of the blue form exhibiting a substantial shift of the absorption spectrum to shorter wavelengths. The purple form may represent a transition state in the conversion to the red form. However, our results indicate that it is energetically favorable for the purple form to revert to the blue, suggesting that the true transition state lies somewhat higher in energy and further along the reaction coordinate toward the red form. This conclusion is supported by the fact that no reversible behavior is seen in these films once they have been converted to the red form; annealing red films does not result in appearance of the purple form or conversion back to the blue form. This conclusion is also consistent with the aforementioned study of Mino et al.,[22] which involved 25-layer samples of Ca^{2+} salts of poly-PCDA. They obtained UV–visible absorption spectra, differential scanning calorimeter (DSC) curves, and IR spectra as a function of temperature. The IR spectra support the hypothesis that at elevated temperatures (~323–346 K), a thermally distorted blue form is present. Specifically, it was found that IR absorption bands corresponding to the side chains (CH_2 scissoring, and $(CH_2)_n$ twisting and wagging vibrations) became significantly weaker above 323 K due to disordering. In addition, the film exhibited a melting transition at 346 K as observed with DSC. As mentioned above, nearly complete conversion to the red form for our film did not occur until annealing at 353 K. Therefore, we can expect the hydrocarbon side chains to exhibit significant disordering in the temperature range ~323–350 K, while the red form has not yet been fully formed thermochromically. This may account for the purple form we observe.

We see no evidence that the three layers within the film change to the red form at different rates. If this were the case, the multicomponent EMA model would not show good agreement with our results; layers with different optical properties can be distinguished using this model. To completely rule out such an effect, future experiments using a monolayer sample are planned, as we have recently succeeded in producing high-quality monolayer PDA samples.[21]

Reaction Scheme. Deckert et al., in a study of thicker Cd^{2+} salt films of 5,7-diacetylenes,[24] have proposed a two reaction scheme from blue (B) to red (R) occurring in series, involving a reversible transition to an intermediate

purple (P) form:

$$B \leftrightarrow P \rightarrow R \quad (3)$$

In that work, the two-reaction scheme provided a consistent model for absorption spectra obtained over the temperature range of 290–360 K. However, a different reaction scheme was proposed by Deckert et al. in an earlier study of 10,12-diacetylene films including PCDA.[23] The data from that study favored a reversible transition between blue and red forms and an irreversible transition from the purple to red form:

$$B \leftrightarrow R, \quad P \rightarrow R \quad (4)$$

We have carried out first-order kinetic simulations to test whether either of the above schemes is consistent with our results. For any reasonable barriers for the B ↔ P reactions, the series kinetic scheme in eq 3 would predict incomplete conversion of B → P upon heating and incomplete reversion of P → B after quenching. This is not consistent with our results, as we observe a complete and reversible transition from the blue form to the intermediate purple form upon heating. As well, there is apparently no energetic barrier to reversion of P → B since the blue absorption features fully recover upon quenching to room temperature. The parallel reaction scheme of eq 4 requires a significant initial presence of the purple form in the film and would predict significant reversibility between blue and red forms at elevated temperatures. Our data are not consistent with these conditions. Thus, according to our kinetic simulations, no kinetic scheme involving a stable or metastable purple form of the poly-PCDA is consistent with our data.

Rather, our data support a mechanism in which the purple form is in fact thermally distorted blue material, involving a substantial shift in the absorption spectrum, as opposed to a significant structural transition that would involve energetic barriers between blue and purple forms. In addition to the observed reversibility between blue and purple forms, we also observe total, irreversible conversion to the red form after heating to 353 K or higher. This is convincingly supported both by the absorption spectra from ellipsometry measurements and from the fluorescence emission experiments. We propose a simple, first-order, irreversible transition from blue/purple to red (B → R) for this film.

Kinetic Analysis from Time-Resolved Fluorescence Emission. The fluorescence intensity measurements confirm that only the red form of poly-PCDA displays strong fluorescence. This is a general property of PDA materials, be they thin films,[6,7] bulk samples,[35,36] or solutions.[37] The blue form does not fluoresce due to the presence of low-lying excited states having the same A_g symmetry as the ground state.[38] This study establishes that the intermediate purple form is nonfluorescent. Therefore, fluorescence emission is a sensitive gauge of the transition to the red form.[7]

We can then obtain kinetic information for the irreversible transition to the red form by examining time-resolved measurements of fluorescence emission. Assuming first-order kinetics at fixed temperature, the amount of blue poly-PCDA [B] is determined by

$$d[B]/dt = -k[B] \quad (5)$$

Thus

$$[B]/[B_0] = e^{-kt} \quad (6)$$

where $[B_0]$ is the initial amount of blue and k is the rate constant. Since only blue and red forms are present, the rate of creation of red poly-PCDA [R] is

$$\frac{[R]}{[R_{max}]} = 1 - \frac{[B]}{[B_0]} = 1 - e^{-kt} \quad (7)$$

where $[R_{max}]$ is the final amount of red poly-PCDA. We assume that the isothermal fluorescence intensity is proportional to [R]. Figure 8a shows a typical plot of fluorescence intensity vs time, in this case at 350 K, with a least-squares fit of eq 7. Along with fitting the rate constant and $[R_{max}]$, we must also account for an offset of the time axis since the sample heating begins after the

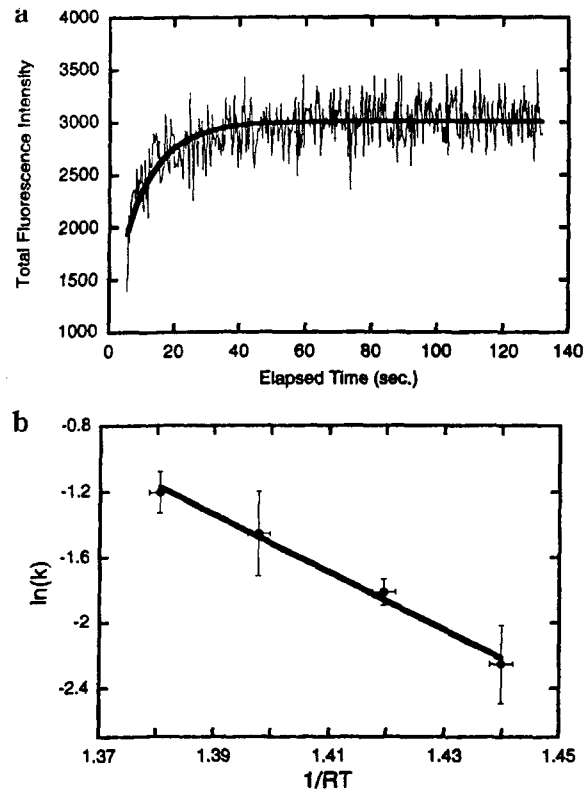

Figure 8. (a) Plot of fluorescence vs time at 350 K (circles) with a least-squares fit of eq 7 (solid line). Each data point represents integrated fluorescence intensity between 585 and 720 nm. The fluorescence spectra are acquired every 250 ms with approximately 50 ms delay between each acquisition. The fit provides a value of k for each measurement. Several fits to each set of data were performed due to uncertainty in the starting time of the measurement. (b) Arrhenius plot [ln(k) vs $1/RT$] of several measurements of fluorescence vs time such as in part a. Measurements of k were acquired at four temperatures (345, 350, 355, and 360 K). The error bars represent the statistical spread of fits at the same temperature. The linear behavior confirms that first-order kinetics provides an accurate description of this system. The energy barrier determined from this plot is $E = 17.6 \pm 1.1$ kcal mol^{-1}.

(35) Yasuda, A.; Yoshizawa, M.; Kobayashi, T. *Chem. Phys. Lett.* **1993**, *209*, 281–6.
(36) Baughman, R. H.; Chance, R. R. *J. Polym. Sci., Polym. Chem. Ed.* **1976**, *14*, 2037.
(37) Bhattacharjee, H. R.; Preziosi, A. F.; Patel, G. N. *J. Chem. Phys.* **1980**, *73*, 1478–80.
(38) Lawrence, B.; Torruellas, W. E.; Cha, M.; Sundheimer, M. L.; Stegeman, G. I.; Meth, J.; Etemad, S.; Baker, G. *Phys. Rev. Lett.* **1994**, *73*, 597–600.

Table 1. Comparisons of activation barriers for various PDA films

ref	monomer	proposed reaction	barrier (kcal mol^{-1})
	Two Reaction Scheme, First Step[a]		
24	DCDA,[b] $CH_3(CH_2)_{11}C{\equiv}CC{\equiv}C(CH_2)_3COOH$[c]	B → P	21.7[d]
24	TTCDA,[e] $CH_3(CH_2)_{15}C{\equiv}CC{\equiv}C(CH_2)_3COOH$[c]	B → P	21[d]
23	TCDA,[f] $CH_3(CH_2)_9C{\equiv}CC{\equiv}C(CH_2)_8COOH$[c]	B → R[g]	22.5
23	PCDA, $CH_3(CH_2)_{11}C{\equiv}CC{\equiv}C(CH_2)_8COOH$[c]	B → R[g]	21.5
	Two Reaction Scheme, Second Step		
23	TCDA[c]	P → R	23
23	PCDA[c]	P → R	22.5
	Single Reaction Scheme		
this work	PCDA[h]	B → R	17.6 ± 1.1

[a] This step is considered to be reversible in the reaction schemes considered. [b] 5,7-Docosadiynoic acid. [c] Film consisted of Cd^{2+} salts of the particular PDA molecule, with 30 layers on both sides of a hydrophobic glass slide. Polymerization was performed after the monomer film was transferred to the glass slide. [d] Barrier is for a "high density" film of molecular area 22 Å^2 molecule^{-1}, comparable to our films. "Low density" films (26 Å^2/molecule) exhibited slightly higher activation barriers.[24] [e] 5,7-Tetracosadiynoic acid. [f] 10,12-Tricosadiynoic acid. [g] Deckert et al. suggest that a reversible reaction step between blue and *purple* forms (B → P) may occur as well.[24] [h] This work. Films in this study were pure PCDA monomers, polymerized on the Langmuir trough as a trilayer and then transferred to hydrophilic Si substrates.

data acquisition has started. Before the sample is in place, a large amount of excitation light is scattered from the stage into the collection fiber. Once the sample is placed on the stage, the scattered light is greatly reduced, allowing us to determine the offset of the time axis to within two spectral acquisition windows (±500 ms). This uncertainty is taken into account in determining the rate constant from the fit. The rate constant at a fixed temperature T is given by

$$k = Ae^{-E/RT} \tag{8}$$

where E is the energy barrier, $R = 1.9 \times 10^{-3}$ kcal mol^{-1} K^{-1}, and A is the pre-exponential factor. Therefore, the slope of an Arrhenius plot [$\ln(k)$ vs $1/RT$] will be the energy barrier E. The result is plotted in Figure 8b. The error bars represent the statistical spread of fits at the same temperature. The linear behavior confirms that first-order kinetics provides an accurate description of this system. From the Arrhenius plot we determine $E = 17.6 \pm 1.1$ kcal mol^{-1}. In Table 1 we compared this to activation barriers measured by Deckert et al. for a range of thicker Cd^{2+} salt PDA films.[23,24] As discussed previously, Deckert et al.'s models consisted of two different two-reaction schemes both involving a distinct purple form separated by an energy barrier from the blue form; this complicates any direct comparison with our results. Nevertheless, all of the activation barriers from the schemes of Deckert et al. are somewhat larger than the present measurement. The fact that our films are only three layers thick and lack metal ion complexation may affect the kinetics of the transition significantly. In particular, our film is likely to exhibit fewer defects and stronger thermal coupling between and within layers due to their crystallinity and structural registry. These factors would likely tend to reduce the energy barrier. The extremely low substrate roughness and lack of metal salt ions in our film may also enhance the ability of the PDA molecules to undergo structural changes compared with the thick films. This would also tend to reduce the energy barrier. Direct comparisons of different films in the same experiment would be needed to verify these effects.

Thermal Reduction of Fluorescence Emission. The decrease in fluorescence emission from red films at elevated temperature is not accompanied by a similar decrease in absorption. Rather, the absorption spectrum of red films remains constant at elevated temperatures, according to ellipsometric measurements. Therefore, the fluorescence emission must be reduced by a substantial enhancement of nonradiative decay processes, as opposed to changes in the absorption characteristics.

As mentioned above, Mino et al.[22] observed significant thermal fluctuations of the side chains of a blue film when annealed above 323 K. Furthermore, these fluctuations lead to a disordered film structure. Unfortunately, they did not perform thermal cycling experiments; only a single increasing temperature ramp was used. Therefore, their study does not establish the degree of order in the film at room temperature in the red form (i.e., after annealing). Recent evidence suggests that the thermochromic red form is in fact *more* ordered than the blue form at room temperature, at least for trilayer poly-PCDA films. In the study of Lio et al.,[9] the CH_2 antisymmetric stretching band in the IR spectrum at room temperature increased in intensity and downshifted in frequency after annealing a blue film to 343 K and remained so after further annealing up to 383 K. These IR spectral changes indicate a more ordered side chain arrangement after the thermochromic transition.[9] Furthermore, Lio et al. obtained molecular-lattice resolved images of blue and thermochromic red poly-PCDA trilayer films using AFM. The images clearly demonstrated that the side chains are more ordered in the thermochromic red form than the blue. This effect may also be related to our observation that fluorescence emission from the thermochromic red film at room temperature is enhanced by further annealing the film at temperatures up to at least 368 K (Figure 6). The additional anneal may promote ordering of the side chains in the thermochromic red film when cooled back to room temperature. Several factors therefore suggest a general correlation between side chain ordering and fluorescence emission.

The above results indicate that we can expect significant fluctuations of the side chains, and presumably the backbones to which they are attached, at elevated temperatures. Furthermore, these thermally induced molecular fluctuations lead to a reduction of molecular order at elevated temperatures. Both of these factors may enhance nonradiative de-excitation pathways. If so, we would then expect that cooling a photochromic red film would increase the fluorescence emission. This is indeed observed (Figure 7). Further studies of the vibration and emission spectra of these films as a function of temperature are required to investigate this hypothesis more rigorously.

Summary

We have shown that spectroscopic ellipsometry can be used to monitor thermochromism in ultrathin poly(diacetylene) films. Spectroscopic ellipsometry reveals that trilayer films of poly-PCDA exhibit a partially reversible transition from the blue form to an intermediate purple form, followed by an irreversible transition to the red form. The purple form appears to be thermally distorted blue material. The purple form is present only at elevated temperatures and exhibits a large, reversible shift in the absorption spectrum to shorter wavelengths. From time-resolved fluorescence experiments we determine an energy barrier of 17.6 ± 1.1 kcal mol^{-1} for the irreversible transition from blue/purple to red forms. Only the red form exhibits significant fluorescence emission. Thermal effects reduce fluorescence emission at elevated temperatures. It is likely that thermal fluctuations of the side chains reduce fluorescence emission.

Acknowledgment. We gratefully acknowledge M. L. Thomas who implemented the heating stage used for these measurements and M. B. Sinclair and J. A. Hunter who assisted in setting up the time-resolved fluorescence experiments. We gratefully acknowledge N. D. Shinn for providing a thorough review of this manuscript. R.W.C. acknowledges the support of the Natural Sciences and Engineering Research Council of Canada. Sandia is a multiprogram laboratory operated by Sandia Corporation, a Lockheed Martin Company, for the United States Department of Energy under Contract DE-AC04-94AL85000.

Appendix

Ellipsometric Analysis. A. Lorentz Oscillator Parametrization. The complex dielectric function of the poly-PCDA "red", "blue", and "purple" forms as a function of photon energy is modeled as a sum of Lorentz oscillators, given by

$$\tilde{\epsilon}(E) = \epsilon_1(\infty) + \sum_{i=1}^{N} \frac{A_i}{(E_{c,i}^2 - E^2 - iB_iE)} \qquad \text{(A1)}$$

We employ the minimum number of oscillators required to characterize the major absorption features of the data, as well as the baseline absorption. The values of $\epsilon_1(\infty)$, amplitude, A, width, B, and the peak energy, E_c, of the the three poly-PCDA forms are given in Table 2. The complex index of refraction is related to the complex dielectric function by

Table 2. Lorentz Oscillator Model Parameters for Poly-PCDA Films for the Wavelength Range 450–700 nm

i	$\epsilon_1(\infty)$	A (eV^2)	B (eV)	E_c (eV)
"red" form				
	3.6958			
1		0.26902	0.05363	2.251
2		0.91248	0.23264	2.4477
3		73.179	1.6481	3.8619
"blue" form				
	1.2455			
1		0.25339	0.093042	1.947
2		3.802	0.76813	2.3277
3		50.508	0.77156	3.5966
"purple" form				
	0.79317			
1		0.21002	0.13649	2.094
2		0.61777	0.20296	2.301
3		2.2458	0.55236	2.529
4		52.152	0.79345	3.5905

$$\tilde{N}^2 = \tilde{\epsilon}^2 \qquad \text{(A2)}$$

B. Effective Medium Model. Inhomogeneous films containing two or more distinct components can be successfully modeled using an effective medium approach.[33] In this procedure the optical constants of an "effective film" are constructed from the optical constants of the constituent materials and treated as a single layer in the optical model. In the Bruggeman effective medium approximation used here,[33] the complex index of the effective film, N_e, is obtained from

$$\sum_i f_i \frac{\tilde{N}_i^2 - \tilde{N}_e^2}{\tilde{N}_i^2 + \tilde{N}_e^2} \qquad \text{(A3)}$$

where N_i and f_i are the complex indices of refraction and volume fractions of the constituent materials. N_i for the poly-PCDA forms are as given in Section A, and f_i are the adjustable parameters in the model.

All ellipsometric models and calculations are included in the standard analysis software provided with the spectroscopic ellipsometer (J. A. Woollam Co., Lincoln, NE).

LA991580K

8. Ramasastry, C. & Ramaiah, A. S. Electrical conduction in $Na_3H(SO_4)_2$ crystals. *J. Mater. Sci. Lett.* **16**, 2011–2016 (1981).
9. Chisholm, C. R. I., Merinov, B. V. & Haile, S. M. High temperature phase transitions in $K_3H(SO_4)_2$. *Solid State Ion.* (in the press).
10. Gaskell, D. R. *Introduction to Metallurgical Thermodynamics* 2nd edn, 574 & 586 (McGraw-Hill, Washington DC, 1981).
11. Srinivasan, S., Velev, O. A., Parthasarathy, A., Manko, D. J. & Appleby, A. J. High energy efficiency and high power density proton exchange membrane fuel cells—electrode kinetics and mass transport. *J. Power Sources* **36**, 299–320 (1991).
12. Croce, F. & Cigna, G. Determination of the protonic transference number for KH_2PO_4 by electromotive force measurements. *Solid State Ion.* **6**, 201–202 (1982).
13. Minh, N. Q. Ceramic fuel cells. *J. Am. Ceram. Soc.* **76**, 563–588 (1993).
14. Minh, N. Q. & Horne, C. R. in *Proc. 14th Risø Int. Symp. on Materials Science: High Temperature Electrochemical Behaviour of Fast Ion and Mixed Conductors* (eds Poulsen, F. W., Bentzen, J. J., Jacobsen, T., Skou, E. & Østergård, M. J. L.) 337–341 (Risø National Laboratory, Roskilde, 1993).
15. Baranov, A. I., Khiznichenko, V. P., Sandler, V. A. & Shuvalov, L. A. Frequency dielectric dispersion in the ferroelectric and superionic phases of CsH_2PO_4. *Ferroelectrics* **81**, 183–186 (1988).
16. Slade, R. C. T. & Omana, M. J. Protonic conductivity of 12-tungstophosphoric acid (TPA, $H_3PW_{12}O_{40}$) at elevated temperatures. *Solid State Ion.* **58**, 195–199 (1992).
17. Haile, S. M., Narayanan, S. R., Chisholm, C. & Boysen, D. Proton conducting membrane using a solid acid. US patent 09/439,377 (15 Nov. 2000).

Supplementary information is available on *Nature*'s World-Wide Web site (http://www.nature.com) or as paper copy from the London editorial office of *Nature*.

Acknowledgements

We thank J. Snyder for assistance with computer automation of the fuel cell test station and S. R. Narayanan for technical discussions. Financial support has been provided by the California Institute of Technology through the Yuen Grubstake entrepreneurial fund.

Correspondence and requests for materials should be addressed to S.M.H. (e-mail: smhaile@caltech.edu).

Self-assembly of mesoscopically ordered chromatic polydiacetylene/silica nanocomposites

Yunfeng Lu*†‡§, Yi Yang†, Alan Sellinger‡§, Mengcheng Lu†, Jinman Huang†, Hongyou Fan‡, Raid Haddad†, Gabriel Lopez†, Alan R. Burns‡, Darryl Y. Sasaki‡, John Shelnutt‡ & C. Jeffrey Brinker†‡

† *The University of New Mexico Center for Micro-Engineered Materials and Department of Chemical and Nuclear Engineering, Albuquerque, New Mexico 87131, USA*
‡ *Sandia National Laboratories, Advanced Materials Laboratory, 1001 University Blvd SE, Albuquerque, New Mexico 87106, USA*
* *These authors contributed equally to this work.*

Nature abounds with intricate composite architectures composed of hard and soft materials synergistically intertwined to provide both useful functionality and mechanical integrity. Recent synthetic efforts to mimic such natural designs have focused on nanocomposites[1–5], prepared mainly by slow procedures like monomer or polymer infiltration of inorganic nanostructures[6,7] or sequential deposition[8,9]. Here we report the self-assembly of conjugated polymer/silica nanocomposite films with hexagonal, cubic or lamellar mesoscopic order using polymerizable amphiphilic diacetylene molecules as both structure-directing agents and monomers. The self-assembly procedure is rapid and incorporates the organic monomers uniformly within a highly ordered, inorganic environment. Polymerization results in polydiacetylene/silica nanocomposites that are optically transparent and mechanically robust. Compared to ordered diacetylene-containing films prepared as Langmuir monolayers[10] or by Langmuir–Blodgett deposition[10], the nanostructured inorganic host alters the diacetylene polymerization behaviour, and the resulting nanocomposite exhibits unusual chromatic changes in response to thermal, mechanical and chemical stimuli. The inorganic framework serves to protect, stabilize, and orient the polymer, and to mediate its function. The nanocomposite architecture also provides sufficient mechanical integrity to enable integration into devices and microsystems.

Owing to extended π-electron delocalization along their backbones, conjugated organic polymers exhibit electronic and optical properties of interest for applications ranging from light-emitting diodes to biomolecular sensors[11]. For example, in blue-coloured polydiacetylene, the optical absorption blue-shifts dramatically when stress is applied to the backbone through the pendant side chains, and this thermally, mechanically, or chemically induced chromatic (blue → red) response has been explored as a colorimetric transduction scheme in a variety of chemically and physically based sensor designs[12,13]. Further improvements of the electronic and optical performance of conjugated polymer devices may require polymer incorporation in nano-engineered architectures[14] that could provide alignment, control charge and energy transfer, mediate conformational changes and prevent oxidation. Recently control of energy transfer was demonstrated in a poly[2-methoxy-5-(2′-ethyl-hexyloxy-)-1,4-phenylene vinylene] (MEH-PPV)/silica nanocomposite[7]. However, this nanocomposite, prepared by MEH-PPV infiltration of a pre-formed, oriented, hexagonal, silica mesophase, was heterogeneous, exhibiting two distinct conjugated polymer environments, that is, polymers inside and outside the hexagonally arranged pore channels of the silica particles. In general, because polymer infiltration into a pre-formed porous nanostructure depends on the partitioning of the polymer from the solvent, we expect it to be difficult to control polymer concentration, orientation and uniformity in the corresponding nanocomposite. Further, when the nanostructure pore size is less than the radius of gyration of the solvated polymer, infiltration proceeds by a worm-like motion referred to as reptation, requiring long processing times at elevated temperatures[7].

We use a series of oligoethylene glycol functionalized diacetylenic (DA-EO$_n$) surfactants (structure **1**, with $n = 3$, 4 5, or 10), prepared by coupling ethylene glycols with the acid chloride of PCA (structure **2**)

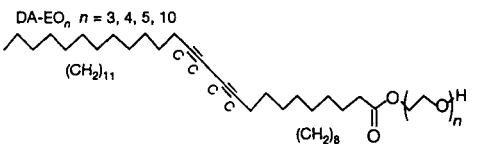

1

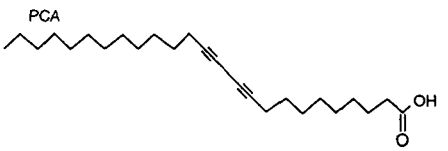

2

both as amphiphiles to direct the self-assembly of thin film silica mesophases[15] and as monomeric precursors of the conjugated polymer, polydiacetylene (PDA). Beginning with a homogeneous solution of silicic acid and surfactant prepared in a tetrahydrofuran (THF)/water solvent with initial surfactant concentration c_o much less than the critical surfactant micelle concentration CMC, we use evaporative dip-coating, spin-coating, or casting procedures to prepare thin films on silicon ⟨100⟩ or fused silica substrates (Fig. 1). During deposition, preferential evaporation of THF

§ Present address: Tulane University Chemical Engineering Department, New Orleans, Louisiana 70118, USA (Y.L.); Canon Research and Development Center Americas, San Jose, California 95134, USA (A.S.).

concentrates the depositing film in water and nonvolatile silica and surfactant species. The progressively increasing surfactant concentration drives self-assembly of diacetylene/silica surfactant micelles and their further organization into ordered, three-dimensional, liquid crystalline mesophases. Ultraviolet-light-initiated polymerization of the DA units, accompanied by catalyst-promoted siloxane condensation, topochemically converts the colourless mesophase into the blue PDA/silica nanocomposite, preserving the highly ordered, self-assembled architecture.

The choice of surfactant greatly influences the resultant mesostructure. This is evident from the X-ray diffraction (XRD) patterns and TEM micrographs shown in Figs 2 and 3 for nanocomposites prepared from diacetylenic surfactants with tri ($n = 3$), penta ($n = 5$) and decaethylene ($n = 10$) glycol head groups. Increasing values of n increase the surfactant head group area a_o. This in turn reduces the value of the surfactant packing parameter, $g = v/a_o l$, where v is the surfactant volume and l the tail length[16], favouring the formation of progressively higher-curvature mesophases: lamellar ($n = 3$) → hexagonal ($n = 5$) → cubic ($n = 10$). From the highly ordered nanocomposite mesostructures observed by transmission electron microscopy (TEM), we infer that the surfactant monomers/structure-directing agents are uniformly organized into precise spatial arrangements before polymerization. These arrangements establish the proximity (topochemistry) of the reactive diacetylenic moieties and thus strongly influence the PDA polymerization process. This is best illustrated by comparing their polymerization behaviour, as shown by the blue (or red) colour of nanocomposite films prepared with different mesostructures (that is, the hexagonal, cubic, and lamellar mesostructures shown in Fig. 3) and contrasting these behaviours with those of planar self-assembled monolayer and trilayer films formed by Langmuir–Blodgett deposition of the neat DA surfactants.

Figure 4 shows a patterned blue PDA/silica nanocomposite film, with a hexagonal mesostructure (prepared using structure **1**, with $n = 5$), formed by ultraviolet exposure through a mask; the corresponding patterned red film was formed subsequently by heating to 100 °C (Fig. 4b). Whereas lamellar mesophases (prepared using structure **1** with $n = 3$) show qualitatively similar behaviour, cubic mesostructures (prepared using structure **1** with $n = 10$) and Langmuir monolayers and trilayers (prepared using neat **1** with $n = 3$, 5 or 10) remain colourless upon ultraviolet exposure and during heating. The different behaviour of lamellar and Langmuir films emphasize the importance of the nanostructured inorganic host on PDA polymerization. In both systems the diacetylenic

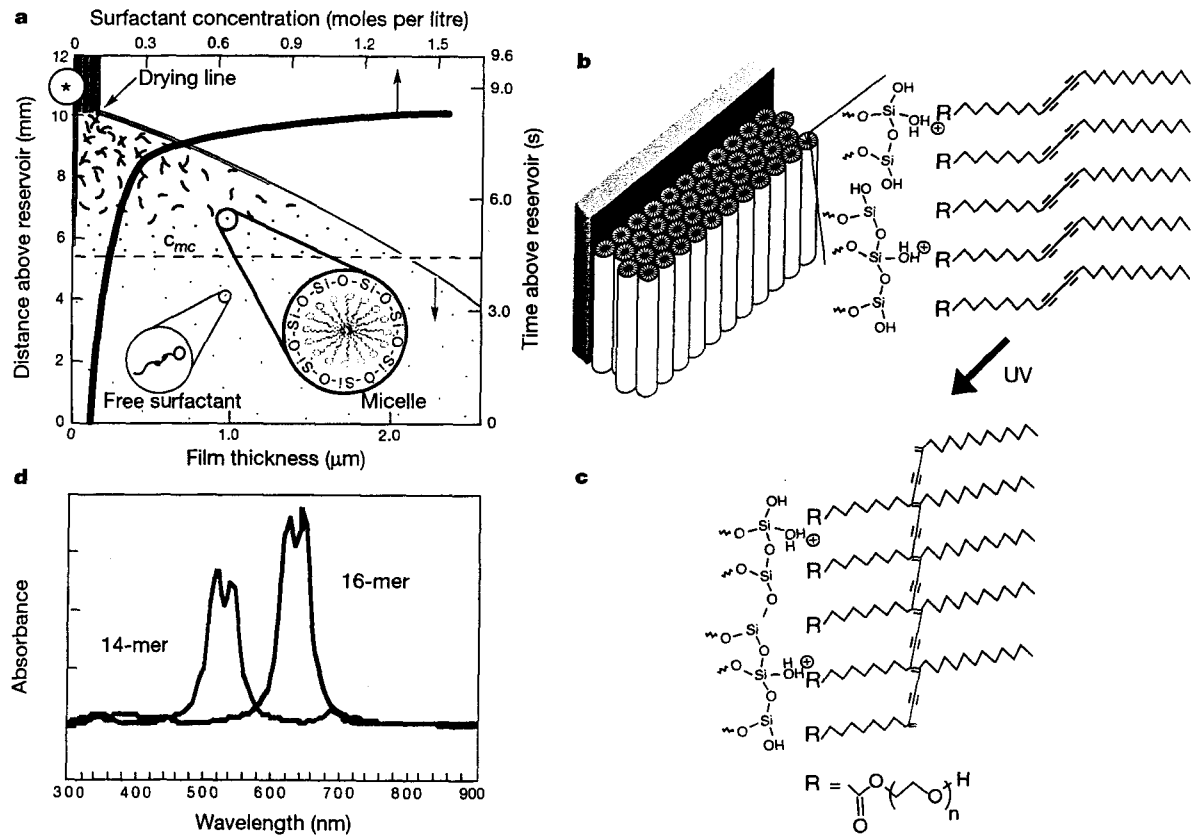

Figure 1 Schematic representation of the PDA/silica nanocomposite evaporation-induced self-assembly process. **a**, Steady-state film thickness and surfactant concentration profiles developed during dip-coating, with vertical axes representing distance and time above reservoir surface and horizontal axes showing film thickness and surfactant (structures **1** or **2**) concentration for $c_o = 0.034$ M. Beginning with a homogeneous solution prepared with $c_o <$ CMC, preferential THF evaporation induces micellization and further self-organization of silica–surfactant composite micelles into ordered thin-film mesophases. The shape and concentration of the DA surfactants influence the mesophase established at the drying line (lamellar, hexagonal or cubic). **b**, Section near asterisk shows a hexagonal mesostructure and hypothetical arrangement of DA surfactants adjacent to the cylindrically structured silicic acid framework. **c**, Hypothetical structure of polymerized PDA/silica nanocomposite formed upon exposure to ultraviolet light and continued acid-catalysed siloxane condensation. **d**, Ultraviolet–visible spectra of cyclic polydiacetylene oligomers determined by INDO/S (Intermediate Neglect Differential Orbital Spectra) quantum calculations after energy-optimization and 10 ps of molecular dynamics. The 16-membered oligomer with diameter of about 2.4 nm absorbs in the red region of the visual spectrum with spectral characteristics commensurate with the blue form of PDA (compare with Fig. 4e). The higher-curvature 14-membered PDA oligomer is strained and has a blue-shifted absorption spectrum consistent with the red form of PDA (compare with Fig. 4e).

surfactants are organized into highly oriented planar configurations with the EO headgroups disposed toward the hydrophilic interface, either water (Langmuir films) or polysilicic acid (nanocomposites). Despite these similar organizations, we suggest that Langmuir films do not polymerize because the reactive DA moieties are spaced too far apart, as indicated by the molecular areas measured at $30\,mN\,m^{-1}$ in a Langmuir trough: DA-EO_1 = 24 Å^2, DA-EO_3 = 38 Å^2, DA-EO_5 = 46 Å^2. Closer spacing of the EO headgroups (and correspondingly the diacetylenic moieties) within the self-assembled nanocomposites (lamellar, hexagonal or cubic) is anticipated from the requirement for charge density matching at the R-$EO_{n-y}[EO{\cdot}H_3O^+]_y{\cdot}{\cdot}yX^-{\cdot}{\cdot}wI^{\delta+}$ interface (where R = alkyl chain, $y \leq n$, $X = Cl^-$, $I^{\delta+}$ = the silica framework carrying a partial charge of δ^+, and w is the 'concentration' of framework needed for charge balance) that reduces the optimal EO headgroup area a_o (ref. 17). This closer spacing is reflected in measurements of the biaxial stress resulting from PDA polymerization, where, for nanocomposites, we observe development of compressive stress upon polymerization (film turns blue) and during the solvatochromic or thermochromic blue → red transformation; this indicates a net expansion of the PDA relative to the silica host (see Fig. A in the Supplementary Information). The corresponding neat DA surfactants prepared as Langmuir monolayers do not polymerize and develop no stress upon ultraviolet irradiation. Polymerizable DA Langmuir monolayers and multilayers (prepared using surfactants with smaller headgroups) contract upon polymerization and the magnitude of this contraction is used to assess the extent of polymerization[18].

The importance of the proximity of the DA moieties on polymerization is further illustrated by our inability to polymerize DA within the cubic mesophase prepared with $n = 10$ (see Fig. 3b and c). The large EO_{10} surfactant headgroups are necessary to direct the formation of the cubic mesophase, but they also serve as spacers preventing polymerization. Introduction of structure **1**, with $n = 3$ or 5 or structure **2** as co-surfactants with smaller headgroups (30–50 wt% relative to EO-DA_{10}) allows us to form cubic mesophases and to polymerize the mixed surfactant assemblies into the blue and red forms of PDA. (We expect that, owing to phase separation[19], this is not possible in Langmuir monolayers or Langmuir–Blodgett films).

The polymerization of the surfactant is highly dependent upon the topological alignment of diacetylenic units within the supramolecular assembly[20,21]. Additionally, for colorimetric materials to form (especially blue-coloured materials), the degree of polymerization and conjugation length of the 'ene'–'yne' backbone must be considerable[22]. The micellar structures that template the silica sol–gel material must thus contain highly oriented, densely packed surfactants. This packing will allow facile topochemical polymerization of the diacetylene units to give coloured polydiacetylene.

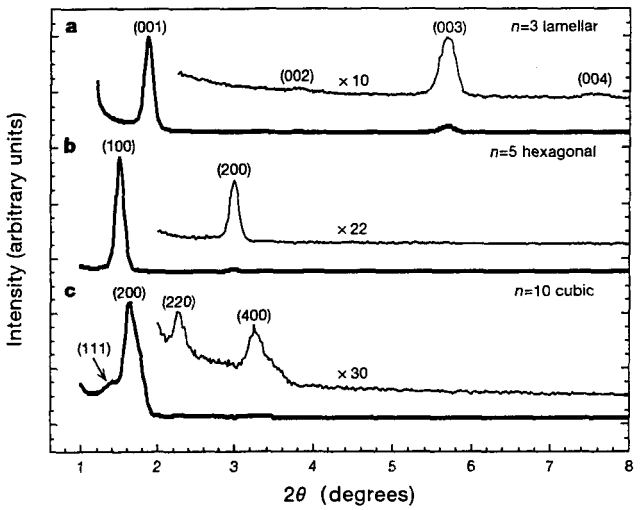

Figure 2 X-ray diffraction (XRD) patterns of nanocomposite thin films prepared using DA-EO_n (where $n = 3$, 5, and 10) surfactants. Increasing values of n increase the surfactant head group favouring the formation of progressively higher-curvature mesophases: lamellar ($n = 3$) → hexagonal ($n = 5$) → cubic ($n = 10$). **a**, Film prepared using 1.86% of DA-EO_3 (wt% DA-EO_3 relative to the solution weight without surfactant) shows a lamellar mesostructure with (001) diffraction peak at 48 Å. The presence of higher-order diffraction peaks (002), (003) and (004) indicate the formation of highly ordered alternating silica/PDA layers. **b**, Film prepared with DA-EO_5 (2.23%) shows a hexagonal mesophase with strong (100) and (200) diffraction peaks at 56 Å and 28 Å, respectively. **c**, Film prepared using 2.23% DA-EO_{10} surfactant exhibits a cubic mesophase with unit-cell parameter a = 108.1 Å. The presence of the (111) diffraction peak at 62.4 Å and the (200) diffraction peak at 54.1 Å clearly establishes a face-centred or primary cubic structure. The presence of higher-order peaks (220) at 38.2 Å and (400) at 27.3 Å provide further evidence of the primary or face-centred cubic mesophase. Introduction of structure **1**, with $n = 3$ or 5 or structure **2**, as co-surfactants with smaller headgroups (30–50 wt% relative to EO-DA_{10}) was necessary to polymerize PDA in the blue or red forms within the cubic mesophase. The XRD patterns were essentially unchanged by these co-surfactant additions.

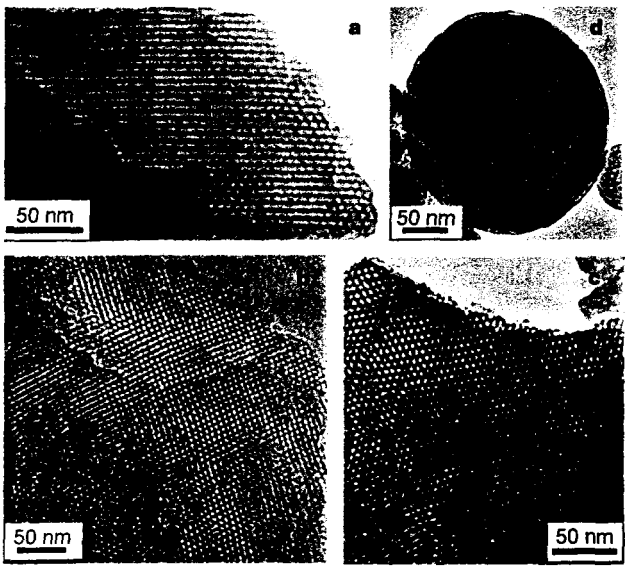

Figure 3 Representative transmission electron microscope (TEM) images of nanocomposite thin films (prepared as in Fig. 2b and c) and particles (formed by a related aerosol-assisted evaporation-induced self-assembly approach[32]). **a**, Hexagonally ordered nanocomposite prepared using 2.23% DA-EO_5 surfactant, showing a striped [110]-oriented mesophase with repeat distance around 48 Å and a region of the corresponding hexagonally patterned mesostructure characteristic of the [001]-orientation (right edge). The smaller spacing measured by TEM versus XRD (48 Å versus 56 Å, compare **a** and Fig. 2b) may be due to the over-focus condition used to achieve high contrast in TEM or electron-beam-induced shrinkage (normal to the substrate) which can occur in general for uncalcined, mesostructured materials. **b**, **c**, Two orientations of a cubic nanocomposite film prepared using 2.23% DA-EO_{10} surfactant. A highly ordered [100] orientation with unit-cell parameter at 108 Å, agreeing well with the XRD results. **c**, The corresponding [111] orientation with repeat distance of 62 Å. As for the corresponding XRD patterns, the cubic mesostructures revealed by TEM were quite comparable with and without the addition of co-surfactants (structure **1**, with $n = 3$ or 5, or structure **2**) needed to polymerize the blue or red forms of PDA within the cubic mesostructure. **d**, PDA/silica nanocomposite particles prepared using an aerosol-assisted evaporation-induced self-assembly technique[32]. The particle exhibits an ordered multi-lamellar exterior and a disordered worm-like mesostructured interior, consistent with a radially directed self-assembly process.

Figure 1 illustrates a postulated length-wise polymerization of surfactants within a cylindrical rod-like micelle to yield the blue form of PDA. Circumferential polymerization, although favoured on the basis of proximity of reactive DA moieties, would impose a high curvature on the PDA backbone because of the small pore size of the mesostructured host (2.5–3.0 nm in diameter, see Fig. B in the Supplementary Information). Although DA surfactants organized into ellipsoidal liposomes (40 nm × 15 nm) are known to polymerize in the blue and red forms[23] we questioned whether circumferential arrangements of DA surfactants (within spherical or cylindrical micelles) could polymerize with the proper 'ene'–'yne' conjugation to produce coloured materials. Molecular mechanics and dynamics calculations indicate that cyclic arrangements of up to 19 DA monomers around the periphery of the 3.0-nm-diameter pore are possible and that an energy-optimized 16-membered cyclic PDA oligomer can exhibit absorption behaviour consistent with the blue form of PDA (see Fig. 1d). Helical conformations[24] represent an alternative configuration that might satisfy DA proximity requirements without severely disrupting the conjugation. In general, nonlinear conformations may be needed for polymer propagation within these self-assembled nano-structured hosts. Such conformations are presumably rare or impossible for Langmuir monolayers and Langmuir–Blodgett films.

The PDA/silica nanocomposite films are optically transparent and mechanically robust. Modulus values measured by nanoindentation (3.50 ± 1.00 GPa) are compared to those of calcined mesoporous silica films that have been successfully integrated into microelectronic devices as low dielectric constant films (Y.L. and C.J.B., unpublished work). Nitrogen sorption experiments performed using a surface acoustic wave technique[25] show the nanocomposite films to be nonporous to nitrogen at −196 °C (Type II sorption isotherm, see Fig. B of the Supplementary Information), meaning that the PDA completely fills the pore channels and that the composite architecture may impart some degree of oxidation resistance (important for extension to other conjugated polymer nanocomposites).

The blue PDA/silica nanocomposites thus exhibit solvatochromic, thermochromic, and mechanochromic properties. When contacted with the series of polar solvents—2-propanol, acetone, ethanol, methanol and dimethylformamide—the films transform to the red, fluorescent form and the differential absorbance (A) at 645 nm ($A_{blue} - A_{red}$) scales linearly with the dielectric constant of the solvent: $A_{645\,nm} = 0.003$ (dielectric constant) − 0.005; for a correlation coefficient of 0.992 (see Fig. 4f), suggesting applications in sensing. We suggest that polar solvents diffuse within the polar, hydrophilic EO_n pendant side chains. The accompanying solvation stresses are transferred to the PDA backbone (evidence for solvation stresses are presented in Fig. A of the Supplementary Information), reducing its conjugation length, and therefore inducing the blue → red transformation[26] as understood by recent molecular mechanics simulations[27]. The solvatochromic behaviour shows very slow reversibility. Heating to temperatures in excess of 47 °C can also cause the blue → red transformation, and preliminary results have shown this thermochromic behaviour to be rapidly reversible (several seconds). This may arise from hydrogen-bonding interactions[26] of the pendant side chains with the silanol moieties

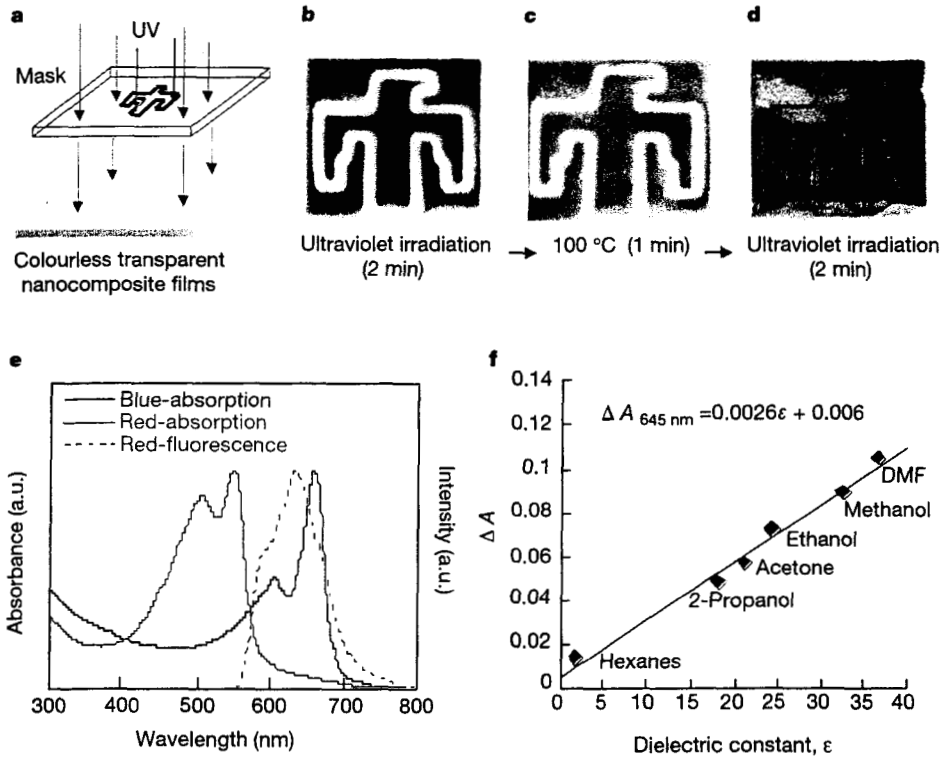

Figure 4 Patterned polymerization induced by ultraviolet irradiation and the thermochromic and solvatochromic transition of a hexagonal PDA/silica nanocomposite film. **a**, Schematic representation of the ultraviolet patterning procedure. **b**, Patterned blue/colourless film formed by ultraviolet irradiation for 2 min. **c**, Patterned red/colourless film formed by heating the film in **b** to 100 °C for 1 min. **d**, Patterned red/blue film formed by ultraviolet exposure of film in **c** for 2 min. **e**, Ultraviolet–visible spectra of the blue PDA/silica hexagonally ordered nanocomposite, the corresponding red film formed by heating at 100 °C, and the fluorescence emission spectrum of the red film (excited at 500 nm). Film formed from structure **1**, with $n = 5$. **f**, Differential absorbance at 645 nm resulting from the solvatochromic transition of blue PDA/silica nanocomposite films to the corresponding red films upon immersion of the blue films in the series of solvents: hexane, 2-propanol, acetone, ethanol, methanol, or dimethylformamide. Immersion times were 3 s followed by drying in nitrogen at room temperature. Without consideration of the nonpolar solvent, hexane, the regression equation is $A_{645\,nm} = 0.003$ (dielectric constant) −0.005, correlation coefficient = 0.992.

of the surrounding inorganic mesophase, supplying a restoring force and enabling recovery of the original side-chain orientation. Mechanical abrasion of the blue nanocomposite film causes local transformation to the red fluorescent form. Thus we envision mechanochromic barrier coatings that could sense excessive mechanical damage by changing from the blue form to the red fluorescent form.

The use of polymerizable surfactants as both structure-directing agents and monomers in the various evaporation-driven self-assembly schemes developed recently[28,29] represents a general, efficient route to the formation of robust and functional nanocomposites. Synthesis of surfactants with polymerizable thiophene, acetylene or phenylenevinylene groups should enable the self-assembly of conductive, conjugated polymer/silica nanocomposites in thin-film forms suitable for integration into devices. Conductive polymers confined within rod-like micellar channels of an electrical insulator conjure ideas of molecular wires. Unlike conduction measurements with two-dimensional films, such as bilayers[30] and monolayers[31], hexagonally ordered nanocomposite mesophases are nearly one-dimensional structures that could allow efficient conductivity along the channel direction. □

Methods

Precursor solutions were synthesized from tetraethylorthosilicate (TEOS, $Si(OC_2H_5)_4$), diacetylenic surfactants (structure 1 with $n = 3, 4, 5, 10$; structure 2, or combinations thereof) and HCl catalyst prepared in a THF/water solvent. The final reactant mole ratios were 1 TEOS:31.4–57.9 THF:4.96 H_2O:0.013 HCl:0.06–1.41 DA surfactant. Films were prepared by casting, spin-coating at 2,000 r.p.m., or dip-coating at a rate of 40 cm min^{-1}. Polymerization of PDA to the blue form was done by ultraviolet exposure at 266 nm for times ranging from 30 s to 30 min. Subsequent transformation to the red form was accomplished by heating at 100 °C for times ranging from 30 s to 2 min or by exposure to a solvent.

Molecular simulations were performed using *Cerius*^{2} and *Polygraf* software and the Burchart–Dreiding 2.21 force field. Ultraviolet–visible spectra of the PDA oligomers were calculated from the transition wavelengths and oscillator strengths obtained from INDO/S calculations on the terminated polymer backbone structure obtained from the molecular dynamics calculation.

Received 3 November 2000; accepted 6 February 2001.

1. Dagani, R. Putting the "nano" into composites. *Chem. Eng. News* **77**, 25–37 (1999).
2. Giannelis, E. Polymer layered silicate nanocomposites. *Adv. Mater.* **8**, 29–35 (1996).
3. Asefa, T., Yoshina-Ishii, C., MacLachlan, M. J. & Ozin, G. A. New nanocomposites: putting organic function "inside" the channel walls of periodic mesoporous silica. *J. Mater. Chem.* **10**, 1751–1755 (2000).
4. Smith, R. C., Fischer, W. M. & Gin, D. L. Ordered poly(*p*-phenylenevinylene) matrix nanocomposites via lyotropic liquid-crystalline monomers. *J. Am. Chem. Soc.* **119**, 4092–4093 (1997).
5. Sellinger, A. *et al.* Continuous self-assembly of organic-inorganic nanocomposite coatings that mimic nacre. *Nature* **394**, 256–260 (1998).
6. Moller, K., Bein, T. & Fischer, R. X. Entrapment of PMMA polymer strands in micro- and mesoporous materials. *Chem. Mater.* **10**, 1841–1852 (1998).
7. Nguyen, T.-Q., Wu, J., Doan, V., Schwartz, B. J. & Tolbert, S. H. Control of energy transfer in oriented conjugated polymer-mesoporous silica composites. *Science* **288**, 652–656 (2000).
8. Kleinfeld, E. R. & Ferguson, G. S. Stepwise formation of multilayered nanostructural films from macromolecular precursors. *Science* **265**, 370–373 (1994).
9. Keller, S. W., Kim, H.-N. & Mallouk, T. E. Layer-by-layer assembly of intercalation compounds and heterostructures on surfaces: Toward molecular "beaker" epitaxy. *J. Am. Chem. Soc.* **116**, 8817–8818 (1994).
10. Sasaki, D. Y., Carpick, R. W. & Burns, A. R. High molecular orientation in mono- and trilayer polydiacetylene films imaged by atomic force microscopy. *J. Colloid Interf. Sci.* **229**, 490–496 (2000).
11. Charych, D., Nagy, J., Spevak, W. & Bednarski, M. Direct colorimetric detection of a receptor-ligand interaction by a polymerized bilayer assembly. *Science* **261**, 585–588 (1993).
12. Cheng, Q. & Stevens, R. Charge-induced chromatic transition of amino acid-derivatized polydiacetylene liposomes. *Langmuir* **14**, 1974–1976 (1998).
13. Cheng, Q., Yamamoto, M. & Stevens, R. Amino acid terminated polydiacetylene lipid microstructures: morphology and chromatic transition. *Langmuir* **16**, 5333-5342 (2000).
14. Mazumdar, S. Prospects for the polymer nanoengineer. *Science* **288**, 630–631 (2000).
15. Lu, Y. F. *et al.* Continuous formation of supported cubic and hexagonal mesoporous films by sol–gel dip coating. *Nature* **389**, 364–368 (1997).
16. Israelachvili, J. N. *Intermolecular and Surface Forces* Ch. 17 (Academic, San Diego, 1992).
17. Monnier, A. *et al.* Cooperative formation of inorganic-organic interfaces in the synthesis of silicate mesostructures. *Science* **261**, 1299–1303 (1993).
18. Day, D. & Ringsdorf, H. Polymerization of diacetylene carbonic acid monolayers at the gas-water interface. *J. Polym. Sci. Polym. Lett. Edn* **16**, 205–210 (1978).
19. Gaines, G. L. (ed.) in *Insoluble Monolayers at Liquid-Gas Interfaces* 281–300 (John Wiley, New York, 1966).
20. Menzel, H., Mowery, M. D., Cai, M. & Evans, C. E. Vertical positioning of internal molecular scaffolding within a single molecular layer. *J. Phys. Chem. B* **102**, 9550–9556 (1998).
21. Collins, M. Optical-properties of poly-diacetylene monolayers. *J. Polym. Sci. B* **26**, 367–372 (1988).
22. Kuriyama, K., Kikuchi, H. & Kajiyama, T. Molecular packings-photopolymerization behavior relationship of diacetylene Langmuir-Blodgett films. *Langmuir* **12**, 6468–6472 (1996).
23. Spevak, W. *et al.* Polymerized liposomes containing *C*-glycosides of sialic acid: Potent inhibitors of influenza virus in vitro infectivity. *J. Am. Chem. Soc.* **115**, 1146–1147 (1993).
24. Frankel, D. A. & O'Brien, D. F. Supramolecular assemblies of diacetylenic aldonamides. *J. Am. Chem. Soc.* **113**, 7436–7437 (1991).
25. Frye, G. C., Ricco, A. J., Martin, S. J. & Brinker, C. J. in *Mater. Res. Soc.* (eds Brinker, C. J., Clark, D. E. & Ulrich, D. R.) 349–354 (Reno, Nevada, 1988).
26. Patel, G. N., Chance, R. R. & Witt. J. D. A planar-non-planar conformational transition in conjugated polymer solutions. *J. Chem. Phys.* **70**, 4387–4392 (1979).
27. Burns, A. R., Carpick, R. W., Sasaki, D. Y. & Shelnutt, J. A. Mechanochromism, shear force anisotropy, and molecular mechanics in polydiacetylene monolayers. *Tribol. Lett.* (in the press).
28. Fan, H. *et al.* Rapid prototyping of patterned functional nanostructures. *Nature* **405**, 56–60 (2000).
29. Brinker, C. J. Lu, Y., Sellinger, A. & Fan, H. Evaporation-induced self-assembly: nanostructures made easy. *Adv. Mater.* **11**, 579–585 (1999).
30. Day, D. R. & Lando, J. B. Conduction in polydiacetylene bilayers. *J. Appl. Polym. Sci.* **26**, 1605–1612 (1981).
31. Suzuoki, Y., Kimura, A. & Mizutani, T. in *Proc. 7th Int. Symp. Electrets* 850–855 (IEEE, New York, 1991).
32. Lu, Y. *et al.* Aerosol-assisted self-assembly of spherical, silica nanoparticles exhibiting hexagonal, cubic and vesicular mesophases. *Nature* **398**, 223–226 (1999).

Supplementary information is available from *Nature*'s World-Wide Website (http://www.nature.com) or as paper copy from the London editorial office of *Nature*.

Acknowledgements

We thank J. Curro and F. van Swol for technical discussions and T. Bucheit for the nano-indentation results. This work was supported by the US Department of Energy Basic Energy Sciences Program, the Sandia National Laboratories Laboratory-Directed Research and Development Program, the National Aeronautics and Space Administration, the UNM/NSF Center for Micro-engineered Materials, and the Defense Advanced Research Projects Agency Bio-Weapons Defense Program. TEM investigations were performed in the Department of Earth and Planetary Sciences at the University of New Mexico. Sandia is a multiprogram laboratory operated by Sandia Corporation, a Lockheed-Martin Company, for the US DOE.

Correspondence and requests for materials should be addressed to C.J.B. (e-mail: cjbrink@sandia.gov).

Early Oligocene initiation of North Atlantic Deep Water formation

Richard Davies*, Joseph Cartwright†, Jennifer Pike† & Charles Line*

* *ExxonMobil International Limited, St Catherine's House, 2 Kingsway, PO Box 393, London WC2B 6WF, UK*
† *Department of Earth Sciences, PO Box 914, Cardiff University, Cardiff CF10 3YE, UK*

Dating the onset of deep-water flow between the Arctic and North Atlantic oceans is critical for modelling climate change in the Northern Hemisphere[1,2] and for explaining changes in global ocean circulation throughout the Cenozoic era[3] (from about 65 million years ago to the present). In the early Cenozoic era, exchange between these two ocean basins was inhibited by the Greenland–Scotland ridge[3,4], but a gateway through the Faeroe–Shetland basin has been hypothesized[3,5]. Previous estimates of the date marking the onset of deep-water circulation through this basin—on the basis of circumstantial evidence from neighbouring basins—have been contradictory[5–9], ranging from about 35 to 15 million years ago. Here we describe the newly discovered Southeast Faeroes drift, which extends for 120 km parallel to the basin axis. The onset of deposition in this drift has been dated to the early Oligocene epoch (~35 million years ago) from a petroleum exploration borehole. We show that the drift was deposited under a southerly flow regime, and conclude that the

DISTRIBUTION

3	MS1413	A. R. Burns, 1140
1	MS1413	T. A. Michalske, 1140
1	MS1413	D. Y. Sasaki, 1140
1	MS1413	J. A. Shelnutt, 1140
1	MS1349	C. J. Brinker, 1846
1	MS0188	LDRD Office, 10300
1	MS9018	Central Technical Files, 8945-2
2	MS0899	Technical Library, 9616
1	MS0612	Review & Approval Desk, 9612
		For DOE/OSTI